The Use of a Distributed Hydrologic Model to Predict Dynamic Landslide Susceptibility for a Humid Basin in Puerto Rico

by

Sameer A. Kamal

M.Eng., Civil and Environmental Engineering, Massachusetts Institute of Technology (2008)
B.Sc., Chemical Engineering, University of Texas at Austin (2006)

SUBMITTED TO THE DEPARTMENT OF CIVIL AND ENVIRONMENTAL ENGINEERING IN PARTIAL FULFILLMENT OF THE REQUIREMENTS FOR THE DEGREE OF

ENVIRONMENTAL ENGINEER

AT THE
MASSACHUSETTS INSTITUTE OF TECHNOLOGY

SEPTEMBER 2009

Signature of Author .....
Department of Civil and Environmental Engineering
September 5, 2009

Certified by .....
Rafael L. Bras
Professor, Civil and Environmental Engineering

Certified by .....
Peter Shanahan
Senior Lecturer, Civil and Environmental Engineering

Accepted by .....
Daniele Veneziano
Professor, Civil and Environmental Engineering
Chairman, Departmental Committee for Graduate Students

The Use of a Distributed Hydrologic Model to Predict Dynamic Landslide Susceptibility for a Humid Basin in Puerto Rico

by

Sameer A. Kamal

Submitted to the Department of Civil and Environmental Engineering
on September 4, 2009 in Partial Fulfillment of the
Requirements for the Degree of Environmental Engineer

ABSTRACT

This thesis describes the use of a distributed hydrology model in conjunction with a Factor of Safety (FS) algorithm to predict dynamic landslide susceptibility for a humid basin in Puerto Rico. The Mameyes basin, located in the Luquillo Experimental Forest in Puerto Rico, was selected for modeling based on the rich ensemble of soil, vegetation, topographical, meteorological and historic landslide data available. The basin was parameterized into the TIN-based Real-time Integrated Basin Simulator (tRIBS) with particular emphasis on vegetation parameters for broadleaf evergreen trees in tropical climates. The basin was forced with precipitation data that included a synthesized rainfall event likely to result in a landslide based on rainfall intensity-duration thresholds. The basin's response was assessed mainly in terms of soil moisture and values of selected vegetation parameters, which served as the dynamic inputs into the FS algorithm.

An off-line FS algorithm was developed and tested using typical values for parameters encountered in the Mameyes basin. Sensitivity analyses indicated that slope angle, soil cohesion and soil moisture were the most sensitive parameters in this FS algorithm. When the tRIBS / FS Algorithm combination was employed over the entire basin, landslides were indicated in 48 out of 13,169 modeled locations. The spatial distribution of landslides compared favorably to a static landslide susceptibility map developed in previous work by Lepore et al. (2008b) while the temporal distribution of landslides was correlated with rainfall events. Landslides were predicted over a range of slope angle values, including on relatively gentle slopes where the modeled soil moisture drove the instability. The results demonstrate that the tRIBS/FS algorithm combination developed in this work is able to capture the key dynamics associated with slope stability, specifically the interactions between the slope angle and the soil moisture state.

Thesis Supervisors:

Rafael Bras
Title: Professor, Department of Civil and Environmental Engineering

Peter Shanahan
Title: Senior Lecturer, Department of Civil and Environmental Engineering

FOR ALTAMASH KAMAL ScD '82

ACKNOWLEDGEMENTS

I would firstly like to acknowledge my advisers Dr. Peter Shanahan and Dr. Rafael L. Bras. Pete's thorough review of my work, thoughtful analysis and detailed critiques of my writing have greatly contributed to my learning as a researcher and as an engineer. His guidance and support have been paramount in the completion of this thesis. Dr. Bras's thoughtful and direct criticism, encouragement, and intuitive sense of what's important have guided the overall direction of this project and have contributed to my academic growth.

It has been a privilege to have been a part of the Bras research group. I've had a wonderful experience working with Dr. Chiara Lepore and am particularly indebted to her for the programming-heavy aspects of the FS algorithm, the organization and presentation of the tRIBS outputs, and for her company during much-needed fresh air breaks. Gajan Sivandran has always made time to share his thoughts as this project has progressed, and his enthusiasm, energy and model troubleshooting support have greatly shaped several aspects of this work. I appreciate the time taken by Gautam Bisht, particularly to familiarize me with and guide me through the use of the tRIBS code. I would also like to acknowledge the other current and former members of the Bras Research Group—Dr. Alejandro Flores, Homero Flores, Dr. Ujjwal Narayan, Dr. Dalia Bach Kirschbaum, Ryan Knox, Tony Parolari and Dr. Jingfeng Wang—whose criticism and counsel have influenced the evolution of this work. I have been touched by their friendship and camaraderie during my time at MIT.

We appreciate the assistance and data provided for the Bisley watersheds by the USDA Forest Service International Institute. Dr. Frederick Scatena's enthusiasm and prompt and practical feedback have been very helpful, particularly in the early modeling stages of this work.

Most of all, I would like to acknowledge my family—my mother Simi, father Altamash, brother Maazin and sister Daanika; my Texas family—Ajam, Asif, Sarmed, Munis and Meraal; and my grandparents for their love and support. To my friends near and far—particularly Ghafoor, Rameez, Suhail, Mahua and Ali—thank you.

TABLE OF CONTENTS

LIST OF FIGURES

LIST OF TABLES

CHAPTER 1: INTRODUCTION

Historically, landslides have been a significant threat to human life. Landslides can be triggered by rainfall, earthquakes, volcanoes or human activity. In the United States, there are an estimated 25-50 deaths and $1 - 2 billion in economic losses annually due to landslides (Schuster 1996). The October 1985 Mameyes landslide in Puerto Rico was the worst landslide disaster in North America. At least 129 people were killed and more than 100 homes were destroyed. More recently, the February 2006 landslide in the village of Guinsaugon in the Philippines resulted in at least 139 deaths, with an additional 980 missing (presumed dead).

In addition to human life, direct costs from landslides include repair, replacement and maintenance of infrastructure, while indirect costs include loss of industrial, agricultural and forest productivity; loss of tourist and other revenues due to damage to land, facilities or transportation networks; loss of human and animal productivity and adverse impacts on water quality. Often, the true impacts of landslides are lost as they may occur as part of multiple-hazard disasters (Schuster 1996).

While there are several complex interactions that ultimately result in rainfall-triggered landslides, this thesis will explore the use of the TIN-based Real-time Integrated Basin Simulator (tRIBS) hydrological model, in conjunction with an off-line landslide algorithm based on the Factor of Safety (FS) equation, to assess dynamic landslide susceptibility of slopes to landslides.

Developed for geotechnical applications by Terzaghi (1925), the FS equation is defined as the ratio of the shear strength (or resisting forces) to the shear stress (or driving forces). A FS value of less than 1 indicates that driving forces will prevail, leading to hillslope failure, while FS values greater that 1 indicate that resisting forces with prevail. A FS value greater than 1 does not indicate unconditional stability, but rather that the probability of stability increases as the FS value increases (Selby 1993). Process-based models have employed variations of the FS equation and coupled them with geomorphic, hydrologic, geologic and vegetation data (Dietrech et al. 1995; Selby 1994; Iverson 2000).

The key dynamic (i.e. time-varying) parameter that appears in the FS equation is the soil moisture at the depth at which the slope failure (i.e. landslide) occurs. Other dynamic parameters include the forces associated with vegetation. As vegetation grows on the hillslope, it exerts a greater force on the hillslope due to its own weight and also the weight of the water it can retain (Greenway 1987). The development of roots can also influence the cohesive strength of soils through root reinforcement (Greenway 1987).

Thus, in order to develop a dynamic process for determining landslide susceptibility, the soil moisture and the vegetation parameters in the FS equation must also be dynamically determined. The tRIBS model, which is a distributed hydrology model that allows for the modeling of hydrologic processes in a time-continuous fashion (Ivanov 2006), provides a good framework due to its ability to distribute soil moisture and also account for

vegetation effects on the slope. The tRIBS model employs a Triangulated Irregular Network , which is a digital data structure used for the representation of a surface primarily in geographic information system (GIS) applications. Previous TIN-based landslide work in the Bras research group at MIT includes the successful use of the Channel-Hillslope Integrated Landscape Development (CHILD) model. The CHILD model employs slope stability equations and incorporates the effects of diffusive processes, rainfall, geology and vegetation (Istanbulluoglu and Bras 2005).

This work sought to demonstrate that the tRIBS distributed hydrology model, in conjunction with a Factor of Safety (FS) algorithm, is a viable tool for predicting dynamic landslide susceptibility via an application to a humid tropical basin in Puerto Rico. The tRIBS model can provide soil moisture and vegetation outputs at hourly time steps, and these dynamic outputs can be employed in the FS algorithm to assess susceptibility of a particular slope to landsliding on an hourly basis. In order to compute these soil moisture and vegetation output values on an hourly basis, the meteorological data used to force the model must be available at hourly intervals. Furthermore, enough soil, vegetation and topographical data must be available so that the basin can be adequately parameterized in the tRIBS framework.

The first step in this work was to select a basin for modeling in tRIBS. The Luquillo Experimental Forest (LEF) in Puerto Rico presents a good setting for this study due to the amount of data available. The basin selected for this work, which lies within the LEF, is the Mameyes basin. It was selected based on the availability of soil, vegetation, topographical and meteorological data, as well as the availability of a landslide data set. Soil data were obtained from the U.S. Department of Agriculture (USDA) Forest Service's International Institute of Tropical Forestry in San Juan, Puerto Rico as published in the USDA Natural Resources Conservation Service (NRCS) Publication titled "Soil Survey of Caribbean National Forest and Luquillo Experimental Forest, Commonwealth of Puerto Rico" (USDA 2002). A vegetation map with general vegetation classifications for the entire island is available in Helmer et al. (2002). Data on landslides were obtained from the United States Geological Survey (USGS) and are available for a large area in the LEF, as outlined by Larsen et al. (1998). Meteorological and rainfall data for sites specific to the LEF are available from the Luquillo Long-Term Ecological Research Program website (*LUQ LTER Data Sets by Category*). The selection of and data assimilation for the Mameyes basin are addressed in Section 3.1.

Once the basin was selected it was parameterized in the tRIBS model framework. This process involved categorizing the various soil types in the Mameyes basin into three classes (clay, loam and silt) and categorizing the vegetation types into two classes (Tropical Broadleaf Evergreen Trees and C4 grasses). The main vegetation type in the Mameyes basin, BET (Broaflead Evergreen Trees) Tropical, had not been modeled previously in tRIBS. Its development was guided by literature on vegetation dynamics and previous vegetation modeling experiences in the Bras group. The parameterization of the basin and particularly the parameterization of the BET Tropical vegetation class are addressed in Section 3.2.

After parameterization and development of the selected basin in tRIBS, the basin had to be forced with hourly meteorological data. Data from the weather station at the Bisley tower site which is located in the north-east of the Mameyes basin was selected. While hourly data from 2002 to 2008 were available, significant temporal gaps exist during time periods that the weather station at Bisley Tower was not operational. However, data for the entire 2005 calendar year was available. The year 2005 was relatively stable in that a major rainfall event of a magnitude typically associated with a landslide did not occur. It thus became necessary to synthesize a rainfall event based on existing duration-intensity thresholds for Puerto Rico (Larsen et al., 2005). An hourly meteorological series for a two-year period was constructed. The 2005 data were repeated twice, with the synthesized rainfall event added in the second year. After assembling and employing the two-year meteorological data record, the response of the basin, specifically in terms of model outputs such as soil moisture distribution, vegetation response and heat flux values, was assessed. The development of the meteorological data, key assumptions and steps in the model initialization, and results from the simulation are presented and discussed in Section 3.3.

Selected outputs (i.e. soil moisture states and vegetation parameters) from the tRIBS simulation of the Mameyes basin were used as inputs into an off-line landslide susceptibility algorithm based on the Factor of Safety (FS) equation. Microsoft Excel was employed for the preliminary development of the FS equation and sensitivity analyses were conducted on selected key parameters in the equation. The sensitivity analyses highlighted the relative importance of terms in the FS equation and formed a basis to check whether the responses of the FS equation to changes in soil moisture, slope angle, soil cohesive strength and vegetation were reasonable. Once the preliminary FS equation in Microsoft Excel had been tested in this way, an algorithm was coded in MATLAB. MATLAB, which allows for efficient manipulation of a large amount of data, provided a good framework for manipulating the outputs files from the tRIBS simulation. A primary advantage of using this off-line approach is that it allowed for the development of the FS algorithm without necessitating time-consuming and demanding modifications to the tRIBS model. The development of the FS equation and results from the sensitivity analyses used to validate the equation are presented in Section 4.2.

Finally, the off-line landslide component based on the FS equation was applied over the entire Mameyes basin for a model period of two years. The off-line landslide component, forced by dynamic meteorological data, was used to flag the location of potentially unstable hillslopes as well as the time step at which they become susceptible. While a highly precise correlation between the location and timing of landslides versus historical records was not feasible nor expected, a qualitative assessment of the off-line landslide component was possible via a comparison to historic landslide records and the static landslide susceptibility map developed previously by the Lepore et al. 2008b. A summary of the results and a comparison to previous results by the author are presented in Section 5.1.

The results from this study set the groundwork for more precise and detailed dynamic landslide modeling in the future. Conclusions and recommendations for future work are

presented in Section 5.2. It is hoped that this work will ultimately contribute towards a real-time landslide warning system that can be applied on the island, and that the methodology employed in this project (and the wider research study) will be applicable to other parts of the world that have had a high historic occurrence of landslides.

CHAPTER 2: BACKGROUND

Puerto Rico

Puerto Rico is located in the northeastern Caribbean, 1,280 miles off the coast of Florida. The island measures approximately 160 km east to west and 55 km north to south. Topographically, a large part of the island is mountainous. The two main mountain ranges include the Cordillera Central mountain range in central Puerto Rico (maximum peak of 1338 m) and the Sierra de Luquillo mountain range in the northeast (maximum peak of 1074 m). The island is largely composed of Cretaceous to Eocene volcanic rocks, which are overlain by younger Oligocene and other sedimentary rocks (Pando 2005).

The climate of Puerto Rico varies significantly due to its varied topography, ranging from humid-tropical in the central mountain range and north coast to seasonal dry in the southern coastal plain (Larsen et al. 1993). The prevailing trade winds are from the east and northeast, and much of the rainfall during the May through December wet season is associated with these winds. Annual rainfall ranges between 760 to more than 5,000 mm, with variations mostly due to the changes in land elevation over the central mountain range. The mean annual temperature varies with elevation, ranging from 23 to 27 °C along the coastal plains to 19 to 23 °C at the higher peaks.

Historically, Puerto Rico has had significant landslide activity. The types of landslides include shallow soil slips, debris flows, debris slides, debris avalanches and slumps (Larsen et al. 1993). One factor contributing to high landslide activity in Puerto Rico is the relatively moist condition of soils. Compared to selected humid cities in the United States, Puerto Rico has almost twice the mean number of days when precipitation exceeds 3 mm. In the forested areas of Eastern Puerto Rico, the average year-long rate of daily moisture loss in the upper 305 mm of soil was found to be about one-half that of the average summer rate in humid climates of the United States (U.S Army Corps of Engineers, 1960). This lower soil moisture depletion rate is likely due to climatic differences between Puerto Rico and the United States, such as shorter summer days and a lower maximum summer temperature (Larsen et al. 1993). Puerto Rico also has a significant historic hurricane frequency, with hurricane season running from June through October and the large majority of hurricanes occurring in August and September.

Landslides and Related Terminology

The term landslide denotes "the movement of a mass of rock, debris or earth down a slope." Varnes (1996) provides useful guidelines on the major types and classifications of landslides. Different types of landslides are typically described by two nouns, the first denoting the material involved and the second denoting the type of movement. A complete description of a landslide would include sets of these two nouns in addition to descriptors that further elaborate the state, distribution and style of the landslide.

According to Varnes, there are three primary types of materials involved in landslides: rock, debris and earth. A rock is defined as a "hard or firm mass that was intact and in its

natural place before the initiation of movement." Debris and earth are both considered a part of soil, which is broadly defined as an aggregate of solid particles (generally minerals or rocks) that either was transported or was formed by the weathering of rock in place. Earth describes material in which 80 percent or more of the particles are smaller than 2 mm (i.e. finer material) while debris describes material where 20 to 80 percent of the material is larger than 2 mm (i.e. coarser material).

In addition, there are five main types of movements: falls, topples, slides, spreads and flows. A fall involves detachment of a soil or rock that descends through falling, bouncing or rolling and where the movement is very rapid to extremely rapid. A topple, which is generally driven by gravity, is the forward rotation out of the slope of a mass of soil or rock about a point or axis below the center of gravity of the displaced mass. A slide is a downward movement of a soil or rock mass that occurs dominantly along surfaces of rupture—in a rotational slide, the surface is curved and concave, while in a translational slide, the surface is planar. Translational slides are typically shallower than rotational slides. A spread is a generally gradual extension and subsidence of a cohesive soil or rock mass into softer underlying material. A flow is a spatially continuous movement in which the distribution of velocities in the displacing mass is similar to that of a viscous liquid. Slides can often turn into flows with increased water content, mobility and evolution of the movement.

The destructive potential of a landslide can usually be gauged by the velocity of the landslide. Landslide velocity is divided into seven categories, three of which classify "slow" landslides (extremely slow, very slow and slow), three of which classify "rapid" landslides (extremely rapid, very rapid and rapid) and the last that classifies a "moderate" landslide.

Further descriptors for landslides include the state of landslide activity (i.e. how "active" the landslide is at a particular time), the style of the landslide activity (i.e. how the different movement processes described above contribute to the overall landslide) and the water content of the landslide materials (i.e. whether the materials are "dry," "moist," "wet" or "very wet.") For a more detailed discussion of landslide terminology, see Varnes (1996).

Slope Stability

In order to quantitatively determine the potential for a landslide, a slope stability analysis is often performed. Duncan (1996) provides an overview of soil slope stability analysis. In general, the stability of a slope is usually analyzed by methods of limit equilibrium. The potential sliding mass is subdivided into a series of smaller units, and each of these units is analyzed by computational methods to determine its potential for failure. A key step in limit equilibrium techniques is the calculation of a factor of safety, which is determined for the critical slip surface (i.e. the surface that is most likely to fail by sliding). The factor of safety is defined as the ratio of the shear strength (or resisting forces) to the shear stress (or driving forces) required for equilibrium of the slope, and effectively represents the factor by which the strength would have to be reduced to bring

the slope to failure and cause a landslide. In other words, a factor of safety value of less than 1 indicates that driving forces will prevail, leading to slope failure. Factor of safety values greater than 1 do not indicate unconditional stability, but rather that the probability of stability increases as the value of the factor of safety increases (Selby 1993).

Process-based models have employed variations of the factor of safety equations and coupled them with geomorphic, hydrologic, geologic and vegetation data (Dietrich et al. 1995; Selby 1994; Iverson 2000). The factor of safety equation to be employed by the tRIBS model, for a particular element at an arbitrary depth Z and at time t, is reproduced below:

$$FS(Z,t)=\frac{\tau_r}{\tau_d}=\frac{\tan\varphi}{\tan\alpha}+\frac{c'(t)}{(\gamma_s Z+B(Z,t))\sin\alpha\cos\alpha}-\frac{\psi(Z,t)\gamma_w\tan\varphi}{(\gamma_s Z+B(Z,t))\sin\alpha\cos\alpha} \quad \text{(Equation 2.1.1)}$$

where τ_r is the shear strength, τ_d is the shear stress, $c'(t)$ is the apparent soil cohesion that is a function of root biomass, α is the slope angle, φ is the internal friction angle of the soil, $B(Z,t)$ is sum of the weight of the biomass above Z and the amount of water retained in the canopy, and $\psi(Z,t)$ is the soil matric potential at depth Z and time t. γ_s and γ_w are the specific weights of the soil and water, respectively (Iverson 2000).

The first term in the equation above represents the friction resistance of soil material, the second resistance due to cohesion and the third the reduction in resistance associated with soil water pore pressures.

Rainfall as a Landslide Triggering Mechanism

While landslides can have many long-term causes, they are generally attributed to a single "trigger." Landslide triggers, which essentially weaken the slope stability enough to cause a landslide, include intense rainfall, rapid snowmelt, water-level change, volcanic eruption and earthquakes (Wieczorek 1996).

The close relationship between rainfall intensity and landslides is well documented in various studies. The mechanism by which shallow landslides are generated during storms is considered to be soil saturation and the rise in pore-water pressures associated with rainfall (Wieczorek 1996). The triggering effect is due to the soil pore pressures and other stresses increasing the internal resisting forces of the combined soil, bedrock and root matrix. Often, soils with low permeability do not have time to drain when such load changes occur, resulting in unequal excess pore pressures that lead to slope failure (Duncan 1996). In addition, lower parts of hillslopes and stream channels may be particularly vulnerable to debris flows due to the high sediment contents in the stream that are a result of intense rainfall. Erosion due to rainfall could also remove the "toe" of a slope through erosion, thereby steepening the slope and increasing the susceptibility to the slope to landsliding.

Previous Landslide Studies in Puerto Rico

A summary of key literature on landslides in Puerto Rico most relevant to this project is presented in the following. Prior studies of landslides have focused on probabilistic approaches that use the historic locations of landslides to infer static susceptibility (e.g. Larsen et al. 1998), on the identification of landslide-triggering rainfall duration-intensity thresholds (e.g. Pando et al. 2005) or on slope stability as determined by the Factor of Safety (FS) equation (e.g. Simon et al. 1990).

Probabilistic approaches to determine static susceptibility

Probabilistic approaches to determine susceptibility are based on the assumption that slope failures in the future will occur with the same probability under the same conditions that led to past and present instability. These approaches determine "static" as opposed to "dynamic" susceptibility because they focus on the characteristics of hillslopes rather than on the response of hillslopes to rainfall events or to other dynamic variables.

Larsen et al. (1998) developed landslide maps from 1:20,000-scale aerial photographs (with a 10m by 10m lower limit of observation) and GIS measurements. The landslides were characterized by a range of geomorphic indicators, which included a sharp break or disruption in vegetation type, bare soil or soil with little vegetation regrowth, steep head, and side scarps and downslope debris deposits. This approach was limited in that landslides masked by thick forest canopy or shadows on steep hillslopes were not detected. Similarly, much older landslides on hillslopes that, over decades, had been restored close to their pre-landslide vegetative conditions were not detected (Larsen 2001). Three regions of Puerto Rico, Blanco, Cayaguas and Coamo, were selected as study areas. A set of simplified matrices that related landslide occurrence to slope angle, slope elevation, slope aspect (the direction the slope faces) and land use were developed. It was found that hillslopes with gradients of 12 degrees or more, elevations in excess of 400 m and slope aspect facing the trade winds corresponded to an appreciable increase in landslide frequency.

Building on this approach, recent work in the Bras Research Group at M.I.T has focused on the development of static susceptibility maps for Puerto Rico (Lepore et al. 2008a and 2008b). These maps have been generated using two procedures, bivariate frequency ratio and multivariate logistic regression, that combine physical features of the hillslope to determine susceptibility. The inherent assumption in this approach is that slope failures in the future will occur with the same probability under the same conditions that led to past and present instability.

Prior work by Lepore et al. 2008b), focusing on the use of the bivariate frequency ratio, concluded that slope angle was the dominant factor in determining static susceptibility for landslides in Puerto Rico. The work highlighted the significance of the resolution of the digital elevation model (DEM) used to infer static susceptibility, in that the "characteristic scale" of a landslide for a particular dataset will be dependent to a large extent on the spatial resolution of the DEM employed. A relatively shallow landslide is

not typically as wide or as long as a relatively deep landslide. Thus, if the length and width of a potentially unstable slope has a lower limit defined by the highest resolution (i.e. smaller grid size) of the DEM, only slides as deep as the depth corresponding to that length or width can be captured (Lepore et al. 2008b). Effectively, this limit of observation provides a definition for what a "landslide" event is. This issue of resolution has significant implications for the current work, since the tRIBS model is based on Voronoi cells of varying sizes.

Rainfall duration-intensity thresholds

Another approach for landslide studies in Puerto Rico has been to focus on the characteristics of rainfall that result in landslides, irrespective of the characteristics of the hillslope where the landslide occurred. Larsen et al. (1993) used data for 256 storms from 1959 to 1990 in the central mountain region of Puerto Rico to develop a threshold relation between rainfall intensity-duration and landslides. This threshold for Puerto Rico was, in turn, compared with a worldwide threshold developed by Caine (1980). For rainfall durations less than 10h, the Puerto Rico threshold indicated that as much as three times more rainfall is required to trigger landslides in humid-tropical PR than the rainfall amount that triggers landslides worldwide. For rainfall approaching 100 h, the difference between humid-tropical and temperate environments may be less significant. More than half of the storms linked to moderate to extensive landsliding were topical disturbances such as hurricanes, tropical storms, tropical depressions, tropical waves or troughs, while 27% were associated with localized heavy rains or convective thunderstorms and 20% with winter cold fronts.

Pando et al. (2005) updated the threshold developed in 1993 based on additional landslide data collected through 2003. They also presented a summary of literature published on rainfall induced landslides in Puerto Rico, and concluded that there is a lack of systematic research and analysis into the causes and consequences of slope stability problems. They recommended additional studies to account for geologic and topographic settings, failure types and land use.

Slope stability

The role of soil processes in determining slope failure as indicated by the FS equation has been addressed in Simon et al. (1990). Simon et al. identified ten different slopes in the Luquillo Experimental Forest (LEF) to analyze through the use of the FS Equation. They sampled soils, tested shear strength, and surveyed vegetation, using the resulting data to solve the FS equation. Pore-pressure response to rainfall events was also monitored, and potential failure depths were identified based on the soils and geology in the region. Ultimately, slope units susceptible to landslides at certain saturation levels were identified from FS values. This study provides a valuable resource in developing and employing the FS Algorithm in the current work.

Summary

While prior landslide studies in Puerto Rico have explored use of the FS equation for specific slopes, the characteristics of rainfall events that trigger landslides and the static susceptibility of areas based on historic landslide occurrences, there is no published work that employs the FS equation to determine dynamic susceptibility in response to rainfall events in Puerto Rico. The current work develops an off-line "landslide component," i.e. an algorithm that is based on the FS equation, that is employed in conjunction with the tRIBS model. Despite their lack of a dynamic component, all three categories of previous landslide studies in Puerto Rico are pertinent to the current work. The slope stability assessments conducted on ten different slopes by Simon et al. (1990) guide the basin-wide, dynamic slope susceptibility assessment in the current work. In particular, the values used for the different FS equation parameters in Simon et al.'s study can be used to guide the development of the FS equation parameters in the current work. Larsen et al.'s (1993) rainfall duration-intensity thresholds form a basis of comparison for results from the current work. The tRIBS/FS algorithm combination, if formulated appropriately, should result in predicted landslides over the basin particularly when the duration-intensity threshold for rainfall is exceeded. Static susceptibility maps also provide a basis of comparison with the spatial aspect of the tRIBS/FS algorithm results. In other words, regardless of when the slopes fail (i.e. the dynamic aspect), there should be a reasonable overlap between the spatial distribution of slides from the current work and the static susceptibility maps developed based on probabilistic approaches.

CHAPTER 3: SELECTION, DEVELOPMENT AND SIMULATION OF BASIN

3.1 Selection of Study Basin and Availability of Data

The basin for this study was selected based on the availability of meteorological, precipitation, soil and vegetation data—all of which are required for the specification of the basin in tRIBS. Furthermore, a basin with an existing landslide dataset was selected to allow for a qualitative comparison of the factor of safety results with actual historic landslides. Soil and vegetation data were largely available across the entire island, so the limiting selection criteria were the availability of landslide data and meteorological/ precipitation data. Areas with prior landslide data were preferred since the presence of historic landslides provides an indication of relative landslide risks (see Lepore et al. 2008b for a more complete discussion of this hypothesis). Meteorological/precipitation data were limiting because an ensemble of hourly data is needed to run tRIBS, and hourly data is available only for select stations on the island.

The basin selected for modeling is the Rio Mameyes basin (hereto referred to as "Mameyes basin"), located within the LEF. For this work, the basin was delineated from a 30m Digital Elevation Model (DEM) of the island (See Figure 3.1.1). The availability of each dataset for this basin is addressed in the text that follows.

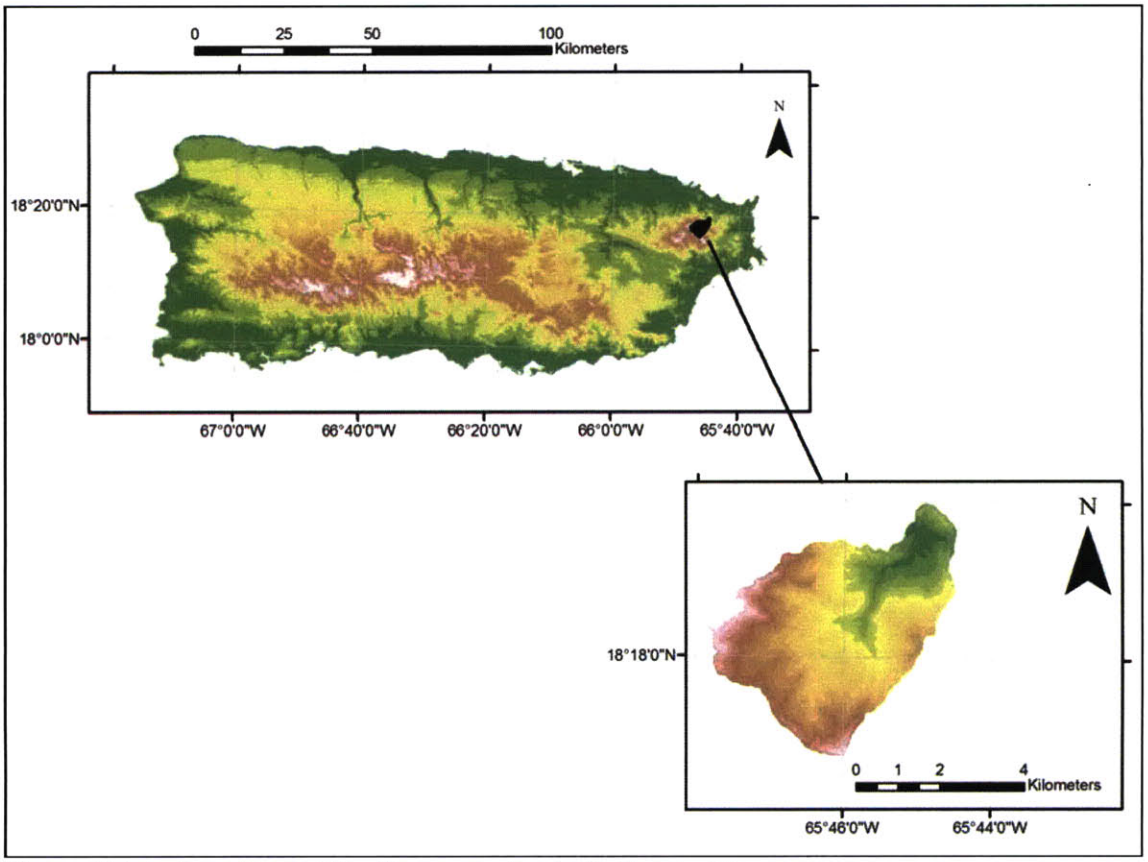

Figure 3.1.1: Location of the Mameyes basin in Puerto Rico.

Landslide Data

The modeling component of this work attempts to develop a dynamic landslide susceptibility map, forced by meteorological data. One point of comparison for this dynamic susceptibility map is the static susceptibility map previously developed by the Lepore et al. 2008b.

Prior landslide work by the Lepore et al. 2008b employed landslide data obtained from the United States Geological Survey (USGS) and includes data sets for the regions of Coamo (1024 landslides), Rio Blanco (1860 landslides) and Cayaguas (82 landslides) (Larsen et al. 1998). The available landslide data are shown in Figure 3.1.2. The Mameyes basin (shown in Figure 3.1.3) encompasses a range of susceptibility index values (from 1 – Highest Susceptibility to 4 – Lowest Susceptibility) as defined by Lepore et al. (2008b).

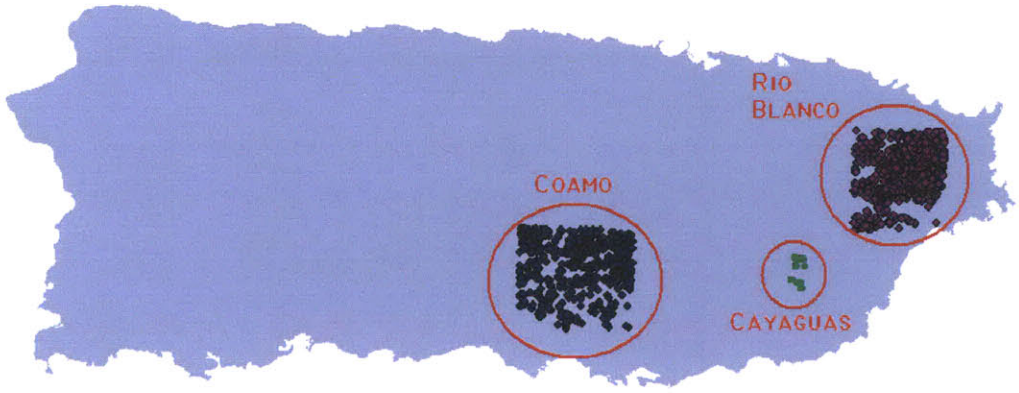

Figure 3.1.2: Regions with available landslide data

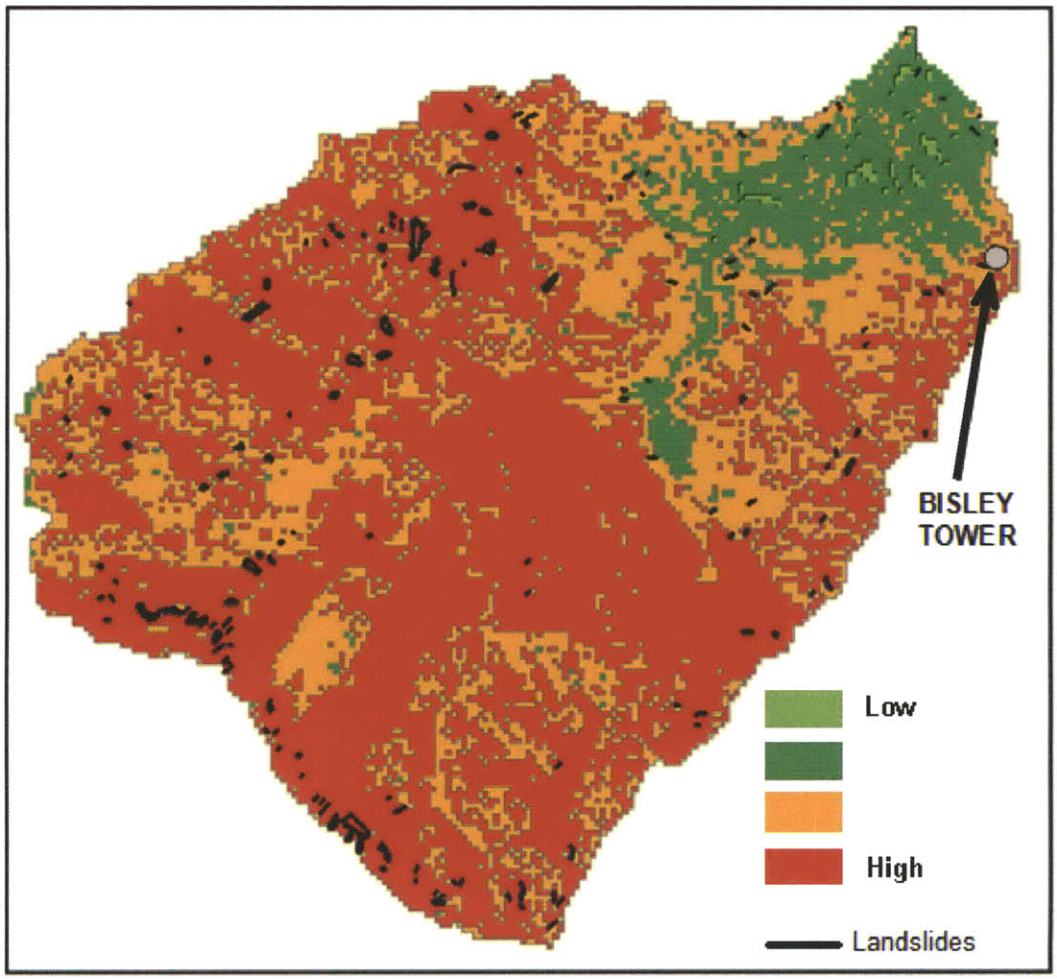

Figure 3.1.3: Landslide susceptibility (1 = Highest susceptibility, 4 = Lowest susceptibility) and historic landslide locations for Mameyes basin as documented by Lepore at al. 2008b. Gray dot represents location of the Bisley Tower.

Meteorological Data

As mentioned above, hourly meteorological data are needed for the tRIBS model. Hourly data are available only for select locations in Puerto Rico. Through the National Climatic Data Center (NCDC), hourly data are available for three locations—but none of these overlap with areas where landslide data are also available. Selected hourly meteorological data are available for several locations in the Luquillo Experimental Forest (LEF) through the Luquillo Long-Term Ecological Research Program (Luquillo LTER) website. These locations are the field sites of El Verde (2001 – 2008), East Peak (2002 – 2008) and Bisley Tower (2002 – 2008). Of these, the Bisley Tower site is located in the northeast part of the Rio Mameyes basin (See Figure 3.1.3).

The meteorological parameters required for the tRIBS model are listed in Table 3.1.1. As seen in Table 3.1.1, two meteorological parameters—atmospheric pressure and net radiation—are not available for the Bisley Tower through the LTER dataset. Atmospheric pressure does not exhibit a very significant variation over the island from a modeling

perspective, and thus daily atmospheric pressure values were obtained from a NCDC weather station at San Juan, with the daily pressure value assigned to each hourly value for that day. Net radiation is generated by the tRIBS weather generator based on the other input weather values and the latitude and longitude of the basin. More details about the weather generator are documented by Ivanov (2006).

Table 3.1.1: Availability of hourly meteorological data for Bisley Tower

Symbol	Description	Unit	Bisley?
PA	Atmospheric Pressure	mb	No
TD	Dew Point Temperature	°C	Yes
RH	Relative Humidity	%	Yes
VP	Vapor Pressure	mb	Yes
XC	Sky Cover	tenths	Yes
US	Wind Speed	m/s	Yes
TA	Air Temperature	°C	Yes
NR	Net Radiation	W/m^2	No
ET	Pan Evaporation	mm/hr	Yes
R	Rainfall	mm/hr	Yes
IS	Incoming Short Wave Radiation	W/m^2	Yes

Significant temporal gaps in the data exist for time periods that the weather station at Bisley Tower was not operational. However, data for the entire 2005 calendar year are available. As described in Section 3.3, this complete dataset from 2005 forms the basis of the meteorological data used to force the tRIBS model.

Soil Data

Data for the LEF was obtained in digital format from the USDA Forest Service's International Institute of Tropical Forestry in San Juan. A description of this soils data is available in the USDA/NRCS publication titled "Soil Survey of Caribbean National Forest and Luquillo Experimental Forest, Commonwealth of Puerto Rico" (USDA 2002). More than 99% of the Mameyes basin lies within the area covered by the LEF Soil Survey. In the LEF soil survey the soil types are defined according to the unified soil classification system used in geotechnical engineering (ASTM, 2001). These data were reclassified into broader soil types by the author. This preliminary soil classification categorized each soil type in the unified soil classification system as a soil type in the USDA soil texture triangle. These textures included: sand, sandy loam, loam, sandy clay loam, clay loam, silty clay loam, silty clay, clay, rock outcrop, and other. Once each soil was put into a USDA soil texture category, a reclassification was conducted based on the Cosby et al. (1984) reclassification triangles, reproduced in Figure 3.1.4. The final classification of soil types is shown in Figure 3.1.5. The three soil types represented in the basin are clay (53.9%), loam (41.1%) and silt (4.9%).

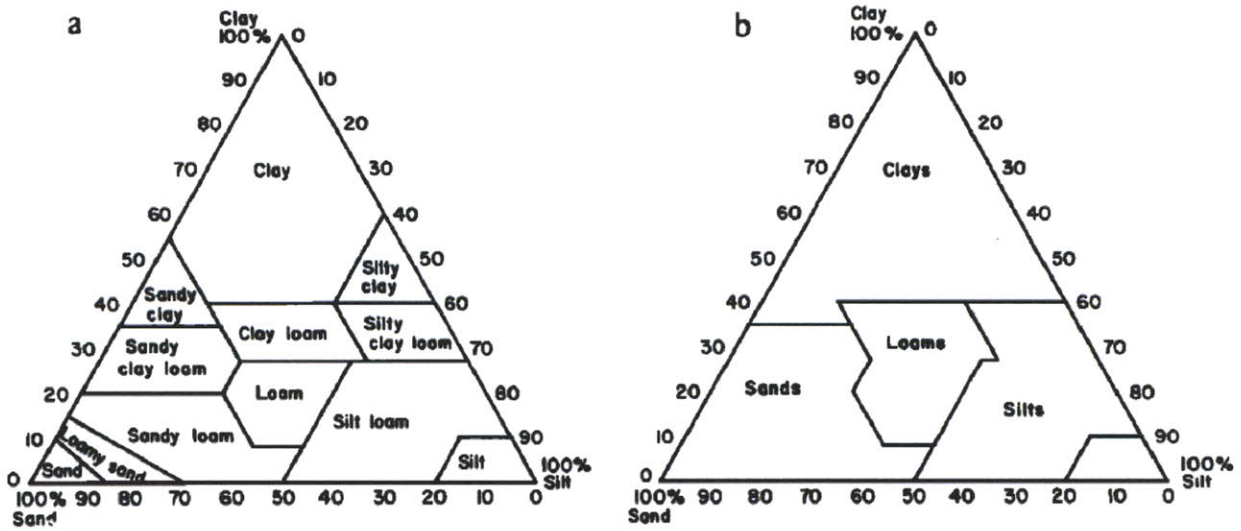

(*a*) The USDA soil texture triangle. (*b*) Reclassification of the texture categories into four broad regions for the two and four group discriminant analyses.

Figure 3.1.4: Figure from Cosby et al. (1984) showing soil reclassifications into four general categories.

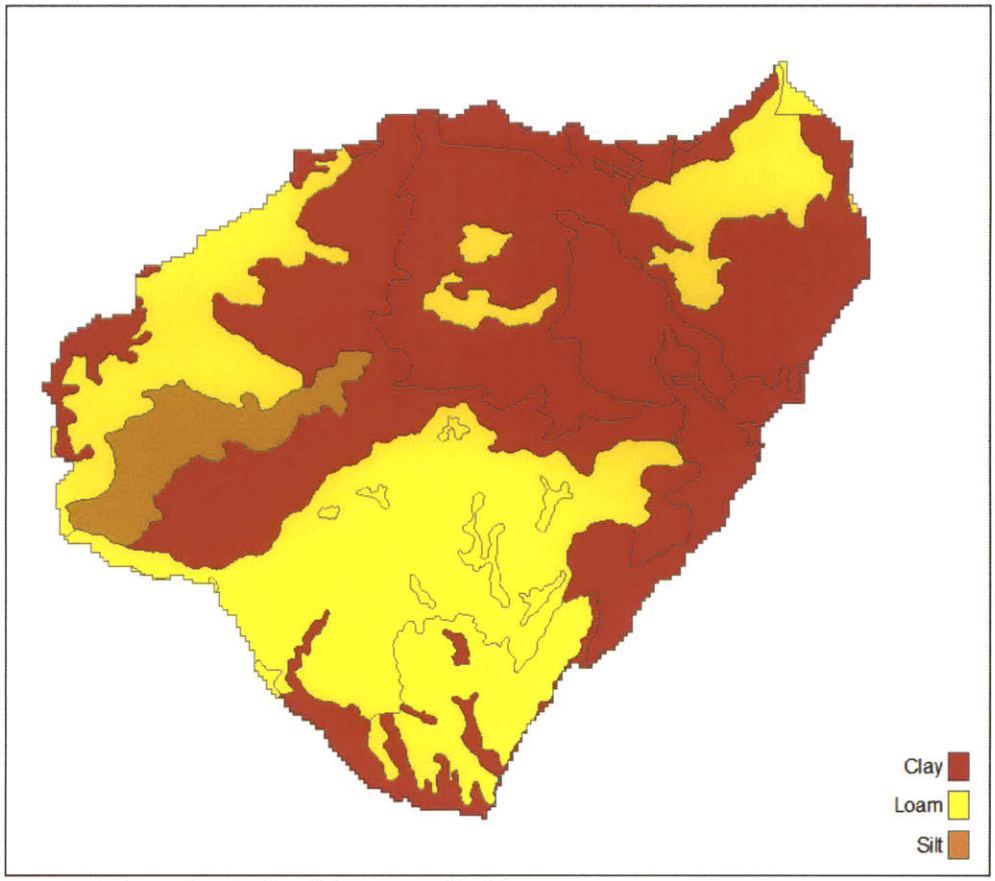

Figure 3.1.5: Final classification of soil types

Vegetation Data

Helmer et al. (2002) produce a digital map of forest type and land cover in Puerto Rico, mapping 26 distinct units. They employed Landsat Thematic Imagery from the time period 1991–1992 to develop a detailed and segmented classification approach for the entire island of Puerto Rico (Helmer et al. 2002). Helmer et al. (2002) estimated the classification accuracy of this map to be ~70–80%, and noted that the forest and land cover may have appreciably changed in some areas between when the data were collected (1992) and when the digital map was produced (2000-2002).

A manual reclassification of the 26 units into vegetation classes consistent with the Community Land Model (CLM) plant functional types used in tRIBS was performed by the author. The plant functional types for forests are differentiated on the basis of whether the forest has trees that are deciduous or evergreen, needle-leaf or broad-leaf, and if they are typically encountered in climates that are tropical, temperate, boreal or drought (Olseon et al. 2004).

This manual reclassification of vegetation and land cover types yields a basin overwhelmingly dominated by one vegetation class: BET Tropical. This is consistent with the U.S. National Atlas map of forest cover types (USDA and USGS, 2001) which also classifies the entire area of the Mameyes basin as BET Tropical. The final vegetation types employed for modeling are shown in Figure 3.1.6. Overall, 99.65% of the area consists of the BET Tropical Vegetation class while the remaining 0.35% of the area is C4 Grass (i.e. grass that follows a C4 (as opposed to a C3) photosynthetic pathway).

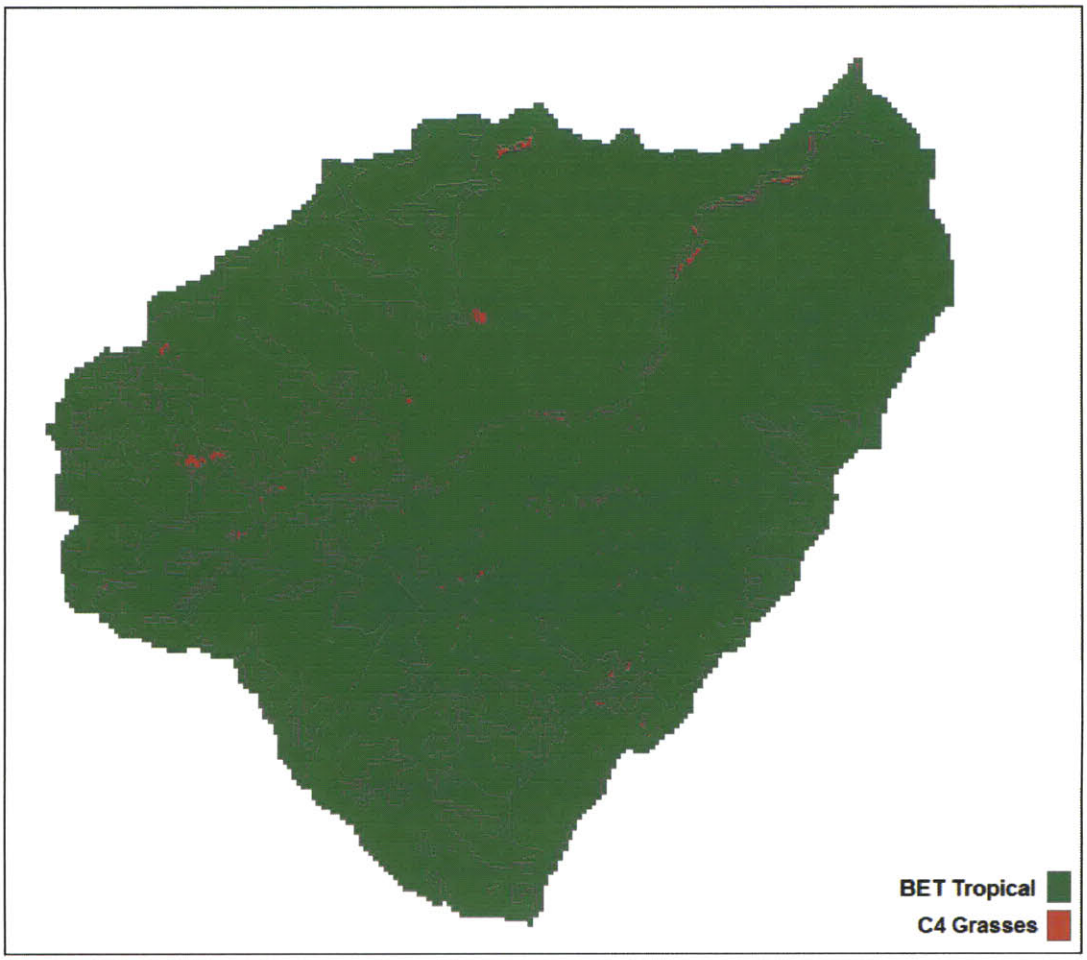

Figure 3.1.6: Final classification of vegetation types.

The BET Tropical vegetation class can be further subdivided into four different forest types (LTER Website). These forest types are the tabonuco (typically found at an elevation of < 600 m), colorado (600 – 750 m), dwarf (> 750 m) and palm (found on steeper slopes with poor drainage and saturated soils). A mapping of these forest types is available through the Luquillo Long-Term Ecological Research (LTER) website and is also documented in Brown et al. (1983). While differentiating between these forest types within the BET Tropical class is beyond the scope of the current work, more detailed modeling in the future could attempt to incorporate these differences in vegetation across different parts of the basin. A map showing the locations of these different forest types, obtained from the LTER website, is shown in Figure 3.1.7.

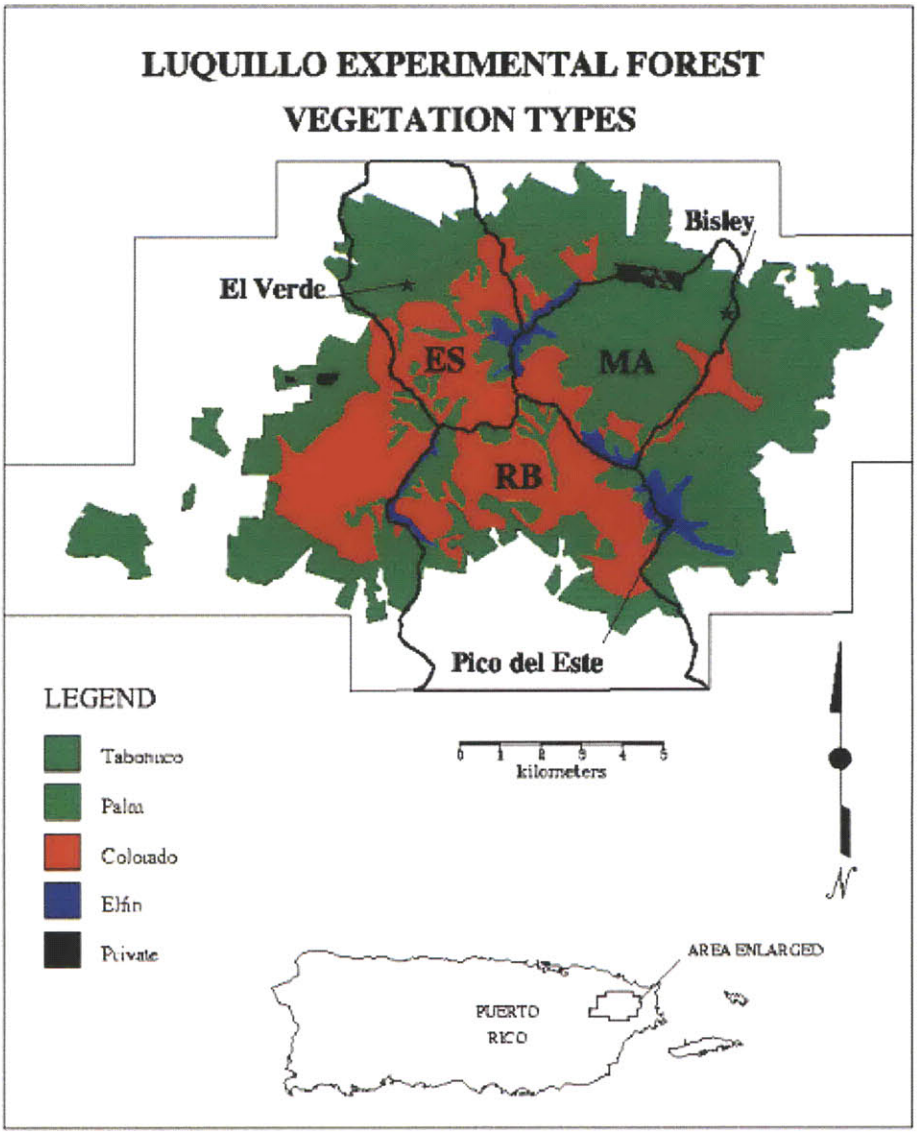

Figure 3.1.7: The four forest types for the Luquillo Experimental Forest, obtained from the LTER website. An outline of the Mameyes basin ("MA") and location of the Bisley tower is also shown.

3.2 Parameterization of Basin in tRIBS

Soil Parameters

The soil parameters required for tRIBS are listed in Table 3.2.1 and corresponding values are provided in Table 3.2.2. Values for the majority of these parameters were documented by Ivanov (2006), who employed the tRIBS model to study the effect of dynamic vegetation and topography on hydrological processes in semi-arid areas. Hydraulic properties for the current study were derived from Rawls et al. (1982) while heat transfer and albedo parameters were derived from Dickenson et al. (1993) and Bonan (1996). Previous applications involving the tRIBS model (Ivanov 2006) have estimated approximate values for the decay parameter (which governs the exponential decay of the saturated hydraulic conductivity for the soil with depth), the saturated anisotropy ratio and the unsaturated anisotropy ratio. These values are employed for the current work.

Table 3.2.1: Required soil parameters

#	Parameter Name	Variable
1	Saturated Hydraulic Conductivity	Ks
2	Soil Moisture at Saturation	thetaS
3	Residual Soil Moisture	thetaR
4	Pore distribution index	m
5	Air Entry Bubbling Pressure	PsiB
6	Decay Parameter	f
7	Saturated Anisotropy Ratio	As
8	Unsaturated Anistropy Ratio	Au
9	Porosity	n
10	Volumetric Heat Conductivity	ks
11	Soil Heat Capacity	Cs

Table 3.2.2: Values for required soil parameters

Variable	Description	Unit	Clay	Loam
Ks	Saturated Hydraulic Conductivity	mm/hr	1	15
thetaS	Soil Moisture at Saturation	-	0.385	0.434
thetaR	Residual Soil Moisture	-	0.09	0.027
m	Pore distribution index	-	0.15	0.22
PsiB	Air Entry Bubbling Pressure	mm	-370	-111
f	Decay Parameter	mm-1	0.0001	0.0001
As	Saturated Anisotropy Ratio	-	1,000	1
Au	Unsaturated Anistropy Ratio	-	1,000	1
ks,dry	Volumetric Heat Conductivity	J/msK	0.475	0.463
n	Porosity	-	0.189	0.196
ks,sat	Volumetric Heat Conductivity	J/msK	1,218,393	1,184,138
Cs	Soil Heat Capacity	J/ m3K	1.706	2.25

Vegetation Parameters

The main classes of vegetation identified in the Mameyes basin are Broadleaf Evergreen Trees in Tropical climates (BET Tropical) and C4 Grass. C4 grasses have been completely parameterized in previous work involving the tRIBS model (Ivanov 2006). BET Tropical forests have not been parameterized for prior basin development in tRIBS. A complete set of vegetation parameters for a particular vegetation class would include general vegetation parameters (14 in number), photosynthesis parameters (5), respiration and turnover parameters (11), allocation parameters (6), phenology parameters (5), survival parameters (2) and dynamic root parameters (4). A summary of these parameters is provided in Table 3.2.3.

Values for a majority of the vegetation parameters have been obtained or calculated from values for plant functional types (PFTs) available in documentation for the Community Land Model (CLM). The CLM is the land model for the Community Climate System Model (CCSM) and the Community Atmosphere Model (CAM), and is a collaborative project between the Terrestrial Sciences Section (TSS) and the Climate and Global Dynamics Division (CGD) at the National Center for Atmospheric Research (NCAR) and the CCSM Land Model Working Group (Oleson et al. 2008). Other principal working groups that also contribute to the CLM are Biogeochemistry, Paleoclimate, and Climate Change and Assessment (Oleson et al. 2008).

The vast majority of general vegetation parameters, photosynthesis parameters, respiration and turnover parameters, and allocation parameters are available in the CLM documentation (Oleson et al. 2004). Parameters for C4 Grasses are consistent with those employed previously for modeling by Ivanov (2006). Parameters for the BET Tropical Class are addressed later in this chapter.

Table 3.2.3: Vegetation parameters

Symbol in tRIBS	Description	Unit	C4	BET Tropical
General Vegetation Parameters (14)				
dleaf	Mean leaf size of mature plant	m	0.005	0.04
chiL	Leaf orientation. Ranges from -1 (vertical) to 1 (horizontal)	-	-0.3	0.1
alf_lf_vis	Leaf reflectance in visible range	-	0.11	0.1
alf_lf_nir	Leaf reflectance in near-infrared range	-	0.58	0.45
alf_st_vis	Stem reflectance in visible range	-	0.36	0.16
alt_st_nir	Stem reflectance in near-infrared range	-	0.58	0.39
tau_lf_vis	Leaf transmittance in visible range	-	0.07	0.05
tau_lf_nir	Leaf transmittance in near-infrared range	-	0.25	0.25
tau_st_vis	Stem transmittance in visible range	-	0.22	0.001
tau_st_nir	Stem transmittance in near-infrared range	-	0.38	0.001
KCanDrain	Canopy drainage coefficient	-	0.1	0.18
KCanExp	Canopy drainage exponent	-	3.2	3.9
SLA	Specific leaf area	m^2 leaf/gC	0.02	0.0155
-	Type of root distribution	-	Uniform	Exponential
Photosynthesis Parameters (5)				
Vmax25	Maximum non-stress catalytic capacity of Rubisco enzyme	µmol CO_2 m^2/s	35	40
Kmean	Canopy nitrogen decay rate to parameterize the Vmax25 decay	-	0.3	0.5
m	Stomatal slope factor	-	4	9
b	Minimum conductance	µmol CO_2 m^2/s	40,000	10,000
-	Quantum efficiency of CO_2 uptake	µmol CO_2/mole photons	0.053	0.08
Allocation Parameters (6)				
e0leaf	Allocation fraction to leaves for non-stressed vegetation	-	0.45	0.45
e0stem	Allocation fraction to stems for non-stressed vegetation	-	0	0.35
e0root	Allocation fraction to roots for non-stressed vegetation	-	0.55	0.30
wsens	Allocation sensitivity parameter	-	0.7	0.02
alloc_eps	Coefficient in the structural biomass-canopy relationship	-	1.25	36
alloc_kap	Exponent in the structural biomass-canopy relationship	-	1	1.6

Table 3.2.3: Vegetation parameters (Continued)

Respiration and Turnover Parameters (11)				
rkstem	Sapwood respiration rate (r*k/C:N ratio) at 10°C	gC/gC.s	2.5×10^{-8}	4.67×10^{-10}
rkroot	Fine root respiration rate (r*k/C:N ratio) at 10°C	gC/gC.s	2.5×10^{-8}	1.74×10^{-9}
al_grw	Fraction of (GPP-Rm) going to growth	-	0.25	0.25
Yleaf	Leaf life span	$Year^{-1}$	1	1
Ystem	Sapwood turnover rate	$Year^{-1}$	1	35
Yroot	Fine root turnover rate	$Year^{-1}$	1	4.5
DH20max	Maximum drought leaf turnover rate	day	30	200
Dtairmax	Maximum cold leaf turnover rate	day	6.67	6.67
bH20	Shape parameter for drought leaf loss	-	3	3
bTair	Shape parameter for cold leaf loss	-	2	3
Tcold	Temperature threshold for leaf loss due to cold	°C	3	5
Phenology Parameters (5)				
ClfInit	Fraction of plant structural biomass to initiate leaf-onset	-	0	0.075
LAIInit	Minimum LAI to initiate the leaf-onset	m^2/m^2	0.2	0.2
DaysFav	Min # of days with favorable conditions for leaf-onset	day	5	7
TminFav	Minimum daily soil temperature for conditions to be favorable	°C	5	15
ClfNorm	Fraction of maximum leaf biomass to transit to normal growth	-	0	0.4
Survival Parameters (2)				
PsiStress	Soil water potential at which stomatal closure begins	MPa	-0.6	-0.5
PsiWilt	Soil water potential at which plant wilting begins	MPa	-6.8	-4
Dynamic Root Parameters (4)				
rootUpdateOpt	Option regarding root profile update time (midnight or threshold)	-	Midnight	Midnight
rootUpdateThreshold	Percentage threshold to update root profile [0-100]	-	5	5
stressType	Option regarding the type of stress factor	-	Integrated	Integrated
rootTrack	Option for keeping the root biomass pool for next year	-	Yes	No

Vegetation Initialization Parameters

Vegetation initialization parameters help establish key vegetation parameters at the beginning of the modeling period. These include the vegetation fraction, carbon pool indicators for canopy, sapwood and root carbon, Leaf Area Index (LAI), Stem Area Index (SAI), vegetation height, root depth and a parameter for the decaying exponential function used to model the root depth.

The Leaf Area Index (LAI) is a ratio of the area of the total upper leaf surface of vegetation to the surface area of the land on which the vegetation grows. Similarly, the Stem Area Index (SAI) is a ratio of the area of one side of the stem to the vegetated land's surface area. The root depth is defined in the tRIBS code as the depth above which 95% of the mass of the root lies. The parameter for the decaying exponential function used to model the root depth is effectively a decay rate of distribution of the root biomass with the soil depth (Ivanov 2006).

Since a very large portion of the Mameyes basin is undisturbed forest, it is reasonable to assume that the vegetation currently present over most of the basin has existed for a very long time period. Therefore a reasonable approach to model the basin is to consider steady-state values for some of the initialization parameters. These steady-state values were simulated by running the tRIBS model with representative rainfall values for a time period of ten years, by which time the model predictions were observed to have converged to approximately steady values. Based on these steady-state values, initialization parameters as listed in Table 3.2.4 were selected for the C4 Grass and the BET Tropical vegetation types.

Table 3.2.4: Vegetation initialization parameters

Description	Unit	C4 Grass	BET Tropical
Vegetation Initialization Parameters (10)			
Vegetation Fraction	-	0	0.7
Phenology State	-	Dormant	Normal
Value of LAI	m^2/m^2	0	5
Value of SAI	m^2/m^2	0	2
Value of Canopy Carbon Pool	gC/m^2	0	300
Value of Sapwood Carbon Pool	gC/m^2	0	200
Value of Root Carbon Pool	gC/m^2	0	50
Value of Vegetation Height	m	0	20
Value of Rooting Depth	m	0.012	0.3
Value of Parameter for Decaying Exponential Function of Rooting Depth	-	9	2

Selection of Parameters for BET Tropical Class

Literature Sources

Parameters for the BET Tropical class were selected based on parameters employed in several models developed by the National Center for Atmospheric Research (NCAR). A summary of literature values and sources is provided in Table 3.2.5.

As mentioned previously, a vast majority of the general vegetation parameters as well as the key photosynthesis parameters are available in the Community Land Model (CLM) documentation (Oleson et al. 2004). The CLM, which is designed to integrate all land processes into a single model through coupling land, atmosphere, ocean and sea ice models (Oleson et al. 2004), contains parameters for each of the major Plant Functional Types (PFTs).

Bonan et al. (2002) address the representation of vegetation as PFTs in order to provide for a unified treatment of vegetation in climate and ecosystem models, specifically the NCAR Land Surface Model (LSM). Bonan et al. utilize a minimum temperature of 15.5°C to favor the growth of broadleaf evergreen trees. Wilson et al. (1987) provide an overview of vegetation parameters employed for modeling of a low-latitude, evergreen forest in the NCAR Biosphere-Atmosphere Transfer Scheme (BATS). Average values for LAI, SAI and vegetation fractions from Wilson et al. (1987) were used to establish the initialization vegetation parameters used in this work.

Other Sources

Additional parameters whose source is listed as "N/A" in Table 3.2.5 were either not explicitly available in the literature, not necessary for the model, or indicate modeling options with predetermined values. Some of the vegetation parameters, such as the initial carbon pools for stems, leaves and roots, are employed mainly for modeling purposes and are usually not explicitly measured or reported in the literature. The values of these parameters were determined by varying them until the vegetation response (e.g. LAI and vegetation fraction) of the model was appropriate. These modeling exercises were conducted on a single Voronoi cell representing a flat slope so that the response of vegetation to these parameters could be isolated. These so-called "element model runs" allowed for a determination of the parameter values prior to a basin-wide application.

Most of the photosynthesis parameters are empirical parameters assigned based on prior modeling experiences with the Broadleaf Deciduous Drought (BDD) vegetation class (Bisht et al., in preparation). The vegetation dynamics are not overly sensitive to these parameters, and values for these parameters were not available in the major sources listed above. The allocation fractions for leaves, stems and roots reach steady-state values based on how the other parameters are specified.

The phenology parameters, in part, govern the transition of the vegetation between different phenology states. In the tRIBS model for this basin, the phenology state was set

to always be in the "Normal" state. In tropical climates, BET trees are never expected to enter the leaf-fall state (Ariora 2005). The presence of vegetation in the basin throughout the year indicates that the Dormant phenology state, which is the alternative to Normal, is not really applicable. Furthermore, because the vegetation is not being grown from scratch in the model (i.e. the initialization parameters reflect steady state rather than early growth values), the "Maximum Growth" phenology state is also not pertinent. Since the phenology state is always Normal, the vegetation dynamics are not very sensitive to the phenology parameters that govern transitions between phenology states.

Due to the humid climate and high rainfall experienced over the Mameyes basin, soil moisture values across the basin are not expected to be so low as to impede the growth of plants. Survival parameters, such as soil water potentials representing when stomatal closure and plant wilting begin, are therefore not considered important since the plant is not expected to come under soil moisture stress. Element model runs confirmed that the model output was relatively insensitive to these variables. The selected values represent values employed in previous models for the Broadleaf Deciduous Drought vegetation class.

Out of the initialization parameters, the most crucial parameters are the values of the carbon pools. These determine the values of the other parameters, and were assigned based on the results of the element analysis.

Table 3.2.5: Sources of vegetation parameters for BET Tropical class

Description	Value used	Literature Value	Source #
General Vegetation Parameters (14)			
Mean leaf size of mature plant	0.04	0.04	2
Leaf orientation par-r Ranges from -1 (vertical) to 1 (horizontal)	0.1	0.01	2
Leaf reflectance in VIS range	0.1	0.1	2
Leaf reflectance in NIR range	0.45	0.45	2
Stem reflectance in VIS range	0.16	0.16	2
Stem reflectance in NIR range	0.39	0.39	2
Leaf transmittance in VIS range	0.05	0.05	2
Leaf transmittance in NIR range	0.25	0.25	2
Stem transmittance in VIS range	0.001	0.001	2
Stem transmittance in NIR range	0.001	0.001	2
Canopy drainage coefficient	0.18	0.18	2
Canopy drainage exponent	3.9	3.9	2
Specific leaf area	0.0155	0.0127	4
Type of root distribution	Exponential	Exponential	2
Allocation Parameters (6)			
Allocation fraction to leaves for non-stressed vegetation	0.45	-	N/A
Allocation fraction to stems for non-stressed vegetation	0.35	-	N/A
Allocation fraction to roots for non-stressed vegetation	0.30	-	N/A
Allocation sensitivity parameter	0.02	0.8	1

Table 3.2.5: Sources of vegetation parameters for BET Tropical class (Continued)

Description	Value used	Literature Value	Source #
Coefficient in the structural biomass-canopy relationship	31	31	1
Exponent in the structural biomass-canopy relationship	1.6	1.6	1
Respiration and Turnover Parameters (11)			
Sapwood respiration rate (r*k/C:N ratio) 10°C	$4.67x10^{-10}$	$4.67 x10^{-8}$	1
Fine root respiration rate (r*k/C:N ratio) 10°C	$1.74x10^{-9}$	$1.74x10^{-8}$	1
Fraction of (GPP-Rm) going to growth	0.25	-	N/A
Leaf life span	1	1.75	1
Sapwood turnover rate	35	35	1
Fine Root turnover rate	4.5	4.5	1
Maximum Drought leaf turnover rate	200	200	1
Maximum Cold leaf turnover rate	6.67	3.33	1
Shape parameter for Drought leaf loss	3	3	1
Shape parameter for Cold leaf loss	3	3	1
Temperature threshold for leaf loss due to Cold	5	5	1
Photosynthesis Parameters (5)			
Maximum non-stress catalytic capacity of Rubisco enzyme	40	75	2
Canopy nitrogen decay rate to parameterize the Vmax25 decay	0.5	-	N/A
Stomatal slope factor	9	-	N/A
Minimum conductance	10,000	-	N/A
Quantum efficiency of CO2 uptake	0.08	-	N/A
Phenology Parameters (5)			
Fraction of plant structural biomass to initiate leaf-onset	0.075	-	N/A
Minimum LAI to initiate the leaf-onset	0.2	-	N/A
Min # of days with favorable conditions for leaf-onset	7	-	N/A
Minimum daily soil temperature for conditions to be favorable	15	15.5	3
Fraction of maximum leaf biomass to transit to normal growth	0.4	-	N/A
Survival Parameters (2)			
Soil water potential at which stomatal closure begins	-0.01	-	N/A
Soil water potential at which plant wilting begins	-6.8	-	N/A
Dynamic Root Parameters (4)			
Option regarding root profile update time 0-Midnight 1-Threshold	0	-	N/A
Percentage threshold to update root profile [0-100]	5	-	N/A
Option regarding the type of stress factor: 0-Integrated	0	-	N/A
Option for keeping the root biomass pool for next year?	Yes	-	N/A
Sources:			
1. Arora et al. (2005), 2. Oleson et al. (2004)			
3. Bonan et al. (2002) 4. Weaver (1990)			

Table 3.2.6: Sources of vegetation initialization parameters for BET Tropical class

Description	Value Used	Lit. Value	Source #
Vegetation Initialization Parameters (10)			
Vegetation Fraction	0.7	0.4 to 0.9	5
Phenology State	Normal	-	N/A
Value of LAI	5	5 to 6	5
Value of SAI	2	~ 2	5
Value of Canopy Carbon Pool	300	-	N/A
Value of Sapwood Carbon Pool	200	-	N/A
Value of Root Carbon Pool	50	-	N/A
Value of Vegetation Height	20	20	5
Value of Rooting Depth	0.3	0.25 to 0.4	6
Value of Rooting Distribution Exponential	2	-	N/A
Sources:			
5. Wilson (1987)			
6. Simon et al. (1990)			

Element Model Set-up

Element model runs, as referred to above, were conducted in order to determine the sensitivity of the basin's response to the key vegetation parameters, as well as the desirable values for highly sensitive parameters. The key files pertinent to these runs are included in Appendix A. The element was defined as having a loam soil class, a BET Tropical vegetation class and was forced by meteorological data from the Bisley tower for 2005. For cases where it was desirable to observe steady-state trends in the vegetation response over several years, the 2005 meteorological data was looped as appropriate. As it was found that steady-state conditions could be observed during a 3-year run, the meteorological data used to force the runs reflected 2005 data repeated three times.

Element Analysis Results

(i) LAI Response

The appropriateness of the basin's response was gauged primarily by considering the Leaf Area Index (LAI) response and by ensuring that the initial carbon allocation fractions were generally consistent with their steady-state values. Values for LAI in the Luquillo Forest are available through NASA's Moderate Resolution Imaging Spectroradiometer (MODIS) website, shown in Figure 3.2.1.

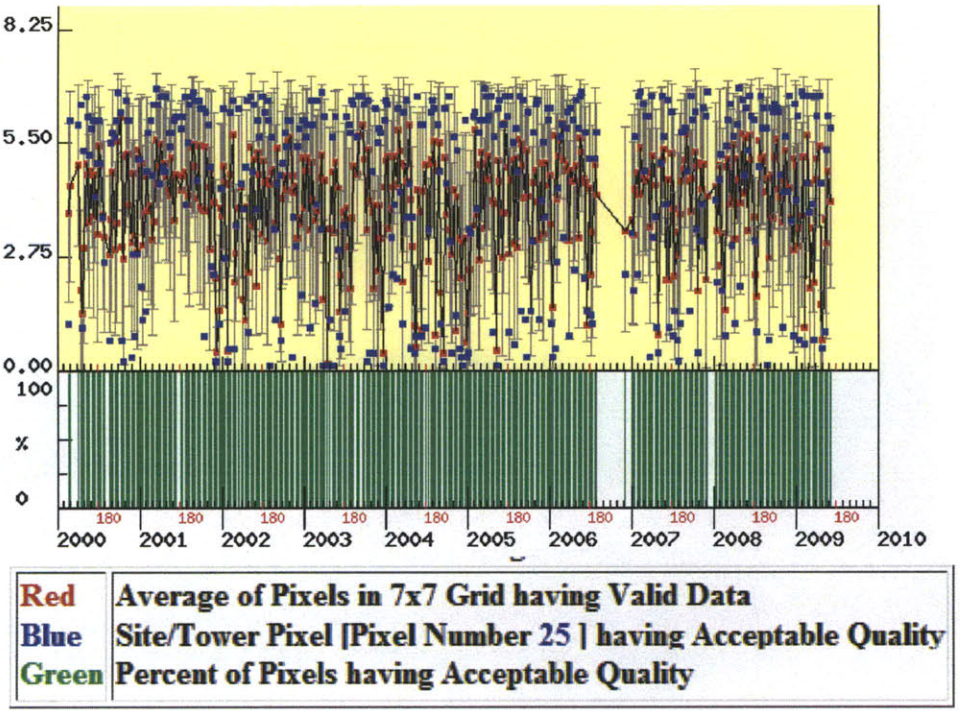

Figure 3.2.1: Range of LAI values for the LEF from MODIS, 2000 – 2009. Average values (shown in red) for 2002 range from approximately 1 to approximately 6.

Figure 3.2.1 shows LAI values for the entire LEF, which contains several forest types. It is important to note that the majority of the Mameyes basin is comprised of the tabonuco forest. LAI measurements by Odum (1970) indicated that the LAI for tabonuco forest is 6 to 7 (Odum 1970 as reproduced by Weaver 1990). For modeling purposes, Bonan et al. (2002) provide a minimum and maximum range for the BET Tropical PFT to be between 0.1 and 7. Similarly, Weaver (1990) summarizes values for the four different forest types (i.e. tabonuco, colorado, palm and dwarf) in the LEF with LAI values ranging from 3 to 7 depending on the forest type. Wilson et al. (1987) employ an LAI range of 5 to 6 for low-latitude, evergreen forest in their NCAR Biosphere-Atmosphere Transfer Scheme (BATS). In sum, an LAI value range of 5 to 7 appears to be a reasonable consensus value for BET Tropical vegetation.

The modeled LAI response, shown in Figure 3.2.2, was obtained by manually varying the initial carbon pools. After a few months during which the model ramps up, the LAI reaches a steady-state value of around 6 with some seasonal variation that relates to looping of the 2005 rainfall cycle observed at Bisley tower, shown in Figure 3.2.3. Troughs in the curve represent the winter season where rainfall is at its lowest. The LAI response is generally consistent with the literature cited above. Again, Figure 3.2.1 shows average values over the LEF, whereas the primary vegetation type in the Mameyes basin is the tabonuco forest which has been associated with a higher LAI value than other forest types in the LEF (Weaver 1990).

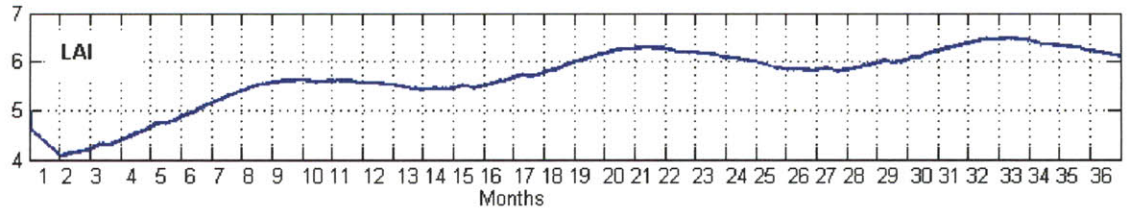

Figure 3.2.2: LAI response (hourly time step) of parameterized BET Tropical vegetation to 2005 meteorological data from Bisley tower.

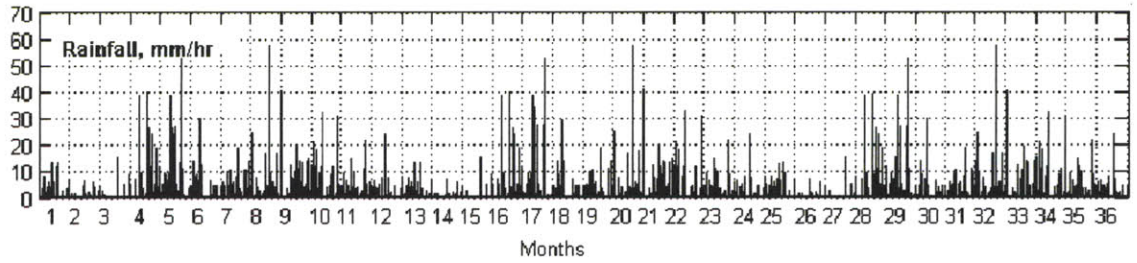

Figure 3.2.3: Rainfall data (hourly time step) used to force the element model run is looped for three years.

(ii) Vegetation Fraction Response

The response of the element model run was also assessed based on the resulting vegetation fraction in the element, shown in Figure 3.2.4. The selected parameters yielded a vegetation fraction very close to 1 (i.e. fully vegetated) for most of the year, with a small but noticeable variation for dry and wet seasons. This is consistent with expectations for a tropical evergreen forest.

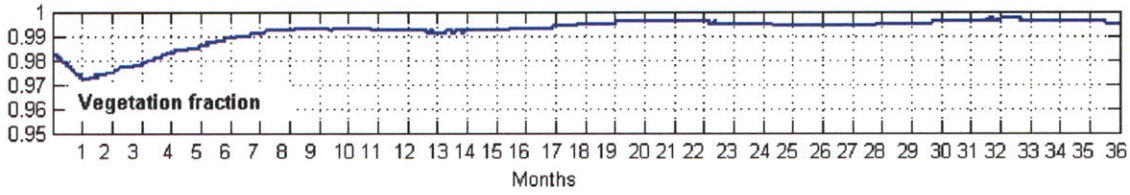

Figure 3.2.4: Vegetation fractions remain close to 1 for most of the year.

(iii) Carbon pools and Specific Leaf Area (SLA)

Element model runs indicate that the carbon pool values effectively determine all the other initialization parameters. Initial carbon pool values were selected such that the other initialization parameters as well as the LAI response were consistent with expectations based on the literature sources cited above. Values for these carbon pools are not typically documented as they are largely empirical values employed for modeling purposes (Ivanov 2006).

From the remaining parameters, the vegetation response was also sensitive to the Specific Leaf Area (SLA) and the allocation parameters governing the structural biomass-canopy

relationship. Specific Leaf Area represents the ratio of leaf area (m^2) to leaf dry mass in terms of carbon. A SLA of 0.0155 m^2 leaf/gC is used for the BET Tropical class. Weaver (1990) documents a value of 0.0127 m^2 leaf/gC for the tabonuco forest. While the SLA value employed in this work is a little higher than the literature value, an SLA of 0.0155 m^2 leaf/gC was the best value in order to obtain the desired LAI response.

(iv) Allocation Fractions

As mentioned previously, the fractions of carbon allocated to leaves, stems and roots were fixed at constant values that reflect the steady-state values observed during the element model runs. The steady-state allocation fractions were approximately 0.20 (root), 0.35 (stem) and 0.45 (leaf).

3.3: Results from Basin-wide Simulations

This section describes the results from the tRIBS simulation conducted on the Mameyes basin. This simulation was performed to test the model's performance in humid climates with special emphasis on the soil moisture and vegetation parameters that are to be employed in the off-line landslide component that is based on the Factor of Safety (FS) equation discussed in Chapter 4. Firstly, the development of the meteorological data used to force the simulation is outlined. Next, key assumptions and steps in the model initialization are summarized. Finally, results from the model simulation are presented and discussed.

Development of Meteorological Data and Simulation of Rainfall Event

As discussed in Section 3.2, hourly meteorological data for the Bisley Tower are available for the entire 2005 calendar year from the Luquillo LTER website. The total annual rainfall for the 2005 calendar year was 3717 mm. The temporal distribution of the rainfall is shown in Figure 3.3.1.

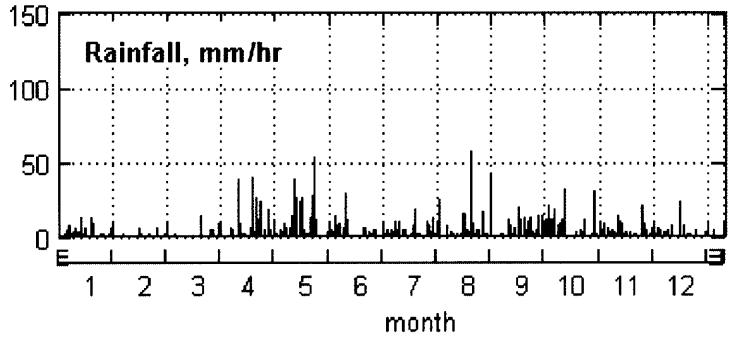

Figure 3.3.1: Hourly rainfall during 2005 calendar year at the Bisley tower

The year 2005 was relatively stable in that a major rainfall event on a magnitude typically associated with a landslide did not occur. The determination of what constitutes a landslide-triggering rainfall event is addressed by Larsen et al., who developed (1993) and updated (2005) a duration-intensity threshold for Puerto Rico based on a global duration-intensity threshold developed by Caine (1980). Figure 3.3.2, adapted from Larsen et al. (2005), presents three landslide thresholds, which are represented by the straight lines. Rainfall events with an intensity (defined as the average rainfall per hour during the storm) and duration that correspond to a point above each of these lines represent events that could likely result in a landslide. The plot shows three thresholds: the original threshold developed by Caine (1980) and two thresholds by Larsen et al. The threshold in Larsen et al. (1993) is based on landslides from 1959 to 1993 while the threshold in Larsen et al. (2005) is based on landslides from 1959 to 2003. White dots represent landslides in Larsen et al. (1993) while black dots represent landslides in Larsen et al. (2005).

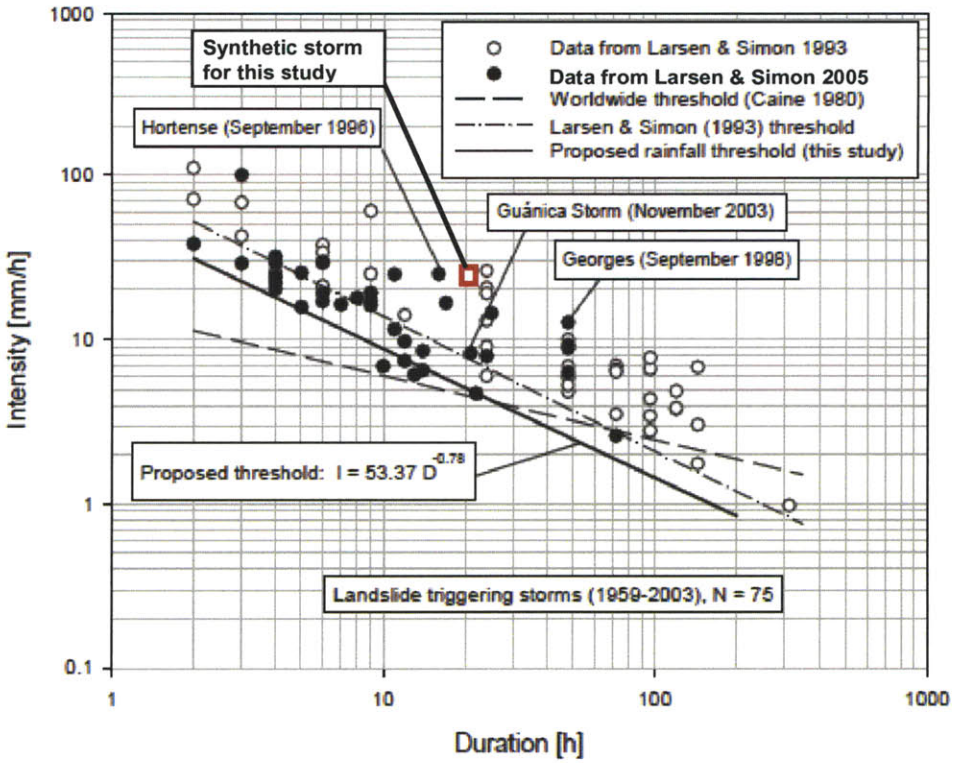

Figure 3.3.2: Rainfall threshold for landslides proposed by Larsen et al. (2005). Synthetic rainfall event is shown by red square and historic landslide-triggering storms are shown by circles. .

Because the actual available rainfall record lacks a storm sufficient to trigger landslides, it was necessary to add to the record a synthetic storm that would be sufficient to test the landslide algorithm. A rainfall event was synthesized in the context of Figure 3.3.2 such that the intensity and duration of the event lay above all three thresholds. A dataset for two calendar years was synthesized by repeating the 2005 meteorological data for a second year (i.e. 17520 hourly time steps) and increasing the rainfall intensity for a rainfall event in May 2005. A new rainfall event was thus simulated such that it had an intensity of 24.6 mm/h and duration of 21 hours for a total of 516.6 mm of rainfall over the length of the storm. The rainfall data with the simulated storm in the second year is shown in Figure 3.3.3.

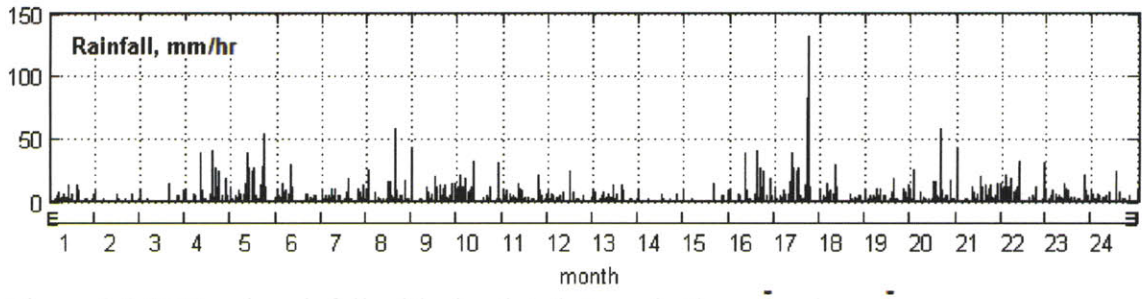

Figure 3.3.3: Hourly rainfall with simulated storm in the second year

As shown in Figure 3.3.2, the duration-intensity point associated with this storm is located above all three threshold lines. It represents a rare but plausible rainfall event for Puerto Rico. Indeed, it represents 14% of the total 2005 rainfall (3717 mm) in a period of less than a day. Using a rainfall event of this magnitude is desirable for testing the off-line landslide component, which can be expected to indicate some unstable slopes after a rainfall event of this magnitude.

Assumptions and Model Initialization

The Mameyes basin was divided into 13169 Voronoi cells with slope angle values in each cell ranging from 0^{o} to 61^{o}. It was assumed that rainfall was uniform over the entire basin. An open-drain boundary condition was imposed on the bottom of the last layer (i.e. at 2m). For simplicity, the small area classified as silt in Figure 3.1.5 was parameterized as a loam in the model run. Since silt and loam soil types are similar, the inclusion of two major soil types (i.e. clay and loam) is sufficient to observe basin responses to different soil types. The initial root depth was set to 0.3 m for BET Tropical vegetation and to 1.2 cm for C4 Grasses. Soil cohesion values of 7.79 kPa and 5.37 kPa for clay and loam, respectively, were assigned.

Initial simulations prompted two modifications to the tRIBS code. As mentioned in Section 3.2, the vegetation phenology state was hard coded to always be in the "normal" state, consistent with the literature on tropical vegetation. The second modification was to assign lower (0) and upper (1) limits on the fraction of canopy that was wet. This is an intermediate term employed in the evapotranspiration module of tRIBS and has implications for the model's stability. Specifically, without these pre-set limits, negative values for the fraction of canopy that is wet can be calculated and result in instability in the latent heat flux calculated by tRIBS. This negative value for the fraction of canopy results because evaporation occurs on an hourly time step, and if the water on the leaf surface reaches 0 before the end of the time step, evaporation in the model continues leaving a negative value for water on the leaf surface (and hence a negative value for the corresponding fraction of canopy that is wet). Consider a simple example: evaporation is occurring on an hourly time step, say at a rate of 1 mm/hr. If there are 0.5 mm of water on the leaf surface at the start of the hour, then the leaf would be dry in 30 minutes and then stay at 0 mm. However, due to the hourly time step for evaporation, the model removes 1 mm from the 0.5 mm resulting in a reservoir of -0.5 mm of water on the leaf's surface. In other words, for a fraction of an hour the model continues to remove moisture from the canopy even though it has already evaporated. Thus, this numerical issue was addressed by ensuring that the fraction of canopy that is wet does not take on a negative value.

Simulation Results

Basin-wide soil moisture response

The soil moisture response of the tRIBS model was validated over the entire basin as well as at specific locations. The soil moisture states immediately preceding and following the

simulated rainfall event are of particular interest from a landslide perspective. Figure 3.3.4 shows the soil moisture state one hour preceding the 21-hour simulated rainfall event. The five plots represent the soil moistures at a depth of 0cm, 13cm, 50cm, 140cm and 160cm from the top, respectively.

One immediate observation is that the two major soil types in the region (see Figure 3.1.5) can be clearly demarcated based on the soil moisture state, which makes sense since the soil types have very different characteristics. The soil moisture values for loam (light green in the first plot) generally increase slightly with increasing depth over the basin, while the soil moisture values for clay (yellow and red in the first plot) generally decrease with increasing depth over the basin (soil types are mapped in Figure 3.1.4). This makes intuitive sense since clay has a much lower hydraulic conductivity (1 mm/hr) than loam (15 mm/hr). In loam, the pulse from the last rainfall (13 mm, 18 hours prior) has quickly dissipated over the depth of the soil column, with the main pulse close to the bottom of the column. In clay, moisture from this pulse is retained closer to the surface, while at depth the soil is very dry. Since there was a long period (more than 3 days) with little or no rainfall preceding the 13mm pulse, these lower moisture values at the higher depths in the clay make sense.

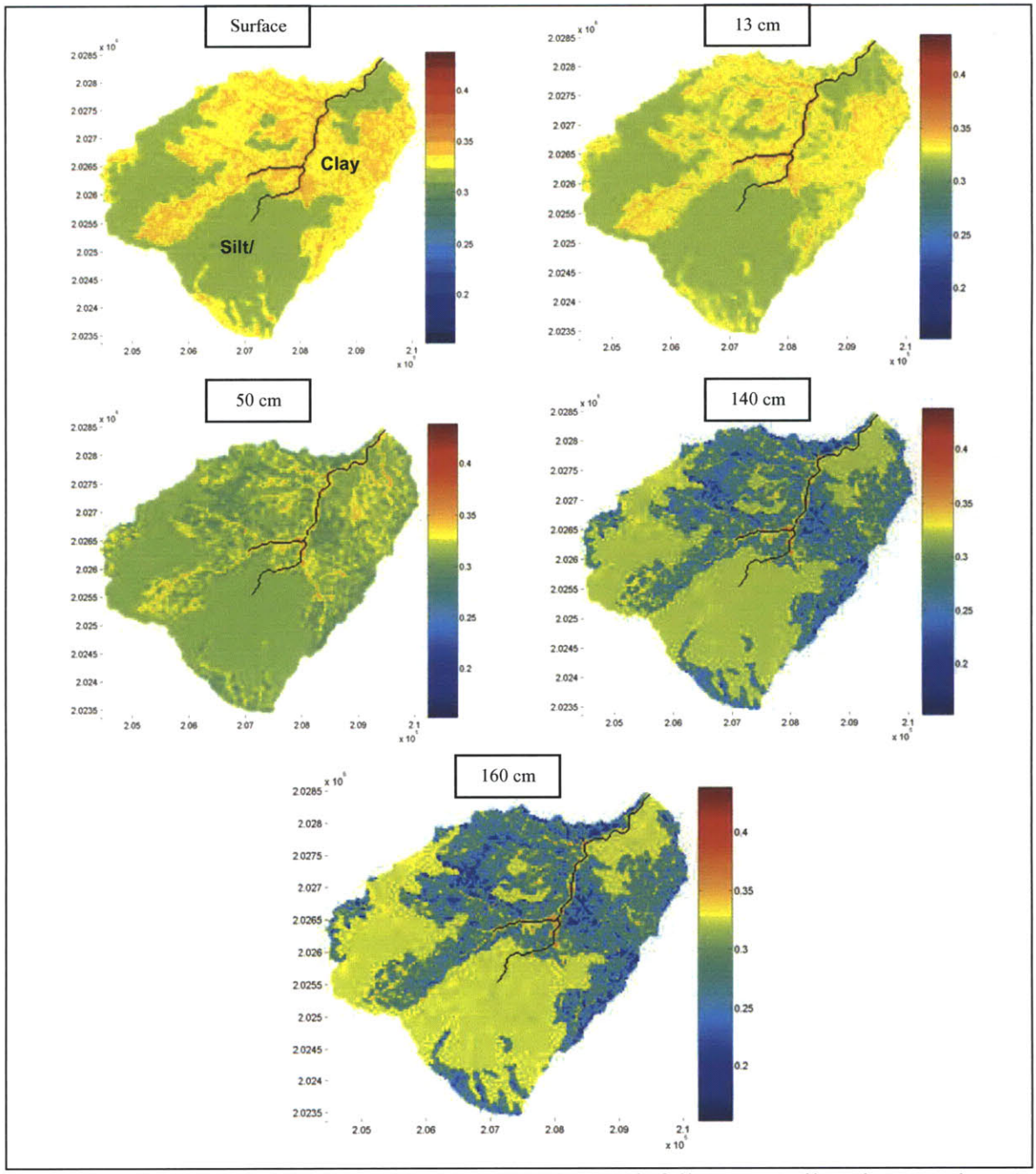

Figure 3.3.4: Soil moisture one hour prior to 21-hour rainfall event. Soil moisture values range from a minimum of ~ 0.15 (blue) to a maximum of ~ 0.434 (red).

Soil moisture states at the end of the 21-hour simulated rainfall event are shown in Figure 3.3.5. The first and second plots show that both the clay and the loam are fully saturated at the surface and at 13 cm, while the loam is also saturated even at 50 cm. The range of soil moisture values for the loam is much narrower than the range of moisture values for the clay. Intuitively, one would expect higher rainfall infiltration into the loam due to its higher hydraulic conductivity and its higher saturation soil moisture content (0.434 vs. 0.385 for clay). Due to this higher infiltration, it takes longer for the loam to fully saturate

at the surface, and longer for pooling to occur on the surface. On the other hand, the clay's lower hydraulic conductivity, lower saturation soil moisture and higher matric potential mean that runoff occurs sooner on the clay, causing it to be drier at lower depths than the loam.

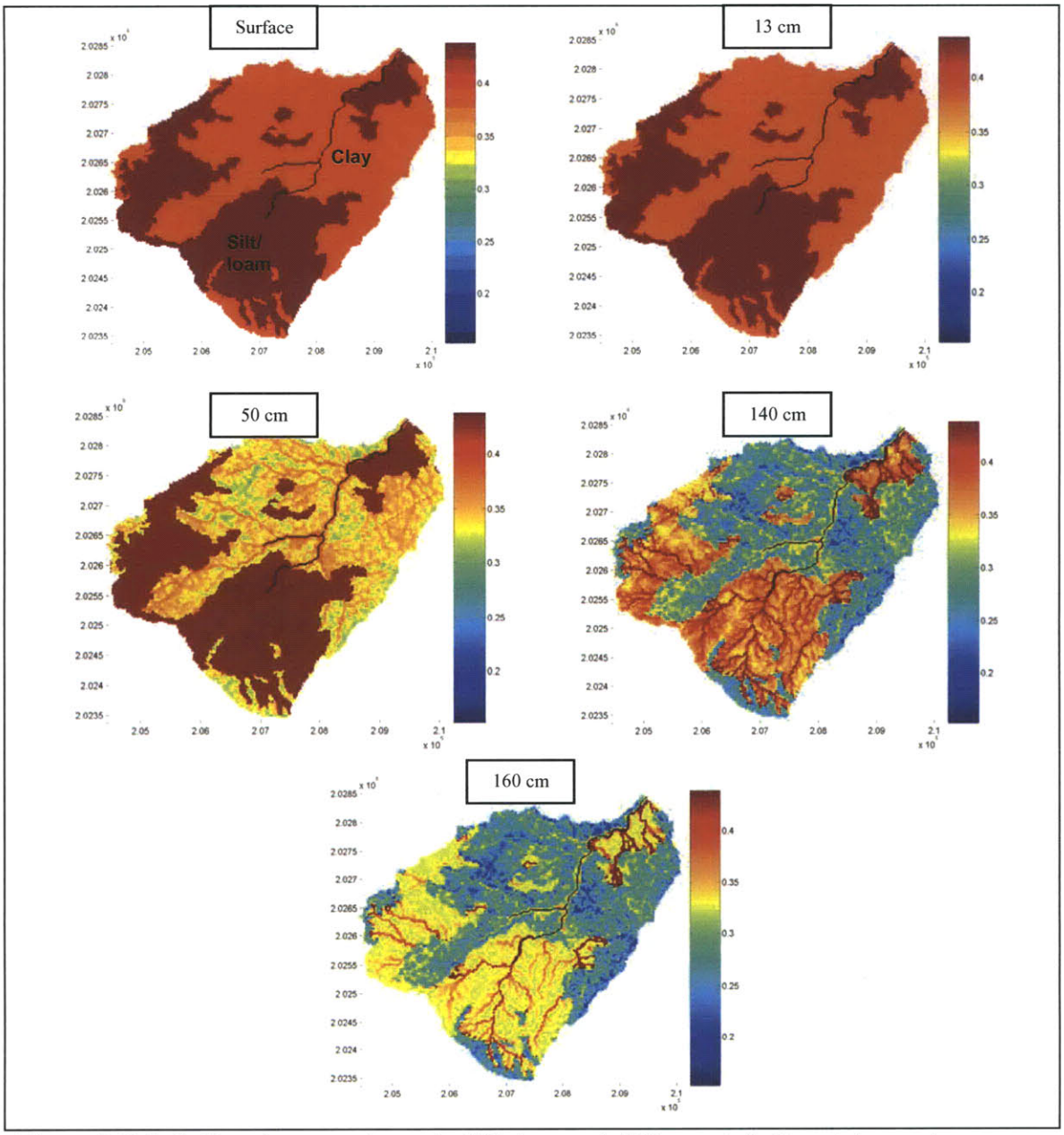

Figure 3.3.5: Soil moisture at the end of 21-hour rainfall event. Soil moisture values range from a minimum of ~ 0.15 (blue) to a maximum of ~ 0.434 (red).

The fact that the clay remains much drier at depth despite having a lower saturation moisture content demonstrates that lower intensity but longer duration storms are more likely to saturate the clay soil over a greater depth than higher intensity events with shorter durations. Thus, the susceptibility of these soils to landslides depends not only on

the duration and average intensity but also on the temporal distribution of the rainfall. This observation has also been noted in prior literature on landslides in Puerto Rico (e.g. Simon et al. 1990).

Figures 3.3.4 and 3.3.5 provided snapshots of the soil moisture for all of the Voronoi cells in the Mameyes basin before and after the 21-hour rainfall event. In addition to these, time series plots of soil moisture are prepared for specific Voronoi cells scattered across the basin. A selection of these plots is reproduced here. The locations of these selected Voronoi cells are shown in Figure 3.3.6, and key properties of each Voronoi cell are shown in Table 3.3.1.

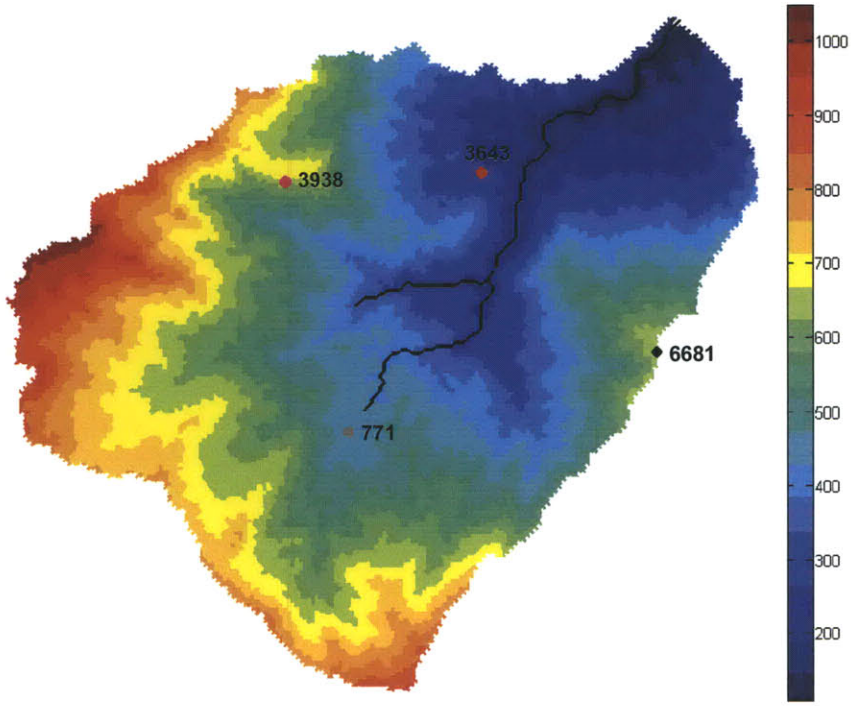

Figure 3.3.6: Location of selected Voronoi cells shown on DEM of Mameyes basin.

Table 3.3.1: Properties for selected Voronoi cells. For corresponding soil moisture plots see Figure 3.3.7.

Color	Cell #	Soil	Slope Angle (°)	Elevation (m)	Vegetation	Cell size (m^2)
Red	3643	Clay	25	296	BET Tropical	1763
Pink	3938	Clay	14	647	BET Tropical	591
Black	6681	Loam	43	648	BET Tropical	2700
Gray	771	Loam	11	451	BET Tropical	1575

Figure 3.3.7 shows the response of the soil moisture for the four selected locations for the length of the rainfall event (t = 12,180 h to 12,200 h) and for an equal duration after the storm (t = 12,200 h to t=12,220 h). The top two plots are for locations with clay (Voronoi cells #3643 and #3938) and the bottom two are for locations with loam (Voronoi cells #6681 and #771).

These plots again emphasize the different soil moisture distributions that result in different soil types. Both soil types become saturated at their surface after the first major burst of rainfall at 12,183 h, and the surface of the clays remains saturated much longer than the surface of the loams due to their lower saturated hydraulic conductivity and higher matric potential. In clay, water from the rainfall event stays near the surface and then slowly dissipates after the conclusion of the rainfall event. In loam, the water drains through much faster, resulting in saturation at greater depths than in the clay. The fact that loams appear to become saturated to greater depth in response to the simulated 21-hour rainfall event indicates that they are likely more susceptible to landslides at greater depth as well.

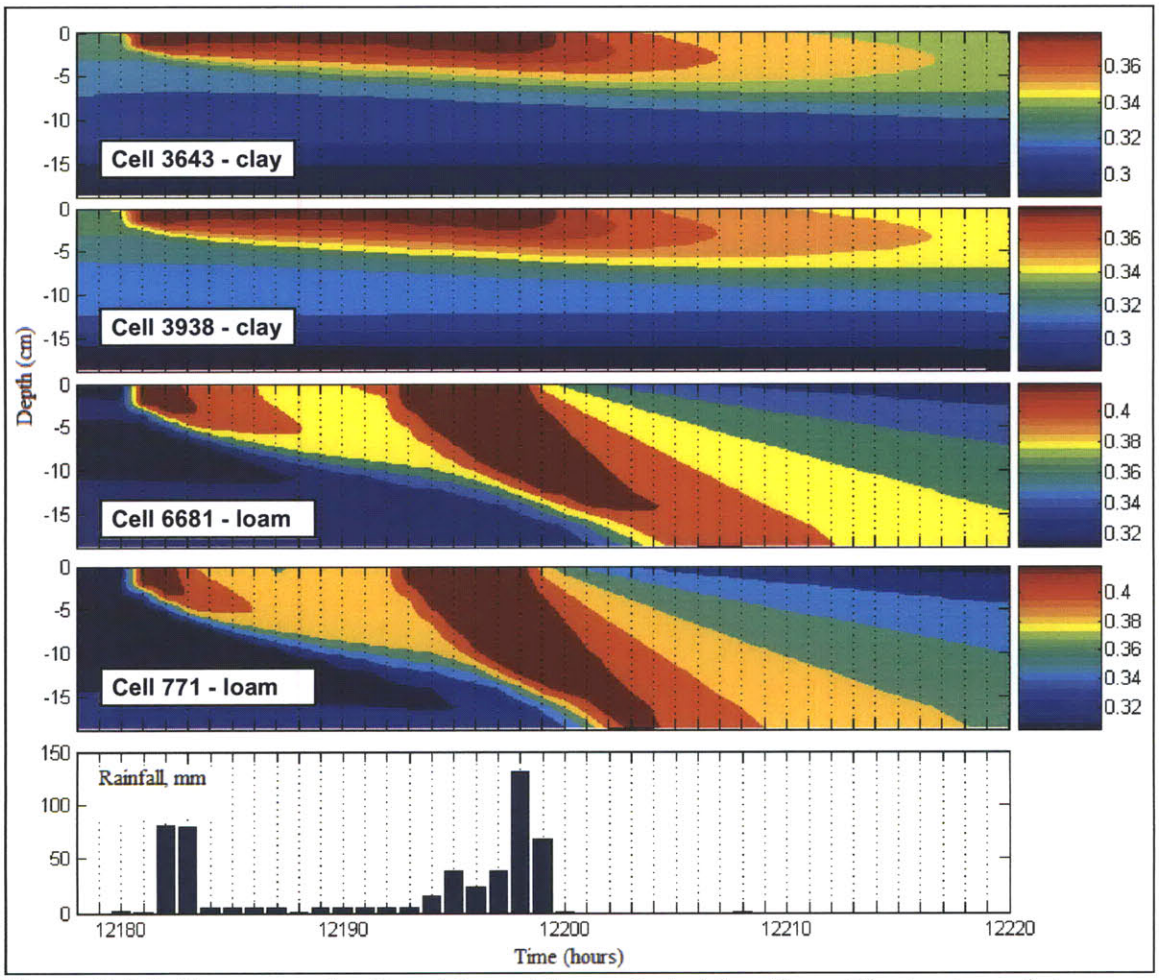

Figure 3.3.7: Response of soil moisture at four selected locations. The top two plots are for locations in clay (Voronoi cells #3643 and #3938), the next two for loam (Voronoi cells #6681 and 771), and the bottom for rainfall during and after the 21-hour rainfall event.

Model response for Bisley Tower

In addition to the basin-wide soil moisture response, the response of other parameters was considered at the locations identified in Figure 3.3.6. The air temperature, surface temperature, soil and root moisture and LAI for Voronoi cell 3643 located near Bisley Tower are shown in Figure 3.3.8. This Voronoi cell was assigned BET Tropical vegetation and a clay soil.

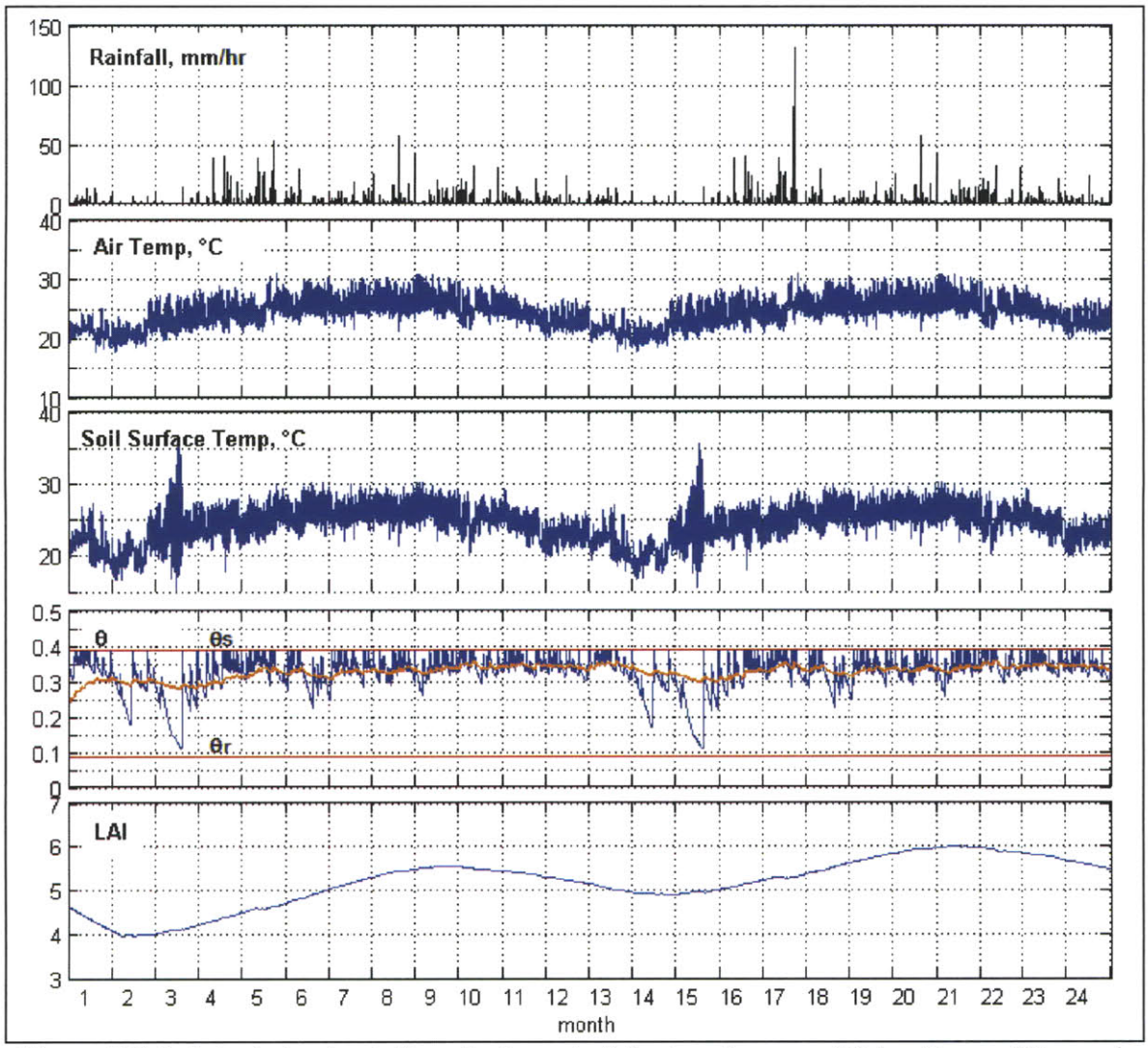

Figure 3.3.8: Selected outputs (hourly time step) for location near Bisley Tower (Voronoi cell #3643). The soil moisture plot shows soil moisture at the surface (blue line), moisture of the root zone (fluctuating red line) and residual and saturation soil moisture limits (straight red lines).

The soil surface temperature, which is calculated by the tRIBS model based on the air temperature and other inputs, has reasonable values with a trend similar to the air temperature. The soil moisture at the surface (blue line) and the moisture of the root zone

(red line) are consistent with the rainfall patterns observed, with the soil being close to (but not reaching) residual soil moisture (lower red line) during the very dry month of March. The surface layer reaches saturation soil moisture (upper red line) at several points during the year in response to rainfall events. The LAI value begins to stabilize after the first year and oscillates within a range of 5 to 6 thereafter. As expected, a seasonal variation in the LAI is observed. The LAI response is generally consistent with the literature values documented in Section 3.1.

Ground heat flux, latent heat flux and sensible heat flux

Ground heat flux, latent heat flux and sensible heat flux values helped identify instabilities in the model during initial simulations. Specifically, during initial simulations, the value for latent heat exhibited extreme values at individual time steps that were clearly numerical instabilities. Such instabilities were not observed in prior model simulations focusing on the semi-arid Walnut Gulch basin in Arizona (Bisht et al., under preparation). These instabilities occurred only in the presence of vegetation and in response to significant rainfall events, which indicated that changes needed to be made in the tRIBS code with regard to how the vegetation dynamics evolved in response to rainfall. Presumably, these instabilities were not observed in the Walnut Gulch semi-arid basin due to the substantially lower rainfall observed there. An investigation into the tRIBS code calculations resulted in the two code changes described previously in this section, i.e. the vegetation phenology state was fixed to always be in the "normal" state, and lower (0) and upper (1) limits were applied to the fraction of canopy that was wet. The implementation of these code changes prevented these instabilities in the latent heat flux. As discussed in the "Model Assumptions and Initialization" portion of this section, the limits on the wet canopy fraction was necessary due to the hourly time step for evaporation in the tRIBS model that resulted in the model continuing to remove moisture from the canopy for a fraction of an hour even though it had already evaporated.

Thus, heat flux values were employed mainly to flag potential instabilities. While a detailed validation of the basin response in terms of the heat flux values is beyond the scope of the current work, it is necessary to ensure that the general response and orders of magnitude of these flux values are reasonable in comparison to measured values. The hourly heat flux values for the entire time two year period are shown in Figure 3.3.9.

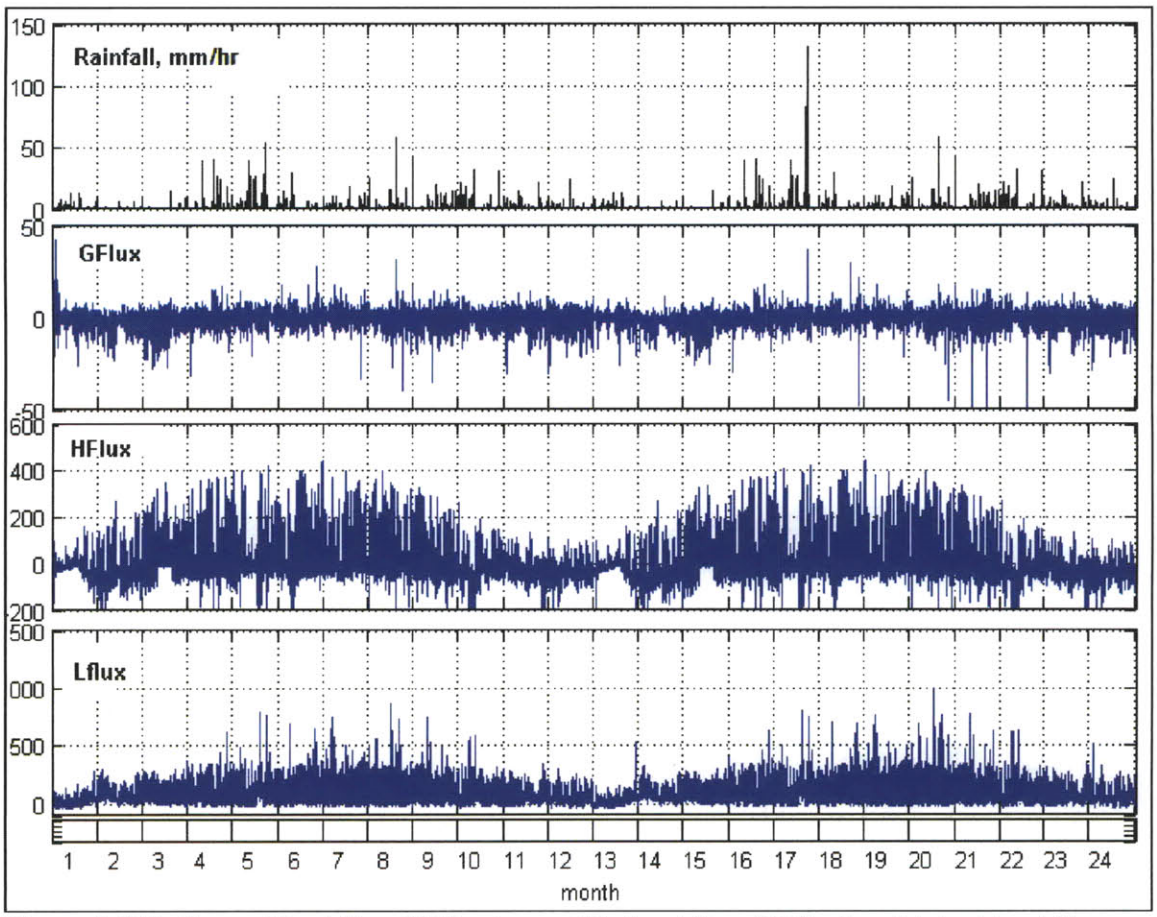

Figure 3.3.9: Ground heat flux (GFlux), sensible heat flux (HFlux) and latent heat flux (LFlux) values [W/m^2] (hourly time step) for location near Bisley tower (Voronoi cell #3643).

While there is limited data on measured flux values in the Mameyes basin, Van der Molin (2002) documents some values for latent heat, sensible heat and net radiation for the months of August 1997 and February 1998 under clear and cloudy conditions for the different forest types in Puerto Rico, including the tabonuco forest (the main forest type near the Bisley tower). Unfortunately, a time series of rainfall or key meteorological data for August 1997 and February 1998 was not available, making a comparison with the 2005 data difficult. Nevertheless, the measured values for August 1997 and February 1998 provide a basis for a preliminary and rough comparison with the simulated results from 2005.

Figure 3.3.10 shows measured monthly average radiation fluxes during August 1997 (Van der Molin 2002) and simulated values for August 2005 as a function of the hour of the day. Averages for clear and overcast days were computed separately. The relative magnitudes of the sensible heat flux, latent heat flux and net radiation, as well as their diurnal trends, are similar in both sets of plots. In addition, overall fluxes are appreciably higher for the clear conditions than the overcast/cloudy conditions in both plots. While the values for measured and simulated overcast conditions match quite well, the measured values for clear conditions are substantially higher than the simulated values.

This is likely due to the value for sensible heat which takes on negative values in the early and late portions of the diurnal cycle in the simulated results but not in the measured fluxes.

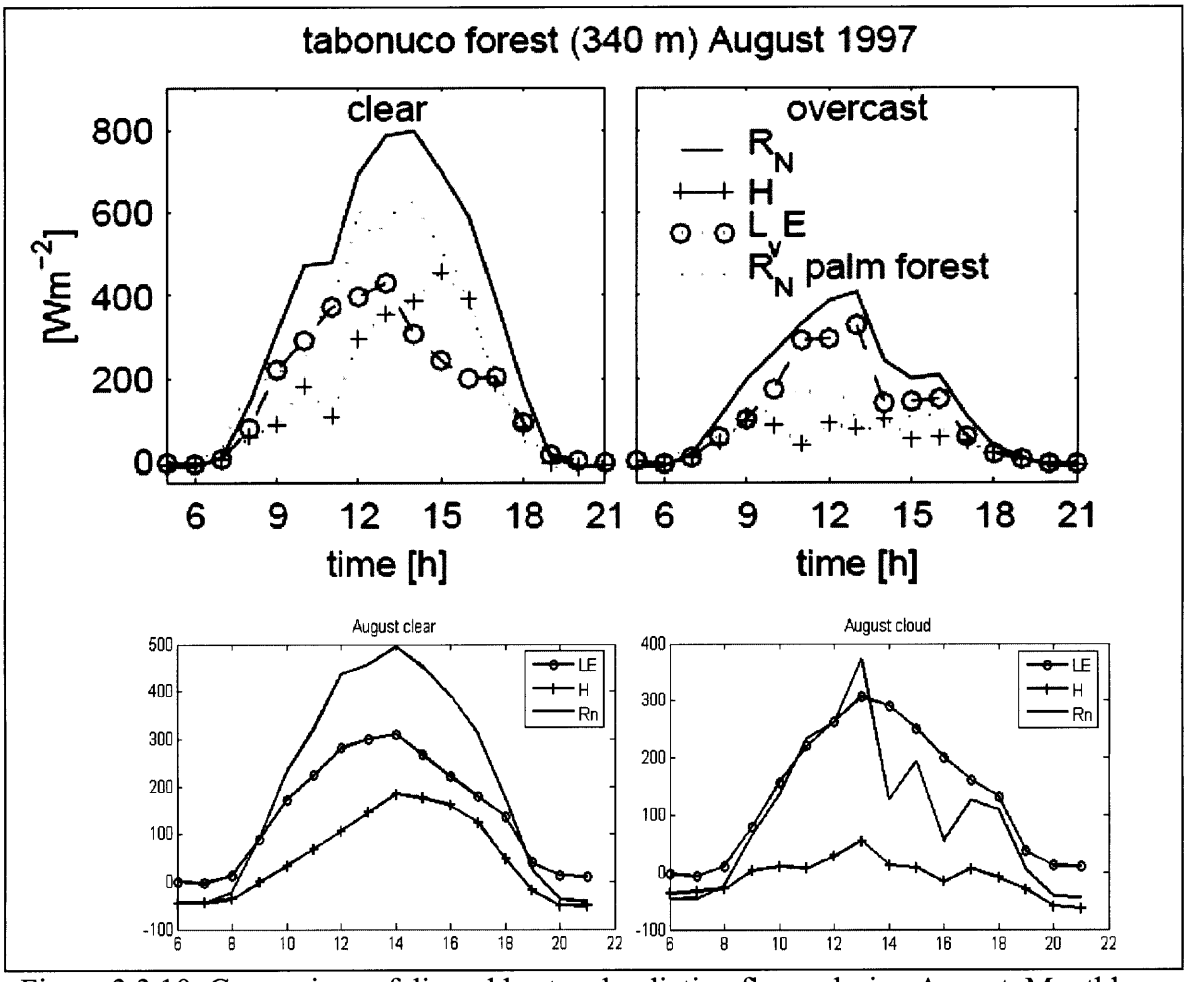

Figure 3.3.10: Comparison of diurnal heat and radiation fluxes during August. Monthly average diurnal fluxes [W/m^2] for latent heat (LE), sensible heat (H) and net radiation (Rn) are shown. The top two figures, reprinted from Van der Molin (2002), show fluxes in August 1997, while the bottom two figures show average modeled fluxes from tRIBS for August 2005.

Similarly, Figure 3.3.11 shows measured monthly average fluxes from February 1998 (Van der Molin 2002) and simulated values for February 2005. The values for overcast conditions for both sets of plots are lower than the values for clear conditions. Like the plots for August, the magnitudes of the measured net radiation and latent heat fluxes for February 1998 are substantially higher than the simulated values for February 2005. In addition, modeled net radiation values for February 2005 are lower than modeled latent heat values, while the opposite is true for measured values in February 1998. This is likely due to the negative values for sensible heat in the simulations, which in turn results from appreciable differences between the air and surface temperature during the month of February. While negative values for sensible heat are possible in nature, these modeled

values are not consistent with the measured values observed for the tabonuco forest in February 1998 (Van der Molin 2002).

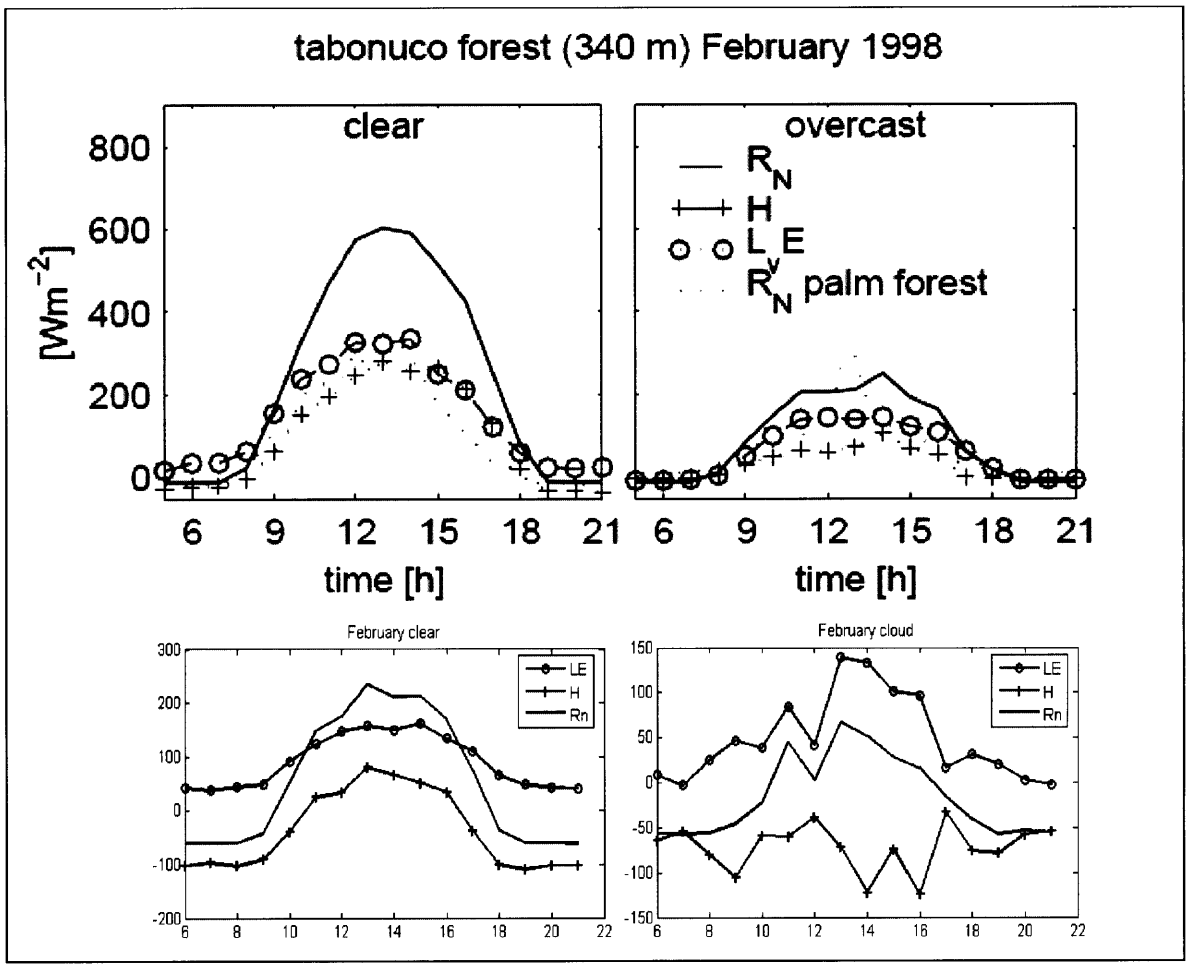

Figure 3.3.11: Comparison of diurnal flux and radiation values for February. Average diurnal values [W/m^2] for latent heat (LE), sensible heat (H) and net radiation (Rn) are shown. The top two figures, reprinted from Van der Molin (2002), show values in February 1998, while the bottom two figures show modeled values from tRIBS for February 2005.

The absence of rainfall and meteorological data with which to simulate August 1997 and February 1998 makes a firm conclusion about the performance of the model difficult. However, the absence of large peaks suggesting numerical instabilities in Figure 3.3.9 is indicative of model stability. In addition, the favorable comparison for predicted LAI values and soil moisture response indicate that simulation results are adequate for use in the off-line landslide component, where the primary dynamic inputs are for soil moisture and vegetation parameters as described in Section 4.2.

Further validation of the basin model in the tRIBS framework, particularly with regard to the sensible heat values given by the model for February, is recommended for future work and is addressed in Section 5.2.

CHAPTER 4: DEVELOPMENT OF OFF-LINE LANDSLIDE COMPONENT

4.1: Development of Landslide Component based on the Factor of Safety (FS) Equation

This section describes the off-line landslide component which is based on the FS equation. An overview of the FS equation is presented, followed by a summary of previous FS work done in the Luquillo Experimental Forest by Simon et al. (1990), whose work provides a basis for several of the static inputs into the FS equation. Next, the impact of vegetation on slope stability is discussed, which provides a context for the term-by-term development of the FS equation.

FS Formulation of Landslide Risk

In order to determine the potential for a landslide, a slope stability analysis is often performed. Duncan (1996) provides an overview of soil slope stability analysis. In general, the stability of a slope is usually analyzed by methods of limit equilibrium. The potential sliding mass is subdivided into a series of smaller units, and each of these units is analyzed to determine their potential for failure. A key step in limit equilibrium techniques is the calculation of a factor of safety, which is determined for the critical slip surface (i.e. the surface that is most likely to fail by sliding).

The FS was originally developed for geotechnical applications under the assumption that L >> H, where H is soil thickness and L is hillslope length (Terzaghi 1925). The FS is defined as the ratio of the shear strength (or resisting forces) to the shear stress (or driving forces). These forces must be equal (FS = 1) for equilibrium of the slope. Thus, the FS effectively represents the factor by which the strength would have to be reduced to bring the slope to failure and cause a landslide. In other words, a FS value of less than 1 indicates that driving forces will prevail, leading to slope failure, while a FS value greater than 1 indicates that resisting forces will prevail (Selby 1993). However, a FS value less than 1 does not indicate unconditional slope failure, and a FS value greater than 1does not indicate unconditional stability. Rather, the probability of stability increases as the FS value increases past 1, and the probability of instability increases as the FS value decreases below 1. Process-based models of landslides have employed variations of the FS equation and coupled them with geomorphic, hydrologic, geologic and vegetation data (Dietrich et al. 1995; Selby 1994; Iverson 2000).

The FS at a particular element at a time t and at an arbitrary depth Z below ground surface can be computed as:

$$FS(Z,t)=\frac{\tau_r}{\tau_d}=\frac{\tan\varphi}{\tan\alpha}+\frac{c'(t)}{(\gamma_s Z+B(Z,t))\sin\alpha\cos\alpha}-\frac{\psi(Z,t)\gamma_w\tan\varphi}{(\gamma_s Z+B(Z,t))\sin\alpha\cos\alpha} \quad \text{(Equation 4.1.1)}$$

where τ_r is the shear strength, τ_d is the shear stress, $c'(t)$ is the apparent soil cohesion that

is a function of root biomass, α is the slope angle, φ is the internal friction angle of the soil, $B(Z,t)$ is sum of the weight of the biomass above Z and the amount of water retained in the canopy, and $\psi(Z,t)$ is the soil matric potential at depth Z and time t. γ_s and γ_w are the specific weights of the soil and water, respectively (Iverson 2000).

The first term on the right hand side of Eq. (4.1.1) represents the frictional resistance of the soil material, the second term the resistance due to cohesion including that due to roots, and the third term the reduction in resistance associated with soil water pore pressures. A term-by-term description appears at the end of this section.

Prior applications of FS framework to Luquillo Forest

Simon et al. (1990) provide the most detailed account of the role of soil processes in slope failure in the Luquillo Experimental Forest. As part of their work, more than 150 landslides were mapped and data from several field tests were used to determine the physical soil properties most pertinent to slope stability across the forest. After calculating FS values for failure depths between 1 and 7 meters, Simon et al. (1990) conclude that failure planes arise from discontinuities in the soil's weathering profile. Such discontinuities often result from relic fractures that commonly occur at depths of 1 to 3 meters. Weathering of the parent rock induces stress-release fractures parallel or subparallel to the surface of the slope, and this fracturing in turn provides a zone for the accumulation of clays. Saprolite, which forms due to the weathering of the two main soil types in the area, i.e. quartz-diorite and marine-deposited volcaniclastics, also begins to accumulate in this zone. The accumulation of low-hydraulic conductivity saprolite and clays in this zone creates a trap for percolating water and leads to excess pore pressures due to perched ground water, particularly after large rainfall events (Simon et al. 1990). A typical quartz-diorite slope profile is depicted in Figure 4.1.1.

Simon et al. note that most of the landslides with known occurrence dates in their dataset were associated with specific storm events in which rainfall ranged from 100 to 600 mm over durations of 1 to 24 hours. The mean slope angle of slopes where landslides occurred was found to be 36.6°, with only four slides (8%) occurring at slopes less than 30°.

A more recent landslide dataset including more than 1,500 landslides in the Rio Blanco region (which includes the Mameyes basin) was obtained by Lepore et al. 2008b from the USGS and employed in the development of a static landslide hazard map for Puerto Rico. After filtering the data to consider only landslides with an area of at least 900m^2 (i.e. dimensions of 30m by 30m), the majority of the slides were found to have depths of 1.75m to 3m.

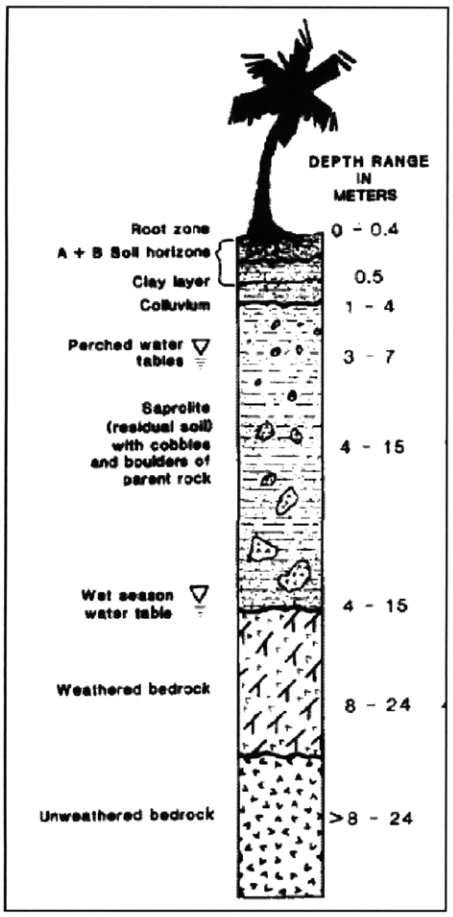

Figure 4.1.1: Soil profile for a quartz-diorite slope, adapted from Simon et al. (1990)

Effects of Vegetation on Slope Stability

Vegetation affects slope stability in several ways, many of which are captured by tRIBS while others are incorporated into the FS equation. The second and third terms in the FS equation are dependent on the state of vegetation on the slope. A discussion of these vegetation effects follows.

Greenway (1987) notes the complex nature of vegetation-slope interactions and outlines the major mechanisms governing the effects of vegetation on slope stability, which are divided into hydrological mechanisms and mechanical mechanisms. Hydrological mechanisms, as described by Greenway (1987), include interception, transpiration, infiltration and desiccation. The first two are beneficial to stability while the latter two are not. The hydrological mechanisms pertinent to slope stability in the Mameyes basin are sufficiently accounted for by tRIBS. Mechanical mechanisms include the reinforcement and binding of soil particles by roots, an increased surcharge on the slope resulting from the weight of trees, and instability resulting from the dynamic force of wind acting on vegetation that is exposed to it. The first mechanism is beneficial to stability, the second potentially beneficial, while the third is adverse to stability. These mechanisms are not explicitly incorporated into tRIBS but are partly accounted for in the FS Equation.

Hydrological Mechanisms

Interception

Interception is advantageous to stability because rainfall is intercepted by the vegetation foliage and part of it is eventually transpired or absorbed, leading to lower infiltration into the soil (Greenway 1987). The tRIBS model estimates interception by the use of the Rutter et al. (1971, 1975) canopy water balance model (Ivanov 2006). Interception losses at each time step as well as cumulative interception losses for each time step can be obtained as outputs from the tRIBS model. While interception data for locations in the Luquillo Forest are not available for 2005 to validate the model results, Schellekens et al. (1999) measured the interception loss over 66 days in 1996 as being 50% of precipitation at the Bisley II catchment area of the Mameyes basin. Similar studies by Gregory and Walling (1973) also report high (66%) losses due to interception in similar evergreen forest environments in Brazil (Gregory and Walling 1973, as reproduced in Greenway 1987). Based on these observations, interception was expected to play a significant role in the soil moisture conditions over the Mameyes basin. Indeed, the average interception value was 51% for the element model runs that were based on 2005 meteorological data from Bisley tower.

Transpiration

The rate at which a plant consumes soil moisture is dependent on a variety of factors, many of which are specific to the type of plant, such as its rooting habit and level of water use (Greenway 1987). Transpiration due to the presence of vegetation is captured in tRIBS through the vegetation parameters discussed previously in Chapter 3.

Infiltration

Studies at several sites indicate that the presence of vegetation in soil can appreciably increase soil infiltration capacity. This increase is attributable to the presence of roots, vacant root channels and increased microscopic surface roughness (Greenway 1987), all of which increase soil permeability and thus infiltration. Greenway (1987) indicates that this increase in permeability cannot be quantified without field permeability tests at the site in question. tRIBS does not account for the increase in infiltration due to the presence of vegetation.

Desiccation Cracking

Desiccation cracking occurs in soils during the dry season when there is high transpiration and low rainfall. Evaporative cracking of the soil has been recorded in several prior studies, particularly in soils with shrinkable clays and soils with a high clay content (Greenway 1987). This mechanism is not expected to play a major role in the Mameyes basin, which receives relatively high rainfall and does not have areas with clays

that are particularly susceptible to cracking. It is not accounted for in tRIBS or the FS Equation.

Mechanical Mechanisms

Root Reinforcement

Studies of root-reinforced soil indicate that it is stronger than soil without roots due to the roots' tensile resistance and frictional or adhesion properties (Greenway 1987). This relationship has been demonstrated through the use of field tests on soils in which the shear strength of soils has been found to increase with increasing root biomass (Ziemer 1981). While the effects of this root reinforcement on soil are well documented, this may or may not be pertinent to slope stability depending on the depth of potential slip surfaces on the slope in consideration (Tsukamoto and Kusakabe 1984).

Tsukamoto and Kusakabe (1984) discuss the potential benefits of root reinforcement on critical slope surfaces. Roots can significantly improve stability in some slopes, and the potential for stabilization is related to the depth of the critical slope surface relative to the vegetation's rooting depth. For soils with a relatively thin soil mantle and discontinuities in the bedrock, roots can penetrate these discontinuities and improve stability. Similarly, soils that have a thick soil mantle and contain a transition layer in which soil density and shear strength increase with depth can benefit from roots that strengthen the upper portions of the transition layer. In contrast, Tsukamoto and Kusakabe (1984) note that slopes with thicker soil mantles and relatively homogenous soil, where deep seated movement occurs below the root zone, will have planes of weakness not reinforced by roots. In this slope type, anchoring of the tree species into the slope does not improve slope stability appreciably.

As indicated in Figure 4.1.1 and documented in Simon et al. (1990), the majority of roots in the Luquillo Experiment forest do not penetrate more than 25 to 40 cm. In contrast, the USDA NRCS Soil Survey (USDA 2002) indicates a root zone of more than 60 inches (152 cm) for the Zarzal/Cristal soil type that is found over the majority of the Mameyes basin. Because the root depths in Simon et al. are based on field samples and vegetation transects, the 25 to 40 cm range appears to be a more reasonable range for the root depth than the estimates by the NRCS. Literature on root development in the tabonuco forest (e.g. Basnet 1992) generally supports the root depth range provided by Simon et al. and also indicates that tabonuco tree roots have a preference for lateral rather than vertical expansion.

Typical landslides in Mameyes and the surrounding areas, as documented by Larsen (1998) and others, are on the order of a few meters deep. While shallow landslides (about 0.5m) have been documented and observed in field studies (Simon et al. 1990), the spatial extent of the vast majority of these slides is smaller than the spatial extent for the majority of the Voronoi cells (i.e. about 30m by 30m). It is very unlikely that the current model could predict landslides that are less than 1m deep because these shallow landslides typically do not have a spatial extent of more than 30m by 30m.

Since the depth reached by the majority of roots (25 to 40 cm) is significantly shallower than the smallest pertinent depth to failure in this study (1 meter), the root reinforcement mechanism is assumed to play an insignificant role for slope stability.

Vegetation Surcharge

Greenway (1987) addresses the surcharge resulting from the weight of vegetation on a slope. This surcharge increases both the normal and downhill force components on potential slip surfaces. This surcharge has an appreciable net stabilizing influence when the slope angle is less than the angle of internal friction of the soil, and a net destabilizing effect when the slope angle is more than the angle of internal friction. This effect is captured through the FS equation which accounts for the sum of the weight of the biomass through the $B(Z,t)$ parameter in terms 2 and 3 of Equation 4.1.1.

Wind Effects

Greenway (1987) indicates that some trees, particularly those with weak or shallow root systems, can become uprooted due to the force of high winds and cause a significant destabilizing force on the hillslope depending on the direction and velocity of the wind. As discussed previously, the root stabilization mechanism is not expected to play a major role in slope stability over the Mameyes basin given the relatively shallow root depth. Brown and Sheu (1975) provide methods to predict the shear stress resulting from wind effects, but these effects are assumed to be negligible for the purposes of the current work.

Development of FS equation

In the context of the prior studies and vegetation effects described above, the development of the FS equation is now presented. For reference, the Equation 4.1.1 is repeated from above:

$$FS(Z,t)=\frac{\tau_r}{\tau_d}=\frac{\tan\varphi}{\tan\alpha}+\frac{c'(t)}{(\gamma_s Z+B(Z,t))\sin\alpha\cos\alpha}-\frac{\psi(Z,t)\gamma_w\tan\varphi}{(\gamma_s Z+B(Z,t))\sin\alpha\cos\alpha} \qquad \text{(Equation 4.1.1)}$$

Frictional resistance of the soil material (1st term)

The first term of Equation 4.1.1 represents the frictional resistance of the soil material and depends on the slope angle of the land surface (α) and the internal friction angle of the soil (φ). The slope angle values are derived from tRIBS and range from 0° to 61° over the basin. Values for the internal friction angle of the soil were determined by Simon et al. (1990) for two major soil types (i.e. diorite and volcaniclastic). The minimum 25th and maximum 75th percentile values are 22.6° and 34.6° for 59 soil samples collected across the forest at depths ranging from 0.2m to 3m. The median values for these soil types are both around 30°. For the purposes of this work, an internal friction angle of 30° is used.

Resistance due to cohesion (2nd term)

The second term of Equation 4.1.1 accounts for the interplay between the apparent soil cohesion (c'(t)) and the overburden on the slope.

Apparent Soil Cohesion

The apparent soil cohesion is the sum of the cohesion associated with the soil alone (c_{soil}) and the cohesion associated with root reinforcement of the soil (c_{root}). Simon et al. (1990) provide values for the cohesive strength of soils that are derived from 25 samples collected over the Luquillo forest. The median value is 5.37 kPa for diorite and 7.79 kPa for volcanoclastic. The 25th and 75th percentile values are, respectively, 2.34 kPa and 8.37 kPa for the former and 3.51 kPa and 14.3 kPa for the latter soil type. The range of these values makes clear that there are considerable differences in soil strengths across the forest. The implications of these differences for the FS value are addressed in Section 4.2. A value of 6.5 kPa, representing an approximate average of the median values for diorite and volcanoclastic, was selected for the current work.

As discussed previously, root cohesion is assumed to play a negligible role for the current work since the observed root depth (25 to 40 cm) does not reach the plane of failure pertinent to this study. This term may prove to be significant for future work focusing on shallow landslides and its calculation is addressed in Section 5.2.

Overburden

The overburden is associated both with the soil itself ($\gamma_s Z$) and with vegetation and soil moisture ($B(Z,t)$). Soil overburden can be calculated by considering the specific weight and the depth of the overlying soil. Simon et al. (1990) provide bulk density values determined from soil tests conducted on 54 soil samples over the Luquillo Forest. Median values of 1.26 g/cm^3 for the diorite soil type and 1.28 g/cm^3 for the volcanoclastic soil type are reported. The 25th and 75th percentile values are 1.15 g/cm^3 and 1.24 g/cm^3 for the former and 1.16 g/cm^3 and 1.38 g/cm^3 for the latter soil type. The average of the medians, 1.27 g/cm^3, was selected for the current work.

The variable $B(Z,t)$ of Equation 4.1.1 accounts for overburden associated with vegetation and consists of the sum of the weight associated with the biomass itself (B_{bm}) as well as the weight associated with the water retained by the plant (B_{cw}) and in the soil (B_{gw}). The weight of biomass (B_{bm}) is calculated from the stem, root and leaf carbon pool values that are predicted by tRIBS at each time step. The stem carbon pool value computed by tRIBS is only for live biomass, and for temperate forests the tRIBS code employs a factor of 0.17 to relate the fraction of live stem biomass to total biomass, consistent with other dynamic vegetation models (Friend et al. 1997). For lack of a corresponding value for tropical forests, this factor was used in this work to calculate the total stem biomass weight. The weight associated with the water retained by the plant is calculated from the canopy water storage (in units of mm) that is computed by tRIBS at each time step.

Water retained by the soil (B_{gw}) is calculated from the soil moisture computed by tRIBS at each time step.

Reduction in resistance associated with soil water pore pressures (3rd Term)

High soil water pore pressures can be detrimental to slope stability and are captured through the third term of the FS Equation. Soil matric potential ($\psi(Z,t)$) is related to soil moisture in the unsaturated zone through empirically based soil moisture retention curves (MRCs). tRIBS uses the Brooks and Corey (1964) MRC, as shown in Equation 4.1.2 (Ivanov 2006).

$$\psi(\theta) = \psi_b \left(\frac{(\theta - \theta_r)}{(\theta_s - \theta_r)} \right)^{-1/\lambda} \qquad \text{(Equation 4.1.2)}$$

$\psi(\theta)$ is the soil matric potential (mm), θ is the dimensionless soil moisture content (volume of water per bulk volume of soil), θ_s is the saturation soil moisture content, θ_r is the residual soil moisture content, ψ_b is the air entry bubbling pressure (mm) and λ is the dimensionless pore size distribution index. All of the variables except for θ are static parameters determined for the soil type. Representative values for these parameters are given by Ivanov (2006). For loam, $\theta_r = 0.027$, $\theta_s = 0.434$, $\lambda = 0.220$ and $\psi_b = -111$ mm. For clay, $\theta_r = 0.09$, $\theta_s = 0.385$, $\lambda = 0.150$ and $\psi_b = -370$ mm. Based on these parameters it was possible to prepare soil moisture curves for both soil types.

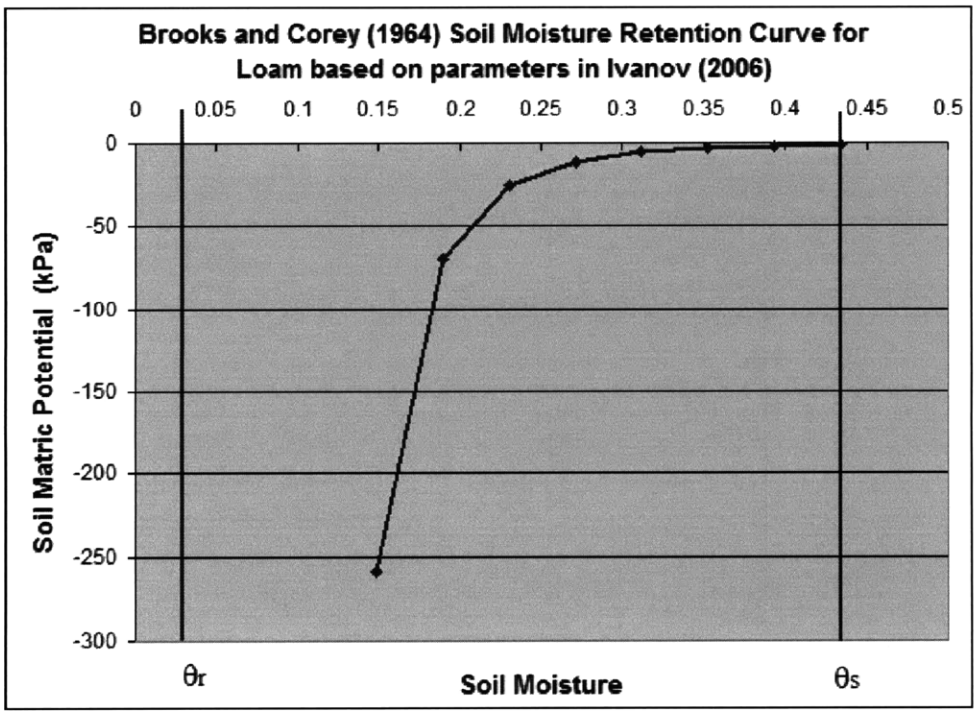

Figure 4.1.2: Moisture Retention Curve for Loam ($\theta_r = 0.027$, $\theta_s = 0.434$.)

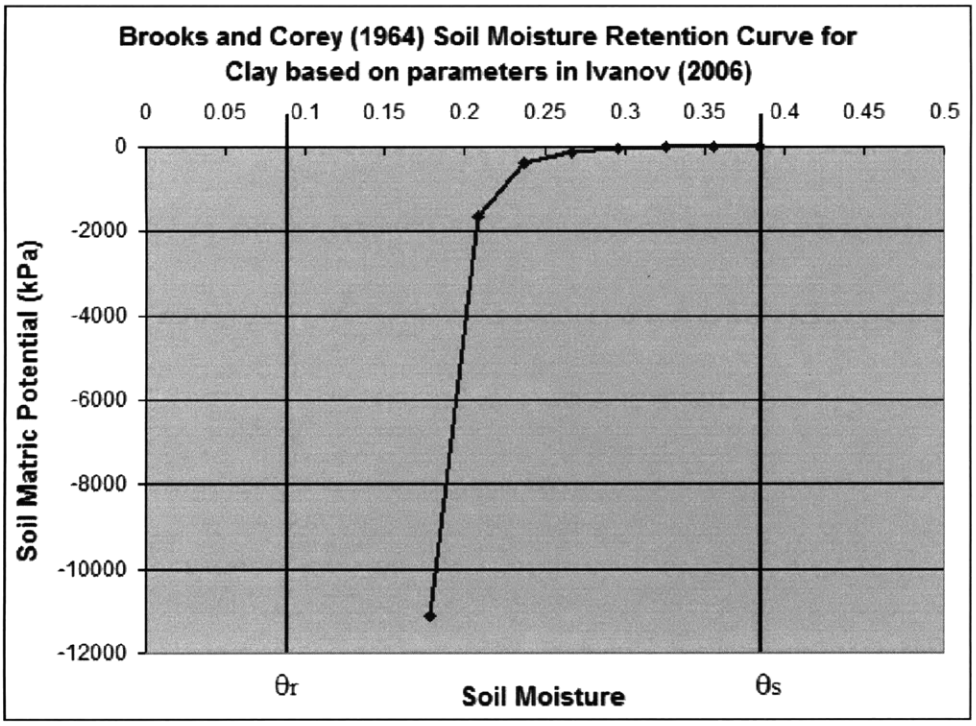

Figure 4.1.3: Moisture Retention Curve for Clay (θ_r = 0.09, θ_s = 0.385.)

Figures 4.1.2 and 4.1.3 show MRCs for clay and loam at soil moisture values ranging from saturation to fairly dry. As each soil approaches its residual soil moisture the absolute value of the (negative) soil matric potential gets exponentially larger due to the relationship shown in Equation 4.1.2. When the (negative) soil matric potential gets exponentially larger in magnitude, it increases the magnitude of the (negative) third term of Equation 4.1.1 considerably. Since the third term is subtracted from the first two terms in Equation 4.1.1, a negative third term value with a large magnitude corresponds to a large increase in the FS value. Thus, the exponential nature of the MRC results in FS values with very large magnitudes as the soil moisture value approaches the residual soil moisture.

As mentioned in Chapter 1, the off-line landslide component is based on the FS equation and FS values will be used to assess the susceptibility of slopes to landslides. Because of the effect of the soil matric potential, it appears likely that the FS value for stable slopes with low soil moisture content will exhibit a large range of positive values. Since all these positive FS values indicate a high degree of stability, values greater than an upper cut-off value (e.g. FS = 2) can be grouped together for simplicity. This grouping of FS values is further discussed in Section 5.2.

This discussion of the effect of soil pore water pressures addresses the calculation of the soil matric potential for failure planes in the unsaturated zone using Equation 4.1.2. For failure planes in the saturated zone it becomes necessary to account for the head due to the overlying water table, which has a destabilizing effect on the FS through the third term of Equation 4.1.1. For the saturated zone, then, the soil potential is calculated from Equation 4.1.3:

$\psi = \rho\, g\, h$ (Equation 4.1.3)

where ρ is the density of water, g is the acceleration due to gravity and h is the height of the saturated layer above the potential failure plane.

Summary

The off-line landslide component is based on the FS Equation (Equation 4.1.1). Selected outputs from tRIBS are used as input into the landslide component and the FS is calculated for each Voronoi cell and at each time step. FS values less than 1 identify slopes that are potentially unstable and also indicate when they become unstable. Five of the variables in the FS Equation (Equation 4.1.1) are directly linked to tRIBS outputs. Four of these terms (i.e. the weight of biomass, below-ground water, canopy water and soil moisture) are dynamic since they are updated at each computational time step, while the slope angle is static for a given Voronoi cell. All other variables are assigned static values in our FS calculations, with the exception of root cohesion which is assumed to be negligible. A summary of these terms is provided in Table 4.1.1.

Table 4.1.1: Summary of terms employed in the FS equation. Shaded terms represent outputs from the tRIBS model that are location dependent, time dependent, or both.

$$FS(Z,t) = \frac{\tau_r}{\tau_d} = \frac{\tan\varphi}{\tan\alpha} + \frac{c'(t)}{(\gamma_s Z + B(Z,t))\sin\alpha\cos\alpha} - \frac{\psi(Z,t)\gamma_w \tan\varphi}{(\gamma_s Z + B(Z,t))\sin\alpha\cos\alpha}$$

Symbol		Description	Value	Range	Unit	Source
α		Slope angle	(tRIBS)	0 to 55	°	DEM / tRIBS
φ		Internal friction angle	30	22.6 to 34.7	°	Simon et al. (1990)
$c'(t)$		Apparent soil cohesion				
	c_{soil}	-- *Soil cohesion*	6.5	2.34 to 14.3	kPa	Simon et al. (1990)
	c_{roots}	-- *Root cohesion*	0	N/A	kPa	Simon et al. (1990)
γ_s		Specific weight of soil	12,459	11,282 to 13,538	N/m^3	Simon et al. (1990)
Z		Depth	5	3 to 7	m	Simon et al. (1990)
B(Z,t)		Vegetation Overburden				
	B_{bm}	-- *Weight of biomass*	(tRIBS)	Varies		tRIBS
	B_{gw}	-- *Below-ground water*	(tRIBS)	Varies		tRIBS
	B_{cw}	-- *Canopy water*	(tRIBS)	Varies		tRIBS
$\psi(Z,t)$		Soil matric potential				
	Θ	-- Soil moisture	(tRIBS)	Varies	-	tRIBS
γ_ω		Specific weight of water	9807		N/m^3	Simon et al. (1990)

4.2: Testing of Landslide Component

This section describes the testing of the landslide component based on the FS equation, Equation 4.1.1, whose formulation is described in Section 4.1. This preliminary landslide component was developed in Microsoft Excel as a precursor to the full, off-line version developed in MATLAB for application to the Mameyes basin. The landslide component was tested by conducting sensitivity analyses on key variables of the FS equation in order to test the performance of the FS equation (Equation 4.1.1). Each sensitivity analysis consisted of systematic parameter variations in the Excel spreadsheet. The key variables considered were soil moisture and water table depth, slope angle, soil cohesive strength and the presence or absence of vegetation.

Assignment of Typical Values

In order to test the FS Equation, typical values were assigned to the variables of the equation as presented in Table 4.1.1. Of these, values assigned to the static variables (i.e. internal friction angle, soil cohesion, specific weights of soil and water, and depth) are discussed in Section 4.1. The assignment of values to the other variables is described in the following. It is assumed that the slope rests on clay and has broadleaf evergreen trees growing on it.

In the following discussion "marginally stable" refers to slopes at which the slope angle is less than the soil's internal friction angle (i.e. 30°), corresponding to the first term of Equation 4.1.1 having a value of just less than 1. "Marginally unstable" refers to slopes at which the slope angle is greater than the soil's internal friction angle, corresponding to the first term of the equation having a value of just greater than 1. Slope angle values of 28° (corresponding to a value of 1.09 for the first term) and 32° (corresponding to 0.92) were used for marginally stable and unstable slopes, respectively.

In order to calculate vegetation overburden, typical values for the weight of biomass and the weight of water associated with this biomass needed to be assumed. The weights associated with biomass can be approximated by the carbon pools in the canopy, stems and roots. In the absence of species-specific data, a ratio of biomass to carbon mass of 2 is often used (Moorecroft et al. 2001).

The tRIBS simulations show that the canopy carbon pool varies slightly over the year with a mean value of approximately 400 gC/m^2, corresponding to a biomass of approximately 0.8 kg that would exert a downward force of about 8 N/m^2. The variation in the canopy carbon pool is associated with the life cycle of leaves. The stem and root carbon values from tRIBS were found to increase with time over the basin, with the most rapid increase during the first year of the simulation. After 18 months (which roughly corresponds to the modeled storm event discussed in Section 3.3), the stem carbon pool is about 1000 gC/m^2. Since the tRIBS model is only considering live and not dead stems, a factor of 5.88 is applied to get an approximate value for the total carbon canopy pool. After also accounting for the biomass-to-carbon ratio of 2, this corresponds to a force of about 115 N/m^2 for the stems. The root carbon pool, which reaches a value of about 500 gC/m^2, similarly corresponds to a force of about 10 N/m^2. Thus,

the total force due to the biomass is about 133 N/m^2.

The forces associated with the above-ground water due to biomass are estimated by considering the water content of the leaves and the stem. For leaves, Gu et al. (2007) used a biomass water-mass-to-dry-mass ratio of 1.5, which is the ratio of the mass of water in the plants to the dry mass of the plants. For stems, they used a biomass water-mass-to-dry-mass ratio of 0.7. The forces of water calculated after accounting for these factors are 12 N/m^2 for water in leaves and 81 N/m^2 for water in stems. Similarly, using a ratio of 0.7 for roots yields a value of 7 N/m^2 due to water in roots. Thus, the total force of water associated with biomass is 100 N/m^2 versus the 133 N/m^2 calculated above for the dry biomass. These estimates indicate that just under half of the weight associated with the vegetation is due to water, which is consistent with intuitive expectations. In addition to the water associated with the biomass itself, there is some weight associated with rainfall interception by the canopy. A typical value of intercepted rainfall as determined from the element model runs discussed in Section 3.3 is about 1.5 mm, corresponding to a force of about 15 N/m^2.

Forces associated with the weight of water retained in the soil (i.e. below-ground water) were determined from the soil moisture content, which theoretically can vary between 0.09 (residual moisture content for clay) and 0.385 (saturation moisture content for clay). In the complete landslide component developed in MATLAB, the weight of water is calculated by considering the soil moisture content of each tRIBS subsurface layer. For the purposes of the sensitivity analyses, it was assumed that the value of the moisture content in the layers above the water table was halfway between the residual and saturation soil moisture (i.e. a moisture content of 0.238). For a water table located at a depth of 2m, this corresponds to a force of 2,300 N/m^2. This force is very large compared to the total force ($100 + 15 + 133 = 248$ N/m^2) associated with biomass.

Soil moisture values close to saturation were selected for the sensitivity analyses. As discussed in Section 4.1, a very dry soil with a moisture content close to its residual content would have a highly negative soil matric potential, resulting in a very high positive value for FS. Soil moisture values closer to the saturation value, or at saturation, are thus selected for testing purposes. In cases where the water table was located above the failure plane, the soil matric potential was determined by considering the elevation head acting on the failure plane due to the water table, as discussed in Section 4.1.

Sensitivity Test Results

Soil Moisture and Water Table Depth

The FS equation is expected to be very sensitive to soil moisture and the depth to the water table, since the increase in pore pressure associated with rainfall is the key landslide triggering mechanism in Puerto Rico. Sensitivity analyses on soil moisture and water table depth for both marginally stable (Table 4.2.1 and Table 4.2.2) and marginally unstable (Table 4.2.3 and Table 4.2.4) soils were performed. Typical values for the soil cohesive strength, internal friction angle and vegetation values were used. Slope angles of 28° and 32° were used for marginally stable and marginally unstable slopes, respectively. Soil moisture conditions were selected

such that the soil at the modeled failure plane located at a depth of 2m was partially and then fully saturated. For cases where this soil was fully saturated, different levels of the water table relative to the failure plane were considered. In the text that follows, a description of "above water table" indicates the location of the failure plane relative to the water table i.e. that the failure plan is located above the water table.

Table 4.2.1: Key assumptions for analysis of sensitivity to soil moisture and water table depth for a marginally stable slope

Key assumptions:	
Cohesive strength of soil (kPa)	6.5
Internal friction angle of soil (°)	30
Slope angle (°)	28
Failure depth (m)	2
Average Vegetation Values	

Table 4.2.2: Effect of soil moisture and water table depth on FS for a marginally stable slope

Soil Moisture	Description	FS
0.32	Above water table	2.38
0.36	Above water table	1.84
0.385	Saturated, 0.5m below water table	1.36
0.385	Saturated, 1m below water table	1.15
0.385	Saturated, 1.5m below water table	0.94

As shown in Table 4.2.2, the calculated FS for an initially stable slope continues to decrease as the water table rises and the soil becomes more saturated. This is consistent with intuitive expectations, since the rising water table results in an increase in the pore pressure acting on the failure plane. In this case, when the water table reaches somewhere between 1m and 1.5m, the FS values switches from a stable (>1) value to an unstable (<1) value. A similar trend is observed in marginally unstable slopes, as shown in Tables 4.2.3 and 4.2.4.

Table 4.2.3: Key assumptions for analysis of sensitivity to soil moisture and water table depth for a marginally unstable slope

Key assumptions:	
Internal friction angle of soil (°)	30
Slope angle (°)	32

Table 4.2.4: Effect of soil moisture and water table depth on FS for a marginally unstable slope

Soil Moisture	Description	FS
0.32	Above water table	2.08
0.36	Above water table	1.60
0.385	Saturated, 0.5m below water table	1.17
0.385	Saturated, 1m below water table	0.98
0.385	Saturated, 1.5m below water table	0.79

Slope Angle

As discussed in previous work by the Lepore et al. 2008b, slope angle is the key variable for inferring static landslide susceptibility in Puerto Rico. Simon et al. (1990) documented a small fraction (8%) of slides that occurred on slopes with slope angles less than 30°. The FS equation is thus expected to be highly sensitive to the slope angle and is also expected to indicate stability for slopes that have low slope angles even if they are fully saturated. The results in Table 4.2.6 meet these expectations: there is significant variation of the FS with slope angle. FS values greater than 1 are observed for slopes inclined at less than 30°, despite the strongly destabilizing influence of being fully saturated and 1m below the water table.

Table 4.2.5: Key assumptions for analysis of sensitivity to slope angle for a fully saturated slope located 1m below the water table.

Key assumptions:	
Cohesive strength of soil (kPa)	6.5
Internal friction angle of soil (°)	30
Failure depth (m)	2
Average vegetation values	
Soil Moisture	0.385
Depth below water table (m)	1

Table 4.2.6: Effect of slope angle on FS for a fully saturated slope located 1m below the water table.

Slope Angle	Description	FS
35°	Higher than internal friction angle	0.88
30°	Equal to internal friction angle	1.06
25°	Lower than internal friction angle	1.31
20°	Lower than internal friction angle	1.67

Cohesive Strength of Soil

As mentioned in Section 4.1, there is considerable variation in the cohesive strength of soils tested in the LEF, which has implications for the 2nd term in the FS equation. In testing sensitivity to cohesive strength, the slope was assumed to be marginally unstable and fully saturated 1m below the water table. Cohesive strengths of 3 kPa, 6.5 kPa and 10 kPa were considered, approximating the 25th, 50th and 75th percentiles for soils tested by Simon et al. (1990). Assumptions and results are shown in Table 4.2.7 and Table 4.2.8, respectively.

Table 4.2.7: Key assumptions for analysis of sensitivity to soil cohesive strength for a saturated, marginally unstable slope located 1m below the water table.

Key assumptions:	
Internal friction angle of soil (°)	30
Slope angle (°)	32
Failure depth (m)	2
Average vegetation values	
Soil Moisture	0.385
Depth below water table (m)	1

Table 4.2.8: Effect of soil cohesive strength on FS for saturated, marginally unstable slope 1m below water table.

Tensile Strength	Description	FS
3 kPa	~ 25th percentile value	0.75
6.5 kPa	~ 50th percentile value	0.98
10 kPa	~ 75th percentile value	1.21

The results show that the FS is highly sensitive to the cohesive strength of the soil, with less cohesive strength leading to a lower FS as expected. They also show that a FS greater than 1 is possible when the soil is located 1m below the water table if the soil has a high enough cohesive strength. These results are generally consistent with FS values calculated by Simon et al. (1990) who also calculated FS values for soils with different cohesive strengths and an internal friction angle of approximately 30°. Their FS analysis concluded that soils with cohesive strengths of 2.34 kPa and 3.51 kPa were unstable while those with cohesive strengths greater than 5.37 were stable at a depth of 1m on a fully saturated slope.

The results regarding sensitivity to cohesive strength support the literature on landslides which highlights that some planes are particularly susceptible to landslides due to the properties of soils located at those depths. While the basin-wide analysis described in the next chapter considers a uniform value of cohesive strength across the area of the basin, the results above suggest that a more localized value of the cohesive strength should be employed in future application of the landslide component. The results further suggest that variations in the cohesive strength over the depth of the soil column, particularly at the discontinuous zones described by Simon et al. (1990), are very significant for the FS.

Vegetation

As described in Section 4.1, the depths reached by vegetation roots in the LEF are typically much less than the depth of the failure plane considered in this study, which means that root cohesion is not expected to contribute to slope stability in this area and thus need not be considered in the FS equation. In the absence of root cohesion, the presence of vegetation is expected to simply increase the force acting on the failure plane and therefore decrease the factor of safety. This was tested in sensitivity simulations using assumptions reported in Table 4.2.9 and results reported in Table 4.2.10. As discussed previously in this chapter, the force associated with vegetation is not as great as the force associated with the pore water pressure and the weight of water for failure planes below the water table, and so the presence of

vegetation should not have a significant impact on the FS. This is confirmed by the results shown in Table 4.2.10.

Table 4.2.9: Key assumptions made to assess the impact of the presence or absence of vegetation for a saturated, marginally unstable slope located 1m below the water table.

Key assumptions:	
Cohesive strength of soil (kPa)	6.5
Internal friction angle of soil (°)	30
Slope angle (°)	28
Failure depth (m)	2
Soil Moisture	0.385
Depth below water table (m)	1

Table 4.2.10: Effect of vegetation on FS for saturated, marginally unstable slope 1m below water table.

Vegetation status	Description	FS
Present	Average Vegetation Values	1.15
Absent	No Vegetation	1.17

As discussed in Section 3.2, the initialization of vegetation parameters (including the carbon pool values) was based on ten-year vegetation simulations. Thus the simulation timeframe does not account for the actual age of the forest, which for the modeling year (2005) has a lower bound of at least sixteen years, since the last major disturbance to cause significant (~50%) tree mortality was Hurricane Hugo in 1989 (Walker 1991). Further refinement of vegetation parameters, particularly the stem carbon pools, to account for the age and growth of the forest is expected to increase the impact of vegetation on the FS Equation. Indeed, Saldarriaga et al. (1988) discuss vegetation dynamics in tropical forests in South and document a near-linear increase in above-ground living biomass during the first forty years. Thus, refinement of the vegetation values for future work should be based on the age of the forest, and is further discussed in Section 5.2.

Summary

Sensitivity analyses based on systematic parameter variations in a Microsoft Excel spreadsheet help to identify the most sensitive parameters in the FS Equation. The FS Equation was found to be very sensitive to the soil moisture and water table depth, slope angle and the soil cohesive strength. The presence or absence of vegetation was found to have a negligible impact on the FS, with the caveat that the initial carbon pools for the vegetation were based on ten-year simulations rather than the actual age of the forest.

CHAPTER 5: RESULTS AND FUTURE WORK

5.1 Results from Application of Landslide Component to Mameyes Basin

This section discusses the results from the application of the off-line landslide component based on the FS Equation over the entire Mameyes basin. The inputs to the FS Equation were driven by the tRIBS model of the Mameyes basin described in Section 3.3. The FS Equation itself was developed and tested prior to this basin-wide application, as discussed in Sections 4.1 and 4.2. The results from the basin-wide application are discussed in terms of the timing of predicted landslides and the location of predicted landslides. Also discussed is the important fact that the tRIBS model does not numerically reach a relative saturation of 1 i.e. "complete saturation" and therefore that a threshold value had to be selected to define the soil moisture as saturated. This section concludes with a note on the sensitivity of the results to the selected threshold value. The algorithm for the off-line component is included in Appendix B.

Threshold for definition of saturated soil moisture

As mentioned in Chapter 1, the tRIBS model cannot numerically reach a saturation value of 100% i.e. a relative saturation of 1. Thus, a saturation threshold had to be specified in order to determine the form of the FS Equation to be applied. In the FS Equation (Equation 4.1.1), the third term accounting for pore pressures is particularly influenced by whether or not saturation is reached, since the soil potential is calculated differently when the soil is not saturated (Equation 4.1.2) versus when it is saturated (Equation 4.1.3). As described in Section 4.2, the saturation status of the soil has a very large impact on the calculated FS. In the absence of an explicit determination of the depth to the water table in tRIBS, the depth to the saturated zone (used in Equation 4.1.3) is approximated based on the soil moisture in each of the 25 vertical layers used to represent soil in tRIBS. This saturation depth is determined from a bottom-up approach; if the bottom layer (i.e. the potential failure surface) is saturated, the next layer up is checked for saturation. The layer at which the soil moisture state is no longer saturated is flagged, and the top of the saturated zone is set between this layer and the underlying saturated layer. The distance from this point to the potential failure surface is then taken as the height of the saturated zone in Equation 4.1.3. The saturation threshold thus plays an important role in terms of influencing the third term of the FS equation. The results reported below employ a relative saturation threshold of 0.99. These results are also compared with results that employ saturation thresholds of 0.95, 9.98 and 0.999999.

Results

Over the modeled two-year period, landslides were indicated in 48 Voronoi cells, representing 0.36% of the total number of Voronoi cells (13,169). All of the predicted failures were in loam, which was shown in Section 3.3 to be more likely to become saturated at the assumed failure depth of 1.5 meters than clay. These results are best presented focusing on (a) the timing of landslides and (b) the location of landslides. The time of landslides is expected to be correlated to rainfall events, including the major storm event synthesized in the second year. The locations of predicted landslides can be directly compared to the static susceptibility map developed by Lepore et al. 2008b.

Timing of predicted landslides

Before a discussion of results, it is important to distinguish between "landslide triggers" and "landslide events." A landslide event is any time step when the FS value is less than 1. It is possible for the FS value to continue to remain less than 1 for multiple continuous time steps, and each time step when this is true is flagged as a "landslide event". An alternative way to view the results is to consider landslide "triggers" i.e. to consider the instant at which a particular Voronoi cell becomes unstable after previously being stable. Each landslide trigger can be associated with multiple landslide events, and a particular Voronoi cells can have more than one landslide trigger. These concepts are discussed further below.

Representing both "landslide events" and "landslide triggers" is important, as is the distinction between them. The total number of landslide events indicates the timeframe over which a particular cell is unstable. As discussed in Section 4.1, a FS value less than one does not indicate unconditional instability i.e. it does not guarantee that a failure will occur in real life. Rather, it is an indication that the slope is unstable and that a landslide is likely. Therefore, accounting for the number of time steps during which the FS value is less than 1 (i.e. the number of landslide events) becomes important, since a slope that has a FS value less than 1 for a greater amount of time than another slope has a higher probability of slope failure. In the following text the term "landslide," if used by itself, it refers to a landslide event.

Landslide triggers, on the other hand, refer to the first time a cell becomes unstable after previously being stable. There can be more than one landslide trigger in a particular cell—for example when a slope becomes unstable due to a rainfall event, becomes stable again as the soil moisture content decreases, and then becomes unstable again in response to another rainfall event. Landslide triggers are important since they offer a means to correlate instances of instabilities with rainfall events that cause those instabilities.

Time series of predicted landslides and the value over time of the third term in the FS equation for each Voronoi unit that fails are shown in Figure 5.1.1. As discussed above, a distinction is made between landslide "triggers" and landslide "events" in Figure 5.1.1. It is clear from Figure 5.1.1 that the temporal distribution of landslides is highly correlated with rainfall events. As the third term in the FS equation (which depends on soil moisture) becomes less negative (i.e. the soil moisture increases and approaches saturation), the number of landslides increases. As expected, there is a sharp increase in the number of landslides triggered in response to the synthetic storm event.

The threshold for complete saturation is only exceeded in a few instances (i.e. when the third term of the FS Equation exceeds 0, a threshold indicated by the horizontal red line in Figure 5.1.1c). There are several landslides, for example in month 8, when the saturation threshold is not reached. The fact that an appreciable number of slides occur without the saturation threshold being reached is supported by the sensitivity analyses in Section 4.1, which indicate that it is not necessary for slopes to be fully saturated for slope failure to occur, particularly in areas with very steep slope angles. Indeed, the average slope angle in the 48 Voronoi cells where failures occurred is about 43°. Higher slope angles lead to lower values of the first two terms in the FS Equation.

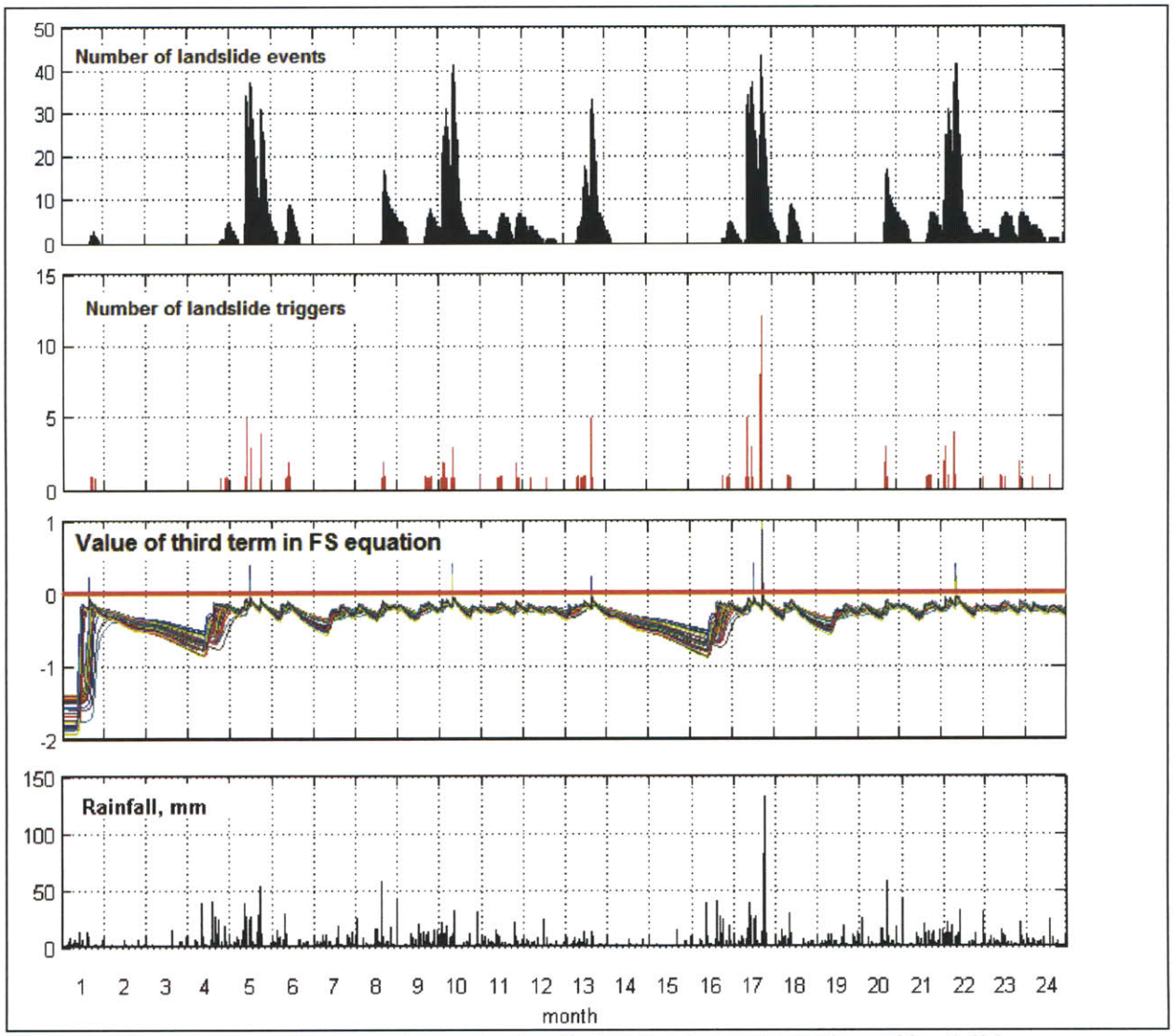

Figure 5.1.1: Results of time series analysis of FS Equation: a) number of landslide events, b) number of landslide triggers, c) value of the third term in the FS equation at Voronoi cells experiencing landslides (different colors for different cells), and d) hourly rainfall for reference.

For a given slope, the values of the first two terms do not vary appreciably with time, and the third term (which depends on the soil moisture) determines whether or not a FS value of less than 1 will be reached. This is best demonstrated by considering two slopes that fail: at Voronoi Cell 4091 which has a slope angle of approximately 50° and at Voronoi Cell 11311, with a slope angle of approximately 30°.

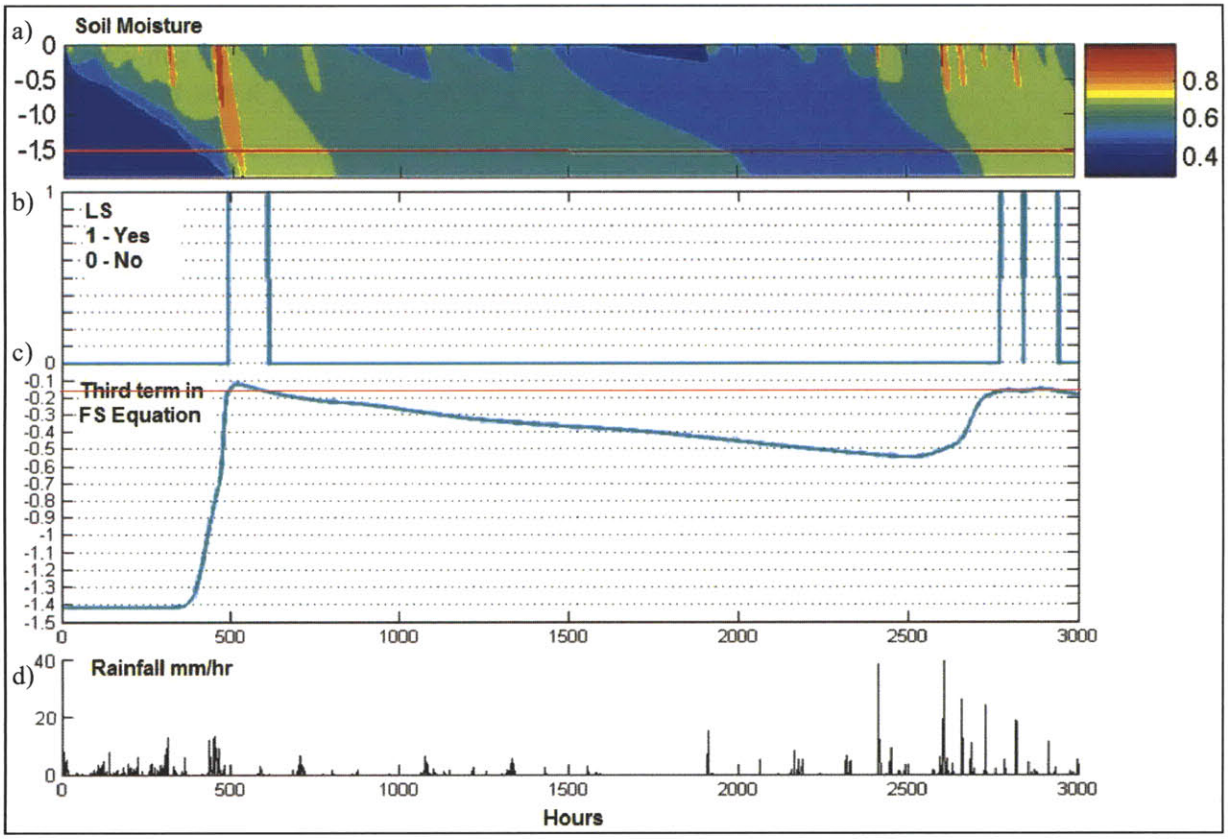

Figure 5.1.2: Results of first 3000 hours (125 days) of simulation for Voronoi Cell 4091 (slope angle of 50°). a) soil moisture vs. depth (color legend indicates soil moisture), b) landslide occurrence, c) value of third term in the FS equation and d) hourly rainfall.

Figure 5.1.2 depicts soil moisture, landslide occurrence, the value of the third term in the FS equation, and rainfall over the first 3000 hours (125 days) of the simulation for Voronoi Cell 4091 with a slope angle of 50°. The soil moisture is represented as relative soil moisture as indicated by the color legend. The darkest red at the top of the legend indicates saturation soil moisture. The landslide occurrence plot has a value of 1 when a landslide occurs and a value of 0 when it does not.

During this time period, three landslides are predicted even though the soil moisture does not reach complete saturation at the depth of the failure plane (1.5m). The sum of the first and second terms of the FS Equation for this slope are approximately 0.86 over the time series, which means that the FS value becomes less than 1 when the magnitude of the third term becomes less than 0.14 (i.e, when the negative third term becomes greater than -0.14). This threshold is crossed three times during the first 3000 hours, resulting in three landslide triggers i.e. three instances when a previously stable cell becomes unstable.

Figure 5.1.3 shows similar plots for Voronoi Cell 11311 with a slope angle of 30°. For this Voronoi cell, only one landslide is predicted in the first 3000 hours even through the soil moisture is greater over greater depths compared to Voronoi Cell 4091 (compare Figure 5.1.3a with 5.1.2a). While there is greater infiltration due to the lower slope angle, the sum of the first and second terms of the FS equation are considerably higher (0.95) at Cell 11311 than Cell

4091. This means that in order for a landslide to be predicted for Voronoi Cell Y, the soil moisture value has to be great enough to make the third term greater than or equal to -0.05. This occurs at about 500 hours, resulting in the single predicted landslide.

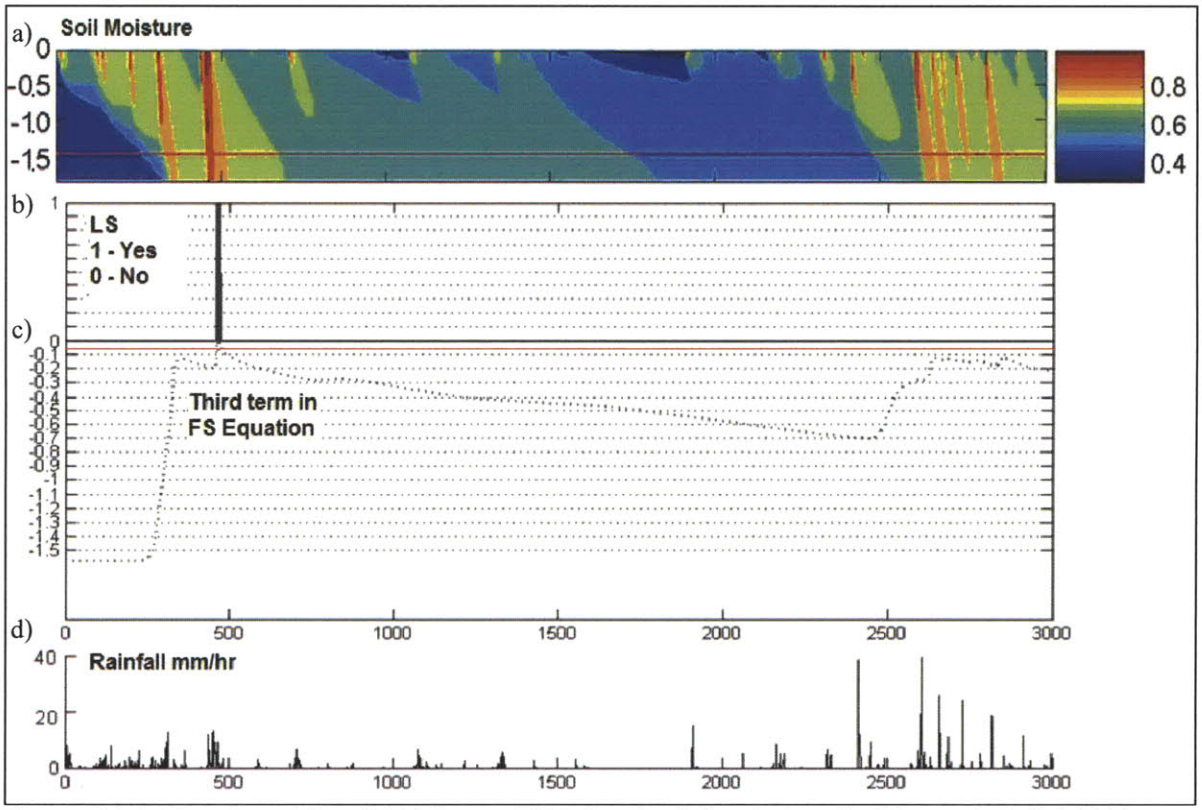

Figure 5.1.3: Results of first 3000 hours (125 days) of simulation for Voronoi Cell 11311 (slope angle of 30°). a) soil moisture, b) landslide occurrence, c) value of third term and d) hourly rainfall.

Figures 5.1.2 and 5.1.3 reaffirm that the slope angle and the soil moisture content are the key determinants of whether a landslide occurs or not. They reaffirm that landslides occur on steep slopes even in the absence of the soil moisture reaching saturation, and also that landslides occur on more gentle slopes if the soil becomes saturated. Whether or not a particular Voronoi cell becomes saturated is, of course, dependent not only on the properties of the Voronoi cell itself but also the interaction of the Voronoi cell with the surrounding cells.

Locations of predicted landslides

The locations of predicted landslides (i.e. the 48 Voronoi cells that reach a FS value less than 1 at least once) are shown in Figure 5.1.4. All of the predicted landslides are located in areas classified previously by Lepore et al. 2008b as the two highest susceptibility categories in the static susceptibility map, with the majority of slides occuring in the highest susceptibility category as shown in Figure 5.1.4. In terms of soil, all of the predicted landslides are shown to be in the loam category. This result is consistent with results from the sensitivity analysis reported in Section 4.2.

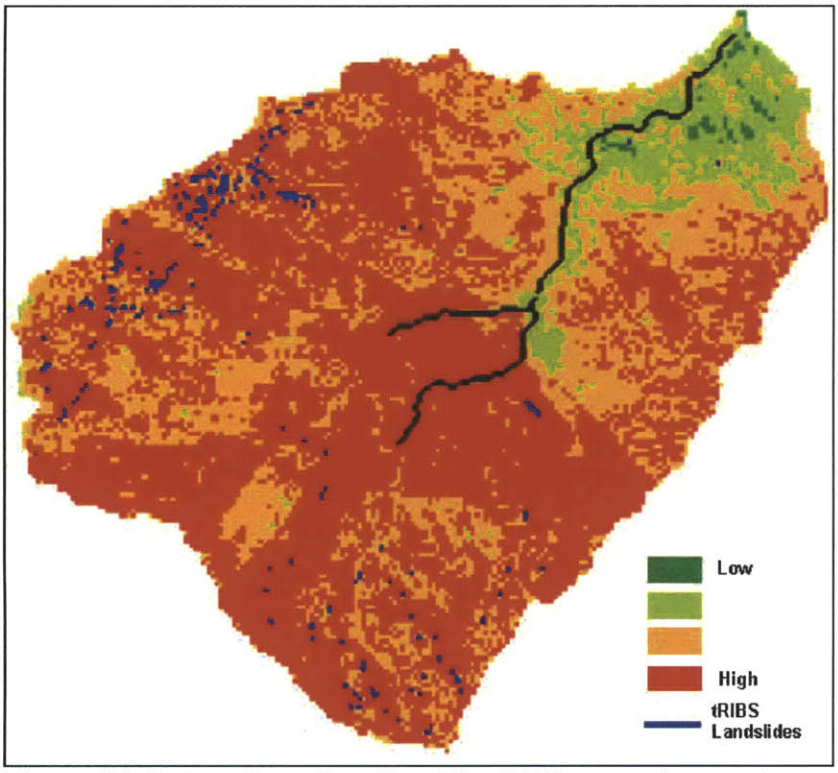

Figure 5.1.4: Location of predicted landslides superimposed on static susceptibility map from Lepore et al. (2008b)

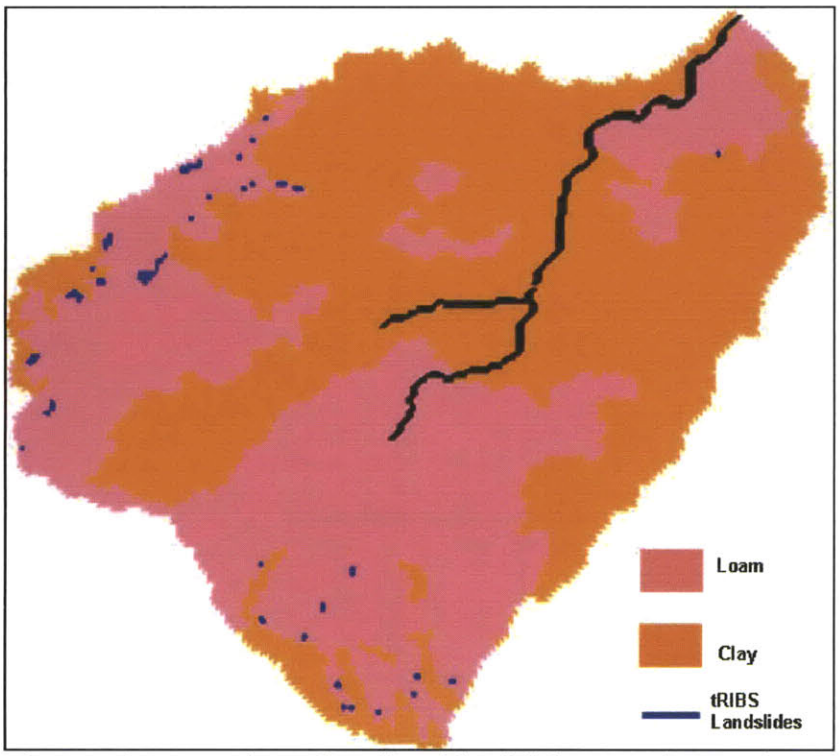

Figure 5.1.5: Location of predicted landslides superimposed on soil map. All failures occur in loam.

The results above indicate good agreement of the tRIBS/FS model results with the static susceptibility map developed previously in that all but one of the 48 predicted landslides are located in the two highest susceptibility categories. In terms of slope angle, there are several predicted landslides associated with steeper slopes, as well as an appreciable number of predicted landslides associated with gentler slopes, as shown in Figure 5.1.6. This slope angle distribution becomes clear by examining the slope angles for locations at which at least one landslide occurs (Figure 5.1.7.) The fact that a range of slope angle values are captured, and that landslides are not exclusively predicted on steep slopes, indicates that the tRIBS/FS algorithm combination developed in this work is able to capture the key dynamics associated with slope stability—i.e. the effects of both slope angle as well as soil moisture.

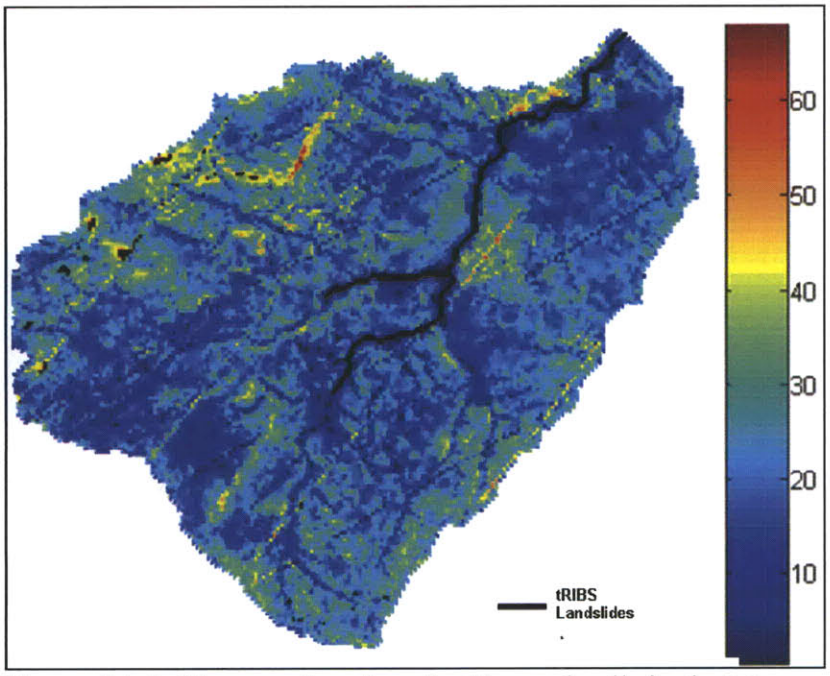

Figure 5.1.6: Slope angle values for Voronoi cells in the Mameyes basin. (Note: lines running southwest to northeast are an artifact of TIN orientation.)

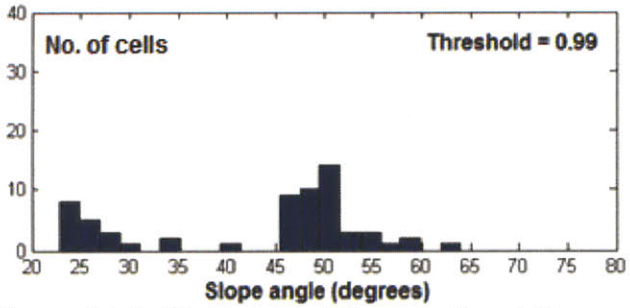

Figure 5.1.7: Histogram of slope angles at Voronoi cells with predicted landslides

A direct comparison between the location of historic landslides and predicted landslides is not necessarily desirable, since the historic landslides (1951 to 1990) predate the DEM used to derive the Voronoi cells. In reality, the basin has a dynamic land surface and current DEMs

may not reflect the past topography that resulted in the historic slides. Figure 5.1.8 shows a) the location of landslides predicted in this study next to b) locations of historic landslides superimposed on the susceptibility map by Lepore et al. (2008b). The predicted landslides appear to follow historic patterns in the west and southern part of the basin, but not the historic patterns along the southwest border of the basin. The reasons for this are not immediately clear, and some insight may be gained by considering the properties of the historic landslides in the southwest of the basin relative to the rest of the historic dataset. For example, if historic landslides in that region were typically shallower relative to other landslides and to the depth of failure in this study, then the lack of slides predicted in that region would make more sense. It is recommended that the properties of these historic landslides be explored in future work.

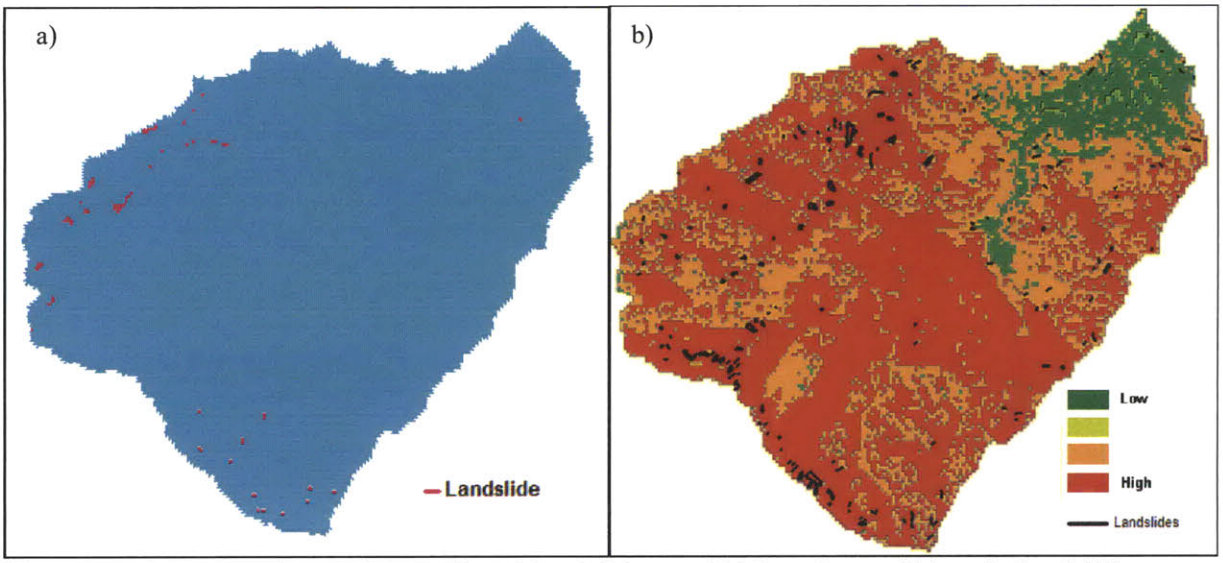

Figure 5.1.8: Comparison of a) predicted landslides and b) locations of historic landslides on susceptibility map by Lepore et al. (2008b)

Sensitivity of results to saturation threshold

The results above were obtained using a saturation threshold of 0.99. As discussed, the use of such a threshold is needed because the relative soil moisture in tRIBS cannot be numerically equal to 1. It is therefore important to understand the impact of the chosen saturation threshold on the overall results. The sensitivity analyses in this section consider how each of the following is affected by the saturation threshold: (a) the number of Voronoi cells at which at least a single landslide is predicted; (b) the number of landslides that are predicted and (c) the slope angles at which a landslide is predicted. Saturation thresholds of 0.999999, 0.99, 0.98 and 0.95 are considered.

(a) Voronoi cells at which a landslide is predicted

When a lower saturation threshold of 0.98 is applied, there is an increase in the number of Voronoi cells where landslides are predicted (i.e. that fail) as well as an increase in the number of landslides. This is consistent with intuitive expectations, since a lower relative saturation threshold means that more cells will be considered saturated and hence more likely to result in

a landslide. Alternatively, if the threshold for saturation is increased to 0.999999, fewer landslides are predicted. The number of cells that fail for saturation thresholds of 0.999999, 0.99, 0.98 and 0.95 are shown in Table 5.1.1.

Table 5.1.1: Impact of soil moisture saturation threshold on the number of Voronoi cells that fail at least once.

Saturation Threshold	Number of cells that fail
0.999999	43
0.99	63
0.98	70
0.95	211

There is an appreciable difference in the number of cells at which landslides are predicted when the saturation threshold is changed. The additional areas where landslides are predicted with lower thresholds are still almost entirely located in the two highest susceptibility categories given by Lepore et al. (2008b). With lower thresholds, many additional landslides are located in the northwestern and the southern parts of the basin, while an appreciable number of slides are added in the central part of the basin. Figure 5.1.8 shows the locations of landslides for saturation thresholds of 0.95 and 0.99. With a threshold of 0.95, landslides were also predicted in two clay cells. On the whole, it can be seen that the threshold affects not only the number of landslides, but also the spatial distribution. However, neither threshold results in a noticeably better match to the distribution of historical landslides shown in Figure 5.1.8.

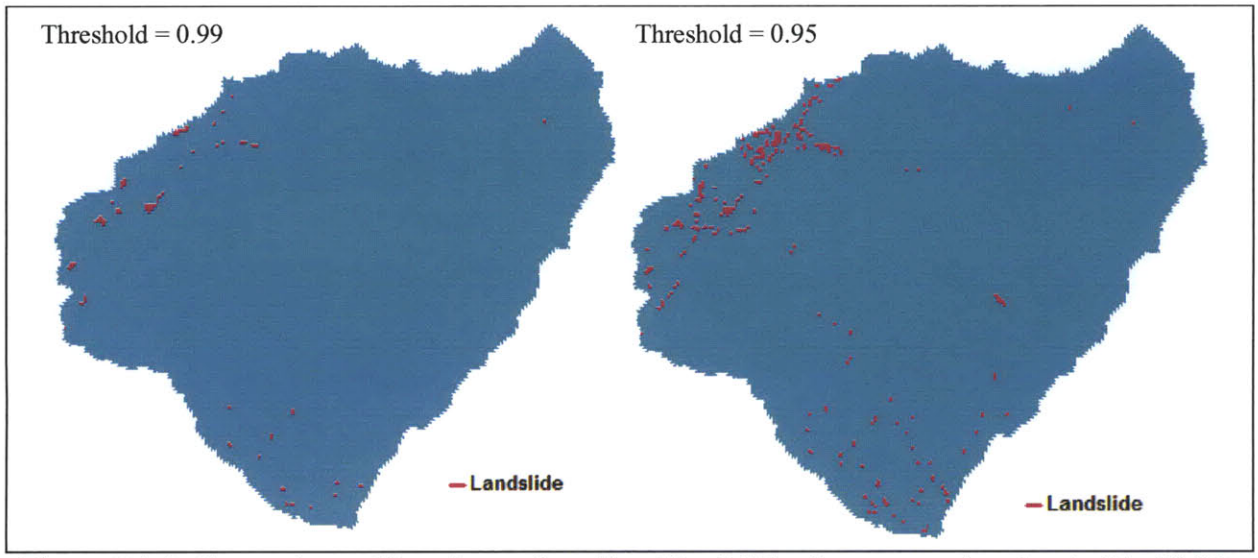

Figure 5.1.9: Comparison of locations of predicted landslides for a saturation threshold of 0.99 and a saturation threshold of 0.95.

(b) Number of landslides predicted

Table 5.1.1 shows the number of Voronoi cells that failed at least once. For some locations, more than one landslide trigger was predicted. With lower soil moisture thresholds, more landslides triggers are predicted, particularly after the synthesized storm event. The

synthesized rainfall event would be expected to increase the soil moisture across the basin significantly, and result in slides even for Voronoi cells that have low slope angles. It therefore makes intuitive sense that a lower soil moisture threshold would significantly increase the number of landslides observed in response to the synthesized rainfall event. A comparison of landslide triggers for saturation thresholds of 0.99 and 0.95 is shown in Figure 5.1.9. A similar trend was observed in landslide events.

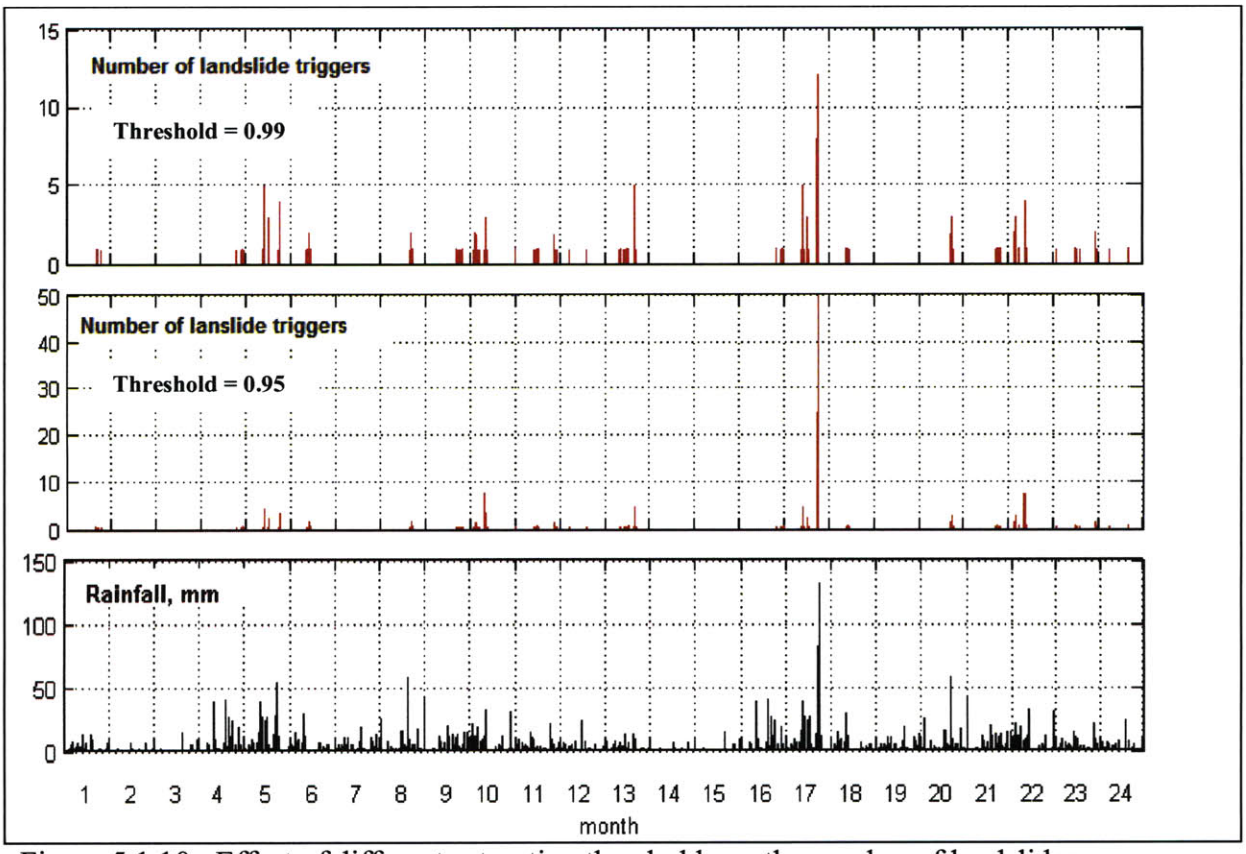

Figure 5.1.10: Effect of different saturation thresholds on the number of landslides

(c) *Slope angles at which a landslide is predicted.*

In addition to influencing the number of cells that fail, different saturation thresholds also influence the distribution of the slope angles for predicted failures. Histograms of the slope angles of cells that are predicted to fail are shown in Figure 5.1.10. As seen in the figure, only slopes above 45° are predicted to fail with a saturation threshold of 0.999999. When the saturation threshold is lowered to 0.99, cells that have low slope angles also become prone to failure. Failure at low slopes angles becomes dramatically more common when the threshold is lowered still more to 0.95. Again, a lower saturation threshold means that saturation will be reached in more cells, increasing the impact that the third term of the FS Equation has on the FS values. As seen in Figure 5.1.10, this impact can be significant enough to predict a landslide in cells with low slope angles that were considered stable with higher thresholds.

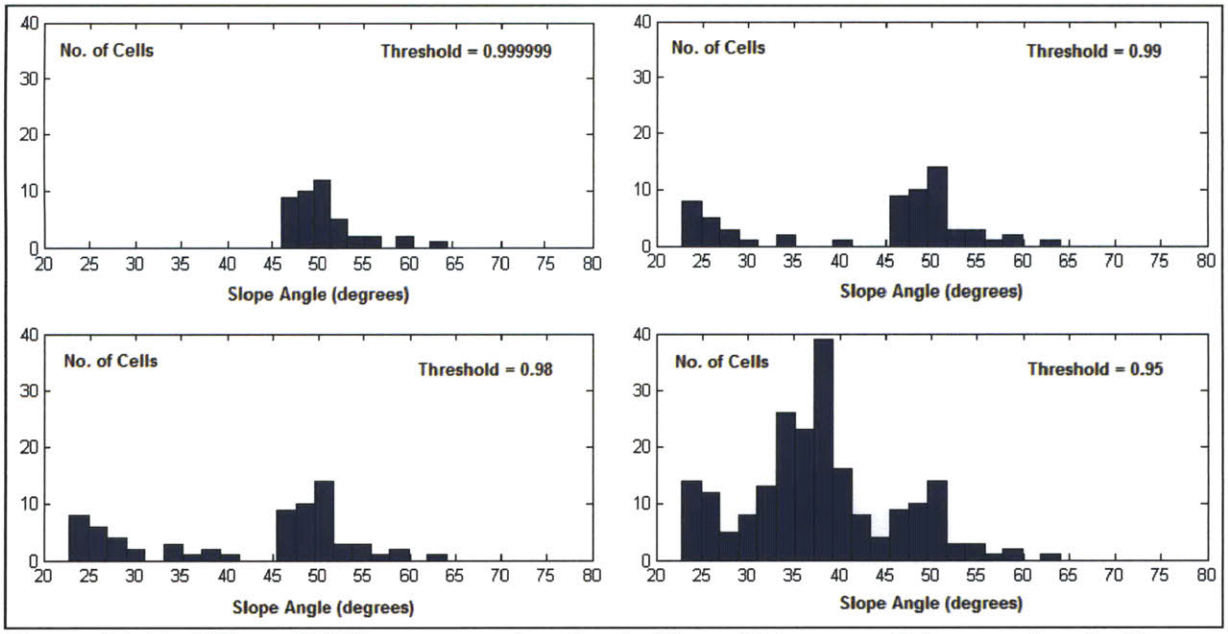

Figure 5.1.11: Effect of different saturation thresholds on histogram of slope angle of cells where landslides are predicted. The total number of cells for each threshold is given in Table 5.1.1.

Conclusion

The application of the off-line landslide component over the Mameyes basin yields landslide predictions in locations that are overwhelmingly located in the two highest susceptibility categories in the static susceptibility map developed previously by Lepore et al. 2008b. Employing a relative saturation threshold of 0.99 for when the soil is considered "fully saturated," 48 out of 13,169 Voronoi cells were predicted to fail at least once, with predicted landslides occurring in response to significant rainfall events. The slope angle and the soil moisture are the key determinants of whether a landslide with occur. The average slope angle at Voronoi cells with predicted landslides is high (43°). However, landslides are also predicted at Voronoi cells with slope angles as low as 23°, indicating that soil moisture also plays an important role in the FS algorithm as formulated.

The results demonstrate that the tRIBS/FS algorithm combination developed in this work is able to capture the key dynamics associated with slope stability. The results depend appreciably on the threshold value selected for soil moisture saturation. While there is no strict rule governing the selection of a particular saturation threshold, it is desirable that the threshold be set such that predicted landslides are not exclusively limited to Voronoi cells with very high slope angle values. Indeed, Simon et al. (1999) found the mean slope angle for 150 slides in the LEF to be at around 36.6°, with 8% occurring at slope angle values less than 30°. A saturation threshold of 0.99 captures an appreciable number of slides at lower slope angle values and therefore appears to be a reasonable value for the saturation threshold. Given the errors in the tRIBS model, one possibility is to approach this threshold issue as a probability matching exercise.

5.2 Future Work

The results reported in Section 5.1 demonstrate that the tRIBS/FS algorithm combination developed in this work is able to capture the key dynamics associated with slope stability and specifically the important effects of both slope angle and soil moisture. This section firstly addresses limitations of the current work, in order to provide context to the preceding results as well as guide perspectives for future work. Since this work has demonstrated that the tRIBS/FS algorithm combination can effectively capture key aspects of slope stability, future work should focus on further refinement of the basin as it is developed in the tRIBS framework and on the FS algorithm itself. Refinements to the basin in the tRIBS framework include more detailed parameterization of the basin, the application of a TIN resolution most appropriate to the scale of landslide events, and a more complete validation of the modeled basin's response. Further improvements in the FS algorithm include the incorporation of more localized values for soil cohesion, and, if the study of shallow landslides is desirable, the incorporation of the root reinforcement mechanism for slope stability.

Limitations of current work

Characteristic scale of landslide events vs. resolution of modeled basin

Prior work by the author and other, focusing on the use of the bivariate frequency ratio, concluded that slope angle was the dominant factor in determining static susceptibility to landslides in Puerto Rico (Lepore at al. 2008b). Lepore et al. (2008b) also highlighted issues around the resolution of the DEM used to infer static susceptibility. Specifically, the "characteristic scale" of a landslide for a particular dataset was found to be dependent to a large extent on the spatial resolution of the DEM employed. A relatively shallow landslide is not typically as wide or as long as a relatively deep landslide. The length and width of a potentially unstable slope has a lower limit defined by the highest resolution (i.e. smallest grid size) of the DEM. Thus, only slides as deep as the depth corresponding to that length or width can be captured (Lepore et al. 2008b).

This issue of resolution has significant implications for the current work, since the tRIBS model is based on Voronoi cells of varying sizes. The use of the tRIBS framework allows for the discretization of the Mameyes basin into Voronoi cells of different dimensions and areas. The resulting TIN (Triangular Irregular Network) with multiple resolutions offers advantages over the use of a traditional grid-based approach, in particular computational savings in areas of low terrain variability (Goodrich 1991). From the perspective of landslides, the use of a TIN-based approach means that hillslopes that are expected to have low susceptibility to begin with can be assigned a coarser resolution than more susceptible areas. However, one effect of this is that the definition of a landslide event in this modeling framework becomes dependent on the size of the Voronoi cell. In other words, if the size of the Voronoi cell is above a certain threshold, there is a corresponding lower limit on the depth of the landslides that could be predicted for that Voronoi cell.

The issue of characteristic scale is best visualized by the following theoretical argument. Consider that an ant walking over a sand pile and causing a slope failure could also be

considered a "landslide" at a small enough scale. If the area around the ant is depicted by a Voronoi cell with the same area as an automobile, it is intuitively clear that any slope instability caused by the ant will not register on the scale of the automobile i.e. will not be considered a "landslide" in the Voronoi cell. However, if the Voronoi cell was slightly larger than the ant, the instability of the slope caused by the ant would suddenly be considered very significant and would be considered a "landslide."

Stated simply, the shallower landslides that are common in Puerto Rico (Simon et al. 1990) are not captured by this study in areas represented by larger Voronoi cells. Effectively, this means that the lower threshold for what defines a landslide event changes throughout the basin. It also means that low susceptibility for large Voronoi cells does not translate to low susceptibility for landslides on a smaller scale that occur within the Voronoi cells. This needs to be accounted for in future work, specifically through the definition of the TIN resolution based on the depth to failure, which is further later in this section.

Temporal discrepancies across datasets

One inherent limitation in work that attempts to consolidate data from different sources (particularly remotely sensed products) is that the data are often obtained at different points in time and thus may not represent actual hillslope conditions at time periods when the model is initialized. In addition, this work does not address hillslope movement and landslide debris transport. This means that once a cell is considered susceptible to landslides there is no mechanism to transport the landslide debris and hence make the hillslope stable again for further analysis.

Saturated zone hydrology in the tRIBS framework

As discussed in Section 5.1, the tRIBS model cannot numerically reach a soil moisture state with an exact value of 1. Because of this limitation, the tRIBS model also cannot simulate the location of the water table. As demonstrated in Section 4.2, the FS value is very sensitive to soil moisture and in particular to the location of the water table. In the absence of a water table depth, it became necessary to estimate the height of the saturated layer above the failure plane as an approximation of the water table. Similarly, the fact that the soil moisture cannot reach a relative soil moisture state of 1 is addressed through the definition of a saturation threshold, with the caveat that different thresholds for what defines "saturation" have a significant impact on whether a landslide will be predicted or not.

Future Work

Barring the broader limitations listed above, there are some key areas that should be addressed in future work. These include refining the Mameyes basin as developed in the tRIBS framework, refining the tRIBS framework itself to better incorporate saturated zone hydrology, and employing localized values for terms such as soil cohesion in the FS Equation. These areas for future work are discussed below.

Refinements to Mameyes basin model in tRIBS

Definition of TIN based on depth to failure

A limitation of this work in that the spatial definition of what constitutes a "landslide" is determined by the size of the Voronoi cell is discussed above. It is therefore proposed that future work initialize the resolution of the TIN based on the desired depth to failure. This would require that the length and width of each Voronoi cell be consistent with the depth of landslides being studied i.e. consistent with the characteristic scale of a landslide with that particular depth. Simon et al. (1990) found specific depths in the soil profile that can act as potential slip surfaces. For each potential slip depth, a TIN with a resolution consistent with that depth is recommended for future work.

Refinement of soil data

Several simplifying assumptions have been made in how the soil is represented in the tRIBS framework. For simplicity, the Mameyes basin is currently represented by two major soil types (clay and loam). It is further assumed the properties of each soil type remain homogenous over the modeled depth of 2m. Simon et al. (1990) indicate that the depth to bedrock for the two dominant rock types in the LEF is 11m and 12m. It is desirable to incorporate this depth to bedrock in future work, since the distribution of soil moisture over the soil column is influenced by the presence of the bedrock. Definition of this depth to bedrock is also important because the very bottom soil layer in the tRIBS framework (centered at 1.883m) is defined as having an open drain boundary condition, which means that all of the water in the layer "drains out" and is not recovered. The presence of this boundary condition likely has significant impacts on soil moisture distribution at the failure depth.

The USDA (2002) documents properties of specific soil units including vertical soil profiles that separate each soil unit into layers with different soil properties. While recent improvements in the tRIBS framework allow for the vertical division of the soil into layers such that each layer has unique soil properties (Bisht et al., in preparation) these capabilities have not been fully employed in the current work. Major differences between soils that occur within the same soil type could be accounted for using this improved framework. Inclusion of these differences within each soil type would present a more representative hydrological picture of the basin, which in turn would lead to more representative soil moisture values.

Refinement of rainfall data

For this work it was assumed that rainfall is uniform over the entire Mameyes basin at the rates measured at Bisley tower. Prior studies have highlighted the differences in rainfall received at different elevations and locations in the LEF, and have related these differences to landslide occurrences (Simon et al. 1990). Since data from two locations close to the Mameyes basin (El Verde and East Peak) are also available for several continuous years, it is possible to employ interpolation techniques in order to establish an hourly rainfall profile across the basin.

Use of NASA's real-time precipitation products

In moving towards real-time dynamic susceptibility determinations, the use of rainfall data from NASA's existing TRMM (Tropical Rainfall Measuring Mission) product and upcoming GPM (Global Precipitation Mission) can be explored in future work. One limitation repeatedly identified in the use of distributed models that are forced by precipitation estimates is that real-time daily precipitation estimates are currently too coarse in time and space for accurate landslide prediction (Casadei et al. 2003). The upcoming NASA GPM product may present an opportunity to improve modeling of infiltration and lateral moisture redistribution, and hence improve modeling of landslides. Precipitation datasets comprising data on a temporal and spatial scale consistent with the TRMM and GPM products can be synthesized from existing hourly data. The tRIBS and off-line landslide component combination can then be run using these precipitation data sets. This exercise can contribute toward identifying the spatial and temporal resolution of real-time precipitation data required to adequately resolve the spatial variability in soil moisture for landslide prediction.

Refinement of BET Tropical vegetation class

The BET Tropical vegetation class developed in this work effectively captures key aspects of the vegetation dynamics at the Mameyes basin, as indicated by the LAI and vegetation fractions observed. As mentioned in Section 3.2 the initial carbon pool values assigned to the canopy, stems and roots play a key role in obtaining the desired LAI, which was a key indicator used to validate the initialization of vegetation parameters. While ten-year simulations were run to validate the long-term impacts of employing these initial carbon pool values, literature on vegetation dynamics in tropical forests in South America (Saldarriaga et al. 1988) documents a near-linear increase in above-ground living biomass during the first forty years. Therefore, it is recommended that the carbon pool values, particularly for the stems and the roots, be initialized based on simulations that are carried through to a time period consistent with the age of the forest in the Mameyes basin at the desired simulation start date.

Literature on the LEF highlights that Hurricane Hugo caused extensive damage to the forest in September 1989 (Lugo 1999). In particular, a high mortality rate—about 50%—of trees was observed near the Bisley tower site. This suggests that a significant portion of the forest is at least 20 years old, with the remaining portion being even older. Accounting for the actual age of the forest is likely to increase the sensitivity of the FS Equation to vegetation, and would involve a more thorough selection of the initial carbon pools and vegetation simulations carried out to a longer time period. Average ages for stems in different parts of the LEF are documented by Scatena and Lugo (1995), while the relation between biomass and the age of tropical forests is address by Weaver (1990).

Detailed validation of Mameyes basin response

As mentioned in Section 3.3, some key indicators were used to perform a first-cut validation of the constructed model for the Mameyes basin. These key indicators were the soil moisture, LAI, and heat flux values. The first two indicators were important from a slope stability perspective, while the later were important to ensure that numerical instabilities did not occur.

A more detailed validation and calibration of the model would firstly involve correlating the predicted basin discharge to the actual basin discharge. Future work should consider a more detailed validation of the model, such as the validation performed for the Walnut Gulch basin (Bisht et al., under preparation).

Further development of landslide component

The first-cut landslide component developed in this work presents a simplified treatment of the factor of safety equation and employs typical values for the parameters not explicitly output by the tRIBS model. Those typical values are applied uniformly across the basin. Where possible, it is recommended that field-measured values specific to the hillslope under consideration be employed in future applications of the landslide component. This would include the value for soil cohesion as discussed in further detail below.

Values for soil cohesion

The soil cohesion values in the current landslide component have been set to a value of 7.79 kPa for clay and 5.37 kPa for loam, representing an average of soil cohesion values determined by Simon et al. (1990). Based on the sensitivity analysis in Section 4.2, it is clear that the value assigned for soil cohesion has a big impact on the calculated FS values. The cohesive strength of soil is currently assumed to be constant throughout the basin, but soil tests in the LEF have demonstrated that there is considerable variation in these values (Simon et al. 1990).

Since the NRCS Soil Survey (USDA 2002) provides some information with regard to soil types encountered at different depths over the LEF, a correlation between tensile strengths documented by Simon et al. to the soil types in the Soil Survey is suggested. The correlation analysis should consider the location and depth at which the tensile strengths were recorded. For example, it is expected that the tensile strengths at the saprolite layer described by Simon et al. (1990) will be considerably lower due to factors such as soil weathering. If more representative tensile strength values for potential failure depths can be determined and incorporated into the FS algorithm, it would greatly improve the accuracy of the landslide component.

Root Reinforcement

Root reinforcement was assumed to be negligible in the current work, but may prove to be significant in studies for areas with greater root depths or higher-resolution modeling where landslides on a smaller scale (i.e. with shallower failure planes) can be captured. Indeed, a majority of landslides caused by Hurricane Hugo occurred at a depth of approximately 0.5m (Larsen 1990). Simon et al. (1990) noted an increase in shear strength in the first 25cm of specific soils that they tested and attributed this increase to the presence of dense root mats in the root zone.

The incorporation of root reinforcement in the FS equation has been address by Greenway (1987), who applies a model developed by Wu (1979) that predicts the shear strength increase

(Δs) due to the presence of roots and presents a framework for determining the root cohesion term. A simplified version of this equation, presented by Wu et al. (1979) and reproduced in Greenway (1987) is:

$$\Delta s = 1.2 * T_r * (A_r / A) \quad (5.2.1)$$

Where T_r is the mean tensile strength of the roots and (A_r/A) represents a root area ratio where A_r is the total cross-sectional area of all roots in a given cross section of soil and A is the area of the soil cross section considered. The value of 1.2 represents a typical value that incorporates the interplay between the angle of internal friction of the soil and the angle of shear distortion in the shear zone.

As a first cut, typical values of tensile strengths for tree roots and root area ratios that were documented for different forest types by Greenway (1987) can be employed. While there is no overlap between the tree species studied by Greenway and those present in the Mameyes basin, estimates of values can be made from tree species that have similar characteristics. Ultimately, employing tensile strength and root area ratios specific to the tree types found in the Mameyes basin would best quantify the stabilizing effects (if any) of these roots. To this end, prior studies that examine the relationship between vegetation and geomorphology in the LEF (e.g. Scatena and Lugo 1995) may provide greater insight.

REFERENCES

Arora, Vivek. (2002). Modeling Vegetation as a Dynamic Component in Soil - Vegetation - Atmosphere Transfer Schemes and Hydrological Models. *Reviews of Geophysics,* 40.2.

Bisht, G., Sivandran, U., Narayan, U., Ivanov, V. Y., and Bras, R. L. (To be submitted), Confirmation of a distributed, physically based eco-hydrologic model in a semi-arid region, *Water Resources Research.*

Bonan, G. B. (1996). A land surface model (LSM version 1.0) for ecological, hydrological, and atmospheric studies: technical description and user's guide. *NCAR Technical Note NCAR/TN-417+STR. National Center for Atmospheric Research.*

Bonan, G.B., and Levis, S. (2002). Landscapes as patches of plant functional types: An integrating concept for climate and ecosystem models. *Global Biochemical Cycles,* 16.2.

Brooks, R.H., and Corey, A.J. (1964). Hydraulic properties of porous media. *Hydrology Paper 3, Civil Engineering Department, Colorado State University, Fort Collins, CO.*

Brown, C.B., and Sheua, M.S. (1975). Effects of deforestation on slopes. *ASCE Journal of Geotechnical Engineering.* 101, GT2: 695-699.

Brown, S., Lugo A. E., Silander S. and Liegel L. (1983). Research history and opportunities in the Luquillo Experimental Forest. *U.S. Department of Agriculture Forest Service, General Technical Report SO-44, Southern Forest Experiment Station, New Orleans, LA,* 128.

Caine, N. (1980). The rainfall intensity-duration control of shallow landslides and debris flows. *Geografiska Annaler*, 62A, 23-27.

Casadei, M., Dietrich, W.E., and Miller, N.L. (2003). Testing a model for predicting the timing and location of shallow landslide initiation in soil-mantled landscapes, *Earth Surface Processes and Landforms*, 28, 925-950.

Cosby, B.G., Hornberger, M., Clapp, B., Ndt, A. and Ginn, R. (1984). A Statistical Exploration of the Relationships of Soil Moisture Characteristics to the Physical Properties of Soils. *Water Resources Research*, 20.6, 682-690.

Dickinson, R.E., Shaikh, M., Bryant, R., and Graumlich, L. (1998). Interactive canopies for a climate model. *Journal of Climate*, 11, 2823-2836.

Dietrich, W.E., Reiss, R., Hsu, M.L. and Montgomery, D.R. (1995). A process-based model for colluvial soil depth and shallow landsliding using digital elevation data. In: Scale issues in hydrological modeling. Kalma, J.D and Sivaplan, M. (Eds.), *John Wiley & Sons: New York.*

Duncan, J.M. (1996). Soil Slope Stability Analysis. In: Schuster, R.L and Krizek, R.J. (1978). Landslides, Analysis and Control. *National Research Council, Transportation Research Board, Special Report,* 176, 12-33.

Friend, A.D., Stevens, A.K., Knox, R.G. and Cannell, M.G.R. (1997). A process-based terrestrial biosphere model of ecosystem dynamics (Hybrid v3.0). *Ecological Modeling* 95, 249–287.

Goodrich, D. C., Woolhiser, D. A., and Keefer, T. O. (1991). Kinematic routing using finite elements on a triangular irregular network, *Water Resources Research*, 27, 995 - 1003.

Greenway, D. R. (1987). Vegetation and Slop Stability in: Slope Stability: Geotechnical Engineering and Geomorphology, Anderson, M.G., Richards, K.S. (Eds), 187-230, *John Wiley & Sons, New York.*

Gregory, K.J., and Walling, D.E. (1973). Drainage Basin Form and Process: A Geomorphological Approach. *Edward Arnold, London.*

Gu L., Riggs, J.S., Sluss, D., Wullschleger, S.D., Yang, B., Heuer, M., Meyers, T., Pallardy, S.G., Hosman, K.P., Liu, Q., and Hanson, P.J. (2007). Influences of biomass heat and biochemical energy storages on the land surface fluxes and radiative temperature. *Journal of Geophysical Research*. 112.D02107.

Gulden, L.E., and Yang Z. (2006). Development of species-based, regional emission capacities for simulation of biogenic volatile organic compound emissions in land-surface models: An example from Texas, USA. *Atmospheric Environment,* 40.8, 1464-1479.

Helmer, E. H., Ramos O.R., López T.M., Quiñones, M., and Diaz, W. (2002). Mapping forest type and land cover of Puerto Rico, a component of the Caribbean biodiversity hotspot. *Caribbean Journal of Science*, 38, 165-183.

Istanbulluoglu, E., and Bras, R.L. (2005). Vegetation-modulated landscape evolution: Effects of vegetation on landscape processes, drainage density, and topography, *Journal of Geophysical Research*, 110.

Ivanov, N.Y., Vivoni, E.R., Bras, R.L. and Entkabi, D. (2004). Catchment hydrologic response with a fully distributed triangulated irregular network model. *Water Resources Research.,* 40, W11102.

Ivanov, V. Y. (2006). Effects of dynamic vegetation and topography on hydrological processes in semi-arid areas. *Thesis (Ph. D.) - Dept. of Civil and Environmental Engineering, Massachusetts Institute of Technology.*

Iverson, R.M. (2000). Landslide triggering by rainfall infiltration, *Water Resources Research*, 36, 1897-1910.

Kamal, S. (2008). Development of a Landslide Hazard Map for the Island of Puerto Rico. *Thesis - Department of Civil and Environmental Engineering, Massachusetts Institute of Technology.*

Larsen, M.C., and Simon, A. (1993). Rainfall-threshold conditions for landslides in a humid-tropical system, Puerto Rico, *Geografiska Annaler*, 75A, 13-23.

Larsen, M.C., and Torres-Sanchez, A.J. (1998). The frequency and distribution of recent landslides in three montane tropical regions of Puerto Rico, *Geomorphology*, 24, 309-331.

Lepore, C., Kamal, S., Bono, E., Noto, V., Shanahan, P., and R. L. Bras (2008). Data Resolution Effects on Landslides Hazard and Susceptibility Assessment of Puerto Rico. *American Geographical Union, Fall Meeting*, H51F-0882.

Lepore, C., Bono, E., Noto V., and R.L. Bras. (2008). Rainfall Induced Landslides Susceptibility and Hazard Assessment in Puerto Rico. *NASA PMM Science Meeting.*

"Long Term Ecological Research Network", <http://www.lternet.edu> (10 Apr 2009).

Lugo, A. E., Scatena, F., and Jordan, C.F. (1999). NPP Tropical Forest: Luquillo, Puerto Rico, 1963-1994. *Oak Ridge National Laboratory Distributed Active Archive Center, Oak Ridge, Tennessee, U.S.A.*

Moorcroft, P.R., Pascala, S.W., and Hurtt, G.C. (2001). A Method for scaling vegetation dynamics: The Ecosystem Demography Model. *Ecological Monographs,* 71(4), 557–586

Odum, H. T. 1970. Summary: an emerging view of the ecological system at El Verde. *In* H. T. Odum and R.F. Pedgeon (Eds.) 1970. A tropical rain forest, USAEC, TID-24720.

Oleson, K. W., Dai, Y., Bonan, G., Bosilovich, M., Dickinson, R., Dirmeyer, P., Hoffman, F., Levis, S., Niu, G. Y., Thornton, P., Vertenstein, M., Yang, Z. L., and Zeng, X. (2004). Technical Description of the Community Land Model (CLM). *NCAR Technical Note (NCAR/TN-461+STR).*

Oleson, K. W., Niu, G. Y., Yang, Z. L., Lawrence, D.M., Thornton, P., Lawrence, P.J., Stöckli, R., Dickinson, R., Bonan, G., Levis, S., Dai, Y., and Qian, T. (2008), Improvements to the Community Land Model and their impact on the hydrological cycle. *Journal of Geophysical Research.*, 113, G01021.

Saldarriaga, J. G., West. D.C., Tharp. M.L., and Uhl, C. (1988). Long-term chronosequence of forest succession in the upper Rio Negro of Colombia and Venezuela. *Journal of Ecology*, 76, 938–958.

Pando, M. A., Ruiz, M. E., and Larsen, M. C. (2005). Rainfall-Induced Landslides in Puerto Rico: An Overview. In: Gabr, M.A., Bowders, J.J., Elton D., and Zornberg, J.G. (Eds). *Geotechnical Special Publication No. 140, Slopes and Retaining Structures under Seismic and Static Conditions. Proceedings of Sessions of the Geo-Frontiers 2005 Congress, Jan. 24–26, 2005, Austin, Texas. ASCE, Reston, VA.*

Rawls, W.J., Brakensiek, D.L., and Saxton, K.E. (1982). Estimation of Soilwater Properties. *Transactions of the ASAE*, 25.5, 1316-1320.

Rutter, A.J., Kershaw, K.A., Robins, P.C., and Morton, A.J. (1971). A predictive model of rainfall interception in forests. Derivation of the model from observation in a plantation of Corsican pine. *Agriculture Meteorology,* 9, 367-384.

Rutter, A.J., Morton, A.J., and Robins, P.C. (1975). Predictive model of rainfall interception in forests. 2. Generalization of model and comparison with observations in some coniferous and hardwood stands. *Journal of Applied Ecology,* 12.1, 367-380.

Saldarriaga, J.G., West, D.C., Tharp, M. L. and Uhl, C. (1988). Long-Term Chronosequence of Forest Succession in the Upper Rio Negro of Colombia and Venezuela. *Journal of Ecology*, 76.4 938-958.

Scatena, F.N., and Lugo, A. E. (1995). Geomorphology, disturbance, and the soil and vegetation of two subtropical wet steepland watersheds of Puerto Rico. *Geomorphology,* 13, 199-213.

Schellekens, J., Scatena, F. N., Bruijnzeel, L. A. and Wickel, A. J. (1999). Modelling rainfall interception by a lowland tropical rain forest in north-eastern Puerto Rico. *Journal of Hydrology*, 225, 168-184.

Schuster, R.L and Krizek, R.J. (1978). Landslides, Analysis and Control. *National Research Council, Transportation Research Board, Special Report,* 176, 12-33.

Selby, M.J. (1993). Hillslope Materials and Processes. *Oxford University Press: Oxford.*

Selby, M.J. (1994). Hillslope sediment transport and deposition, In: Pye, K. (1994). Sediment transport and depositional processes. *Blackwell Science*, 61-87.

Simon, A., Larsen, M. C., and Hupp, C. R. (1990). The role of soil processes in determining mechanisms of slope failure and hillslope development in a humid-tropical forest: eastern Puerto Rico. In: Kneuper, P.L.K., McFadden, L.D. (Eds), Soils and Landscape evolution, *Geomorphology*, 3, 263-286.

"Soil Data Mart – Home". United States Department of Agriculture - National Resources Conservation Service. <http://soildatamart.nrcs.usda.gov> (10 Apr 2009).

Terzaghi, K., Erdbaumechanik, *Franz Deuticke, Vienna*, 1925.

Tsukamoto, Y., and Kusakabe, O. (1984). Vegetative influences on debris slide occurrences on steep slopes in Japan, *Proceeding Symposium on Effects of Forest Land Use on Erosion and Slope Stability, Environmental and Policy Institute, Honolulu, Hawaii.* 1, 156–160.

U.S. Army Corps of Engineers, (1960). Trafficability Predictions in tropical soils-Puerto Rico study, *Waterways Experimental Station Miscellaneous Paper.* No. 4-355, *Rept 2, Viskburg, Mississippi,* 72.

USDA (2002). Soil Survey of Caribbean National Forest and Luquillo Experimental Forest, Commonwealth of Puerto Rico, Natural Resources Conservation Service, Washington, DC.

USDA Forest Service and US Geological Survey. Forest Cover Types of the United States. United States Department of Interior. Web. May 2002. 1 Aug. 2009. <http://nationalatlas.gov/atlasftp.html>.

Van der Molen, M. K. (2002). Meteorological Impacts of Land Use Change in the Maritime Tropics. *Thesis (Ph. D.) - Faculty of Earth and Life Science, Vrije Universiteit Amsterdam.*

Varnes, D. J. (1996). Slope Movement Types and Processes. In: Schuster, R.L and Krizek, R.J., Landslides, Analysis and Control. *National Research Council, Transportation Research Board, Special Report*, 176, 12-33.

Walker, L.R. (1991). Tree Damage and Recovery From Hurricane Hugo in Luquillo Experimental Forest, Puerto Rico. *Biotropica*, 23.4A, 379-385.

Wang, H., and Hall, C.A.S. (2004). Modeling the effects of Hurricane Hugo on spatial and temporal variation in primary productivity and soil carbon and nitrogen in the Luquillo Experimental Forest, Puerto Rico. *Plant and Soil.* 263.1, 69-84.

Weaver, P.L., and Murphy, P.G. (1990). Forest Structure and Productivity in Puerto Rico's Luquillo Mountains. *Biotropica*, 22.1, 69-82.

Wieczorek, G.F. (1996). Landslide Triggering Mechanisms. In: Schuster, R.L and Krizek, R.J., Landslides, Analysis and Control. *National Research Council, Transportation Research Board, Special Report* 176, 12-33.

Wilson, M.F., Henderson-Sellers, A., Dickinson, R.E., and Kennedy, P.J. (1987). Sensitivity of the Biosphere–Atmosphere Transfer Scheme (BATS) to the Inclusion of Variable Soil Characteristics. *Journal of Applied Meteorology,* 341-362.

Wu, T. H., McKinnell, W. P., and Swanston, D.N. (1979). Strength of tree roots and landslides on Prince of Wales Island, Alaska. *Canadian Geotechnical Journal,* 16, 19-33.

Ziemer, R. R. (1981). Roots and the stability of forested slopes. *In:* Davies, T.R.H. and J. Pearce, A.J. (Eds.), Erosion and Sediment Transport in Pacific Rim Steeplands, Proceedings of the Christchurch Symposium, 25-31 January 1981, Christchurch, New Zealand. *International Association of Hydrology Science*, 132, 343-361.

APPENDIX A: KEY tRIBS INPUT FILES FOR ELEMENT RUNS

VEGETATION PARAMETERS

```
## Number of PFTs considered (##THERE MUST BE_NO_SPACES AFTER LAST
VALUE##)
3
## Phenotypes: 'G'-grass,   'B'-Broadleaf, 'N'-needleleaf
          'C3'-C3 type  'D'-deciduous, 'E'-evergreen
          'C4'-C4 type  'T'-tropical,'M'-temperate,'B'-Boreal,'D'-Drought
BDD  BDD  GC4

GENERAL_VEGETATION_PARAMETERS:
/=/=/=/=/=/=/=/=/=/=/=/=/=/=/=/=/=/=/=/=/=/=/=/=/=/=/=/=/=/=/=/=/=/
## Number of parameters (variables) in this group
14
## Mean leaf size of mature plant                (dleaf)          [m]
0.04  0.04  0.005
## Leaf orientation par-r (-1-vert. 0-random 1-horiz.) (chiL)          [-]
0.01  0.01  -0.30
##    Leaf reflectance in VIS range              (alf_lf_vis)      [-]
0.10  0.10  0.11
##    Leaf reflectance in NIR range              (alf_lf_nir)      [-]
0.45  0.45  0.58
##    Stem reflectance in VIS range              (alf_st_vis)      [-]
0.16  0.16  0.36
##    Stem reflectance in NIR range              (alf_st_nir)      [-]
0.39  0.39  0.58
##    Leaf transmittance in VIS range            (tau_lf_vis)      [-]
0.05  0.05  0.07
##    Leaf transmittance in NIR range            (tau_lf_nir)      [-]
0.25  0.25  0.25
##    Stem transmittance in VIS range            (tau_st_vis)      [-]
0.001  0.001  0.22
##    Stem transmittance in NIR range            (tau_st_nir)      [-]
0.001  0.001  0.38
## Canopy drainage coefficient                   (KCanDrain)       [-]
0.18  0.18  0.10
## Canopy drainage exponent                      (KCanExp)         [-]
3.9   3.9   3.2
## Specific leaf area              (SLA)         [m^2 leaf g C^-1]
0.0155  0.0155  0.020
##    Type of root distribution       (1-UNF, 2-EXP, 3-PWR, 4-FREE)   [-]
2   2   0
```

```
PHOTOSYNTHESIS_PARAMETERS:
/=/=/=/=/=/=/=/=/=/=/=/=/=/=/=/=/=/=/=/=/=/=/=/=/=/=/=/=/=/=/=/=/=/=/=/=/=/=/
## Number of parameters in this group
5
## Max non-strs catalytic capac. of Rubisco enz. (Vmax25) [umol CO2 m^-2 s^-1]
40   40   35.0
## Canopy nitrogen decay rate (Kmean) to parameterize the decay of Vmax25  [-]
0.5     0.5     0.3
## Stomatal slope factor: (m) 9 - C3; 4 - C4; 6 - coniferous              [-]
9       9       4
## Minimum conductance    (b): 1.0E+4 - C3; 4.0E+4 - C4   [umol CO2 m^-2 s^-1]
1.0E+4  1.0E+4  4.0E+4
## Quantum effic. of CO2 uptake: 0.08 - C3; 0.05 - C4 [mol CO2 mol^-1 photons]
0.08    0.08    0.053

RESPIRATION_TURNOVER_PARAMETERS:
/=/=/=/=/=/=/=/=/=/=/=/=/=/=/=/=/=/=/=/=/=/=/=/=/=/=/=/=/=/=/=/=/=/=/=/=/=/=/
## Number of parameters in this group
11
## SAPWOOD Respiration rate   (r*k/C:N ratio) (rkstem) 10^oC [g C g C^-1 s^-1]
4.76E-10   4.76E-10   250.0E-10
## FINE ROOT Respiration rate (r*k/C:N ratio) (rkroot) 10^oC [g C g C^-1 s^-1]
1.74E-9  1.74E-9  250.0E-10
## Fraction of (GPP-Rm) going to growth         (al_grw)              [-]
0.25     0.25     0.25
##      LEAF life span                  (Yleaf)             [year]
1.00    1.00      1.00
##      SAPWOOD   turnover rate ^-1          (Ystem)             [year]
35.0     35.0     1.00
##      FINE ROOT turnover rate ^-1          (Yroot)             [year]
4.5      4.5      1.00
##      Maximum DROUGHT leaf turnover rate     (DH20max)             [day]
200      200    30.0
##      Maximum COLD    leaf turnover rate     (DTairmax)            [day]
6.67     6.67     6.67
##      Shape parameter for DROUGHT leaf loss   (bH20)                [-]
3.0      3.0      3.0
##      Shape parameter for COLD    leaf loss   (bTair)               [-]
3.0      3.0      2.0
##      Temperature threshold for leaf loss due to COLD (Tcold)       [^oC]
5.0      5.0      3.0
```

ALLOCATION_PARAMETERS:
/=/
Number of parameters in this group
6
Allocation fraction to LEAVES for NON-STRESSED vegetation (e0leaf) [-]
0.45 0.45 0.45
Allocation fraction to STEM for NON-STRESSED vegetation (e0stem) [-]
0.35 0.35 0.00
Allocation fraction to ROOTS for NON-STRESSED vegetation (e0root) [-]
0.20 0.20 0.55
Allocation sensitivity parameter (wsens) [-]
0.02 0.02 0.70
Coefficient in the structural biomass-canopy relationship (alloc_eps) [-]
1.25 1.25 1.25
Exponent in the structural biomass-canopy relationship (alloc_kap) [-]
1.00 1.00 1.00

PHENOLOGY_PARAMETERS:
/=/
Number of parameters in this group
5
Fraction of plant structural biomass to initiate leaf-onset (ClfInit) [-]
0.075 0.075 0.0
Minimum LAI to initiate the leaf-onset (LAIInit) [m^2 m^-2]
0.20 0.20 0.20
Min # of days with favorable conditions for leaf-onset (DaysFav) [day]
7 7 5
Minimum daily soil t-re for conditions to be favorable (TminFav) [^oC]
15.0 15.0 5.0
Fraction of MAX leaf biomass to transit to normal growth (ClfNorm) [-]
0.4 0.4 0.0

SURVIVAL_PARAMETERS: /=/
Number of parameters in this group
2
Soil water potential at which stomatal closure begins (PsiStress) [MPa]
-0.01 -0.01 -0.6
Soil water potential at which plant wilting begins (PsiWilt) [MPa]
-6.8 -6.8 -6.8

DYNAMIC_ROOT_PARAMETERS:
/=/
Number of parameters in this group. For deatils look at DynamicRoot.README
4
Option regarding root profile update time (rootUpdateOpt) 0-Mid-ngt 1-Thres
0 0 0
Percentage threshold to update root profile (rootUpdateThreshold) [0-100]
5 5 5
Option regarding the type of stress factor (stressType) 0-Intg 1-Current
0 0 0
Option for keeping the root biomass pool for next yr (rootTrack) 0-No 1-Yes
1 1 1

VEGETATION INITIALIZATION PARAMETERS

INITIALIZATION_VARIABLES: /=/
----- THERE MUST BE_NO_SPACES AFTER THE LAST VALUE IN A GIVEN ROW -----
Number of parameters (variables) in this group
10
== INITIALIZATION == vegetation fraction [-]
0.7 0.7 0.0
== INITIALIZATION == phenology state: 0-DORM 1-MAX 2-NORM 3-LEAF-FALL [-]
2 2 0.0
== INITIALIZATION == value of LAI [m^2 m^-2]
5.0 5.0 0.0
== INITIALIZATION == value of SAI [m^2 m^-2]
2.0 2.0 0.0
== INITIALIZATION == value of CANOPY carbon pool [g C m^-2]
300 300 0.0
== INITIALIZATION == value of SAPWOOD carbon pool [g C m^-2]
200 200 0.0
== INITIALIZATION == value of ROOT carbon pool [g C m^-2]
50 50 0.0
== INITIALIZATION == value of vegetation height [m]
20.0 20.0 0.0
== INITIALIZATION == value of rooting depth [m]
0.30 0.30 0.012
== INITIALIZATION == value of rooting distribution exp. 3.046 4.919 [-]
2 2 9.0

APPENDIX B: LANDSLIDE COMPONENT BASED ON FS EQUATION

EXPLANATORY NOTES

Highlighted portions indicate key parts of the code:

- t values shown below are from 1 to 3000. For computational efficiency, the total modeled period was split into different periods and results from each time period were saved in different output files (e.g. Out_1_1.)

- thresh_sat is the threshold value for a saturated soil moisture value, shown below as 0.99.

MATLAB SCRIPT

```
%% DEFINITION OF RUN VARIABLES
thresh_sat=0.99;
t_start=1;
t_end=3000;
nomefile='Out_1_1';
LS_final_totb


%%%%%%%%%%%%%%%%%%%%%%%%%%%%%%%%%%%%%%%%%%%%%%%%%%%%%%%%%%%%
% Landslide Component based on FS Equation
% Sameer Kamal and Chiara Lepore
% August 2009
%%%%%%%%%%%%%%%%%%%%%%%%%%%%%%%%%%%%%%%%%%%%%%%%%%%%%%%%%%%%

%%% STATIC VARIABLES %%%

%%%%%%%%%%%%%%%%%%%%%%%%%%%%%%%%%%%%%%%%%%%%%%%%%%%%%%%%%%%%

load type_soil.mat %(vectors with 1, 2 and 3; 2 and 3 are the same thing)
phideg1 = 30.1;
phi1 = phideg1*3.142/180;% phi = Internal friction angle of soil (radians)
phideg2 = 30.8;
phi2 = phideg2*3.142/180;% phi = Internal friction angle of soil (radians)
csoil1=7790;%Clay
csoil2=5370;%Loam
clear phideg
% gammas = 12458.7; % gammas = Specific weight of soil (N/m3) DRY???
```

```
gammat1=1.28*(1+0.33)*1000*9.81;
gammat2=1.26*(1+0.38)*1000*9.81;
gammaw = 9806;
% gammaw = Specific weight of water (N/m3)
Z = 1.75;
% Z = z/cos(angle) Depth to failure as a vertical(m)

% biomass = Force due to biomass (Pa). For now, assume constant.
% FS analysis indicates this ~ negligible.
biomass = 220;
%%%layers
depth=[0,
25,50,76,103,131,161,193,227,264,304,348,396,449,508,574,649,734,831,943,1073,1225
,1405,1621,1883];
d_depth=diff(depth);
thicknesslayers = [25+12.5,d_depth(2:end-1)/2+d_depth(3:end)/2,d_depth(end)/2+(2000-
1883) ];
clear depth d_depth
%%%%%%% BEGIN LOOP ON TIMESTEP %%%%%%%
% tstep = Number of timesteps (hourly)
% For two year run = 17520
counter_col=1;

for t =
t_start:1:t_end%%%%%%%%%%%%%%%%%%%%%%%%%%%%%%%%%%%%%%%%
%%%%%%%%%%%%%%%%%%%%%%%%%%%%%%%%%%%%%%%%%%%%%%%%%%%%
%%%%%%%
   t
   if t<10
      stringnum=strcat(['000',num2str(t)]);
   elseif t<100
      stringnum=strcat(['00',num2str(t)]);
   elseif t<1000
      stringnum=strcat(['0',num2str(t)]);
   else
      stringnum=strcat([num2str(t)]);
   end

   eval(['dfile=importdata("fsand.',stringnum,'_00d");'])

%%% DYNAMIC VARIABLES %%%

soilm=dfile(:,53);
angle_alpha=dfile(:,3);% angle_alpha = slope angle in radians
waterweight = dfile(:,31:53).*repmat(thicknesslayers(1:end-
1),(size(dfile,1)),1)/1000.*gammaw;%Pa
```

```
% Bvalue = waterweight + biomass;% Bvalue = Total weight due to biomass and water
(Pa)
Bvalue = biomass;% Bvalue = Total weight due to biomass and water (Pa)
clear waterweight
% Bvalue=sum(Bvalue,2);

%%% Evaluate presence and depth of saturated layer

sat_yes = zeros(size(soilm,1),1);
head_saturated=zeros(size(soilm,1),1);
sat_yes(type_soil==1)= ((dfile(type_soil==1,53) - 0.09)/(0.385 - 0.09))>thresh_sat;
sat_yes(type_soil==2|type_soil==3)= ((dfile(type_soil==2|type_soil==3,53) -
0.027)/(0.434 - 0.027))>thresh_sat;
if sum(sat_yes)>0
   tmp_sat=zeros(size(soilm,1),23);
   tmp_sat(type_soil==1,:)=(dfile(type_soil==1,31:53) - 0.09)/(0.385 - 0.09);
   tmp_sat(type_soil==2|type_soil==3,:)=(dfile(type_soil==2|type_soil==3,31:53) -
0.027)/(0.434 - 0.027);
   tmp_sat(sat_yes==0,:)=0;
   indexsat=find(sat_yes==1);
   length_waterlevel=[2000 2000-cumsum(thicknesslayers)];
   length_waterlevel=length_waterlevel(1:end-2)-length_waterlevel(end-1);
   for is2 = 1 : length(indexsat)
      is=indexsat(is2);
     if sum(tmp_sat(is,:)>=thresh_sat)==23
     head_saturated(is)=max(length_waterlevel);
     elseif tmp_sat(is,23)>=thresh_sat&tmp_sat(is,22)<thresh_sat
     head_saturated(is)=min(length_waterlevel);
     elseif tmp_sat(is,23)>=thresh_sat&tmp_sat(is,22)>=thresh_sat
        ii=22;
        while sum(tmp_sat(is,23:-1:ii)>=thresh_sat)==length(tmp_sat(is,23:-1:ii))
            ii=ii-1;
        end
     head_saturated(is)= length_waterlevel(ii+1);
     end
   end
  clear tmp_sat
end
clear sat_yes
head_saturated=head_saturated/1000;
%
clear dfile

psi = zeros(size(soilm,1),1);
psi(type_soil==1)= -0.370*((soilm(type_soil==1) - 0.09)/(0.385 - 0.09)).^(-
1/0.15);%Clay
```

```
psi(type_soil==2|type_soil==3)= -0.111*((soilm(type_soil==2|type_soil==3) -
0.027)/(0.434 - 0.027)).^(-1/0.22);%Loam
clear soilm
if sum(head_saturated)>0
   psi(head_saturated>0)=head_saturated(head_saturated>0);
end

%%%%%% CALCULATION OF TERMS %%%%%%

term1=1000000000000*ones(size(psi,1),1);
term2=1000000000000*ones(size(psi,1),1);
term3=1000000000000*ones(size(psi,1),1);
%%% TERM 1
term1(type_soil==1)  = tan(phi1)./tan(angle_alpha(type_soil==1));
term1(type_soil==2|type_soil==3) =
tan(phi2)./tan(angle_alpha(type_soil==2|type_soil==3));
%%% TERM 2
% term2(type_soil==1) =
csoil1./(((gammas*Z)+(Bvalue)).*(sin(angle_alpha(type_soil==1)).*cos(angle_alpha(typ
e_soil==1))));
% term2(type_soil==2|type_soil==3) =
csoil2./(((gammas*Z)+(Bvalue)).*(sin(angle_alpha).*cos(angle_alpha)));
term2(type_soil==1) =
csoil1./(((gammat1*Z)+(Bvalue)).*(sin(angle_alpha(type_soil==1)).*cos(angle_alpha(ty
pe_soil==1))));
term2(type_soil==2|type_soil==3) =
csoil2./(((gammat2*Z)+(Bvalue)).*(sin(angle_alpha(type_soil==2|type_soil==3)).*cos(a
ngle_alpha(type_soil==2|type_soil==3))));
%%% TERM 3
% term3
(type_soil==1)=(psi(type_soil==1)*gammaw*tan(phi1))./(((gammas*Z)+(Bvalue)).*(sin(
angle_alpha(type_soil==1)).*cos(angle_alpha(type_soil==1))));
% term3
(type_soil==2|type_soil==3)=(psi(type_soil==2|type_soil==3)*gammaw*tan(phi2))./(((g
ammas*Z)+(Bvalue)).*(sin(angle_alpha(type_soil==2|type_soil==3)).*cos(angle_alpha(t
ype_soil==2|type_soil==3))));
term3
(type_soil==1)=(psi(type_soil==1).*gammaw.*tan(phi1))./(((gammat1*Z)+(Bvalue)).*(si
n(angle_alpha(type_soil==1)).*cos(angle_alpha(type_soil==1))));
term3
(type_soil==2|type_soil==3)=(psi(type_soil==2|type_soil==3).*gammaw.*tan(phi2))./(((
gammat2*Z)+(Bvalue)).*(sin(angle_alpha(type_soil==2|type_soil==3)).*cos(angle_alph
a(type_soil==2|type_soil==3))));
clear angle_alpha

FS = term1 + term2 - term3;
```

```
Output(:,counter_col) = FS;
if t==t_start
TT1= term1;
TT2 = term2;
end
TT3(:,counter_col) = term3;

counter_col=counter_col+1;

%%%%%% END LOOP FOR TIME STEP %%%%%%
clear term*
end

save(nomefile,'Output','TT1','TT2','TT3')
clear Output TT1 TT2 TT3
```